

Side Chain Length Dependent Chiroptical Switching in Si-Si Bond Polymer Aggregates

(シリコン原子を主鎖に有する高分子の凝集状態における
側鎖長依存的な光学活性反転)

Nozomu SUZUKI

鈴木 望

Nara Institute of Science and Technology

Graduate School of Materials Science

Advanced Polymer Science Laboratory

(Prof. Fujiki Michiya)

24 February 2016

Index

Chapter 1. General Introduction.....	1
1.1. Materials with Switching Ability	1
1.2. Chirality, Optical Activity, and Switching	4
1.3. Polysilane as switching molecule	4
1.4. Switchable Molecules in Solid State.....	5
1.5. Cholesteric Hard-Core Model.....	6
1.6. Purpose of This Research.....	9
1.7. Outline of Each Chapter.....	9
1.8. References	10
Chapter 2. Experimental Approach: Chiroptical Inversion of Polysilane Aggregates.....	13
2.1. Introduction.....	13
2.2. Experimental	14
2.2.1. Synthesis of Dialkylpolysilanes.....	14
2.2.2. Sample Preparation and CD Measurement in Solution State	14
2.2.3. Sample Preparation and CD Measurement in Aggregate States	15
2.3. Results and Discussion on Chiroptical Properties	16
2.3.1. Chiroptical Properties in Solution State	16
2.3.2. Chiroptical Properties in Aggregate States.....	17
2.3.3. Membrane Filter Experiment of Aggregates	21
2.3.4. Molecular Weight Dependency of UV/CD Spectra	24
2.4. TEM Image of the Polymers.....	27
2.5. References	29
Chapter 3. Theoretical Approach: Higher Order Structure and Chiroptical Activity	30
3.1. Introduction.....	30
3.2. Cholesteric Hard-Core Model.....	31
3.2.1. Qualitative Description of Cholesteric Hard-Core Model.....	31
3.2.2. Quantitative Description of Cholesteric Hard-Core Model.....	34
3.2.3. Consideration of Solvophobic Effects and Number of Molecules	35
3.3. Exciton Chirality Method	39
3.4. Combination of Cholesteric Hard-Core Model and Exciton Chirality Method.....	42
3.5. Applying the Combined Model to Dialkylpolysilane System	43
3.5.1. Obtaining p and D values from PM3 model.....	43
3.5.1. Estimation of p and D values from WAXD data.....	44

3.5.2. Applying the Model to the Dialkylpolysilane System.....	47
3.6. References	49
Chapter 4. Computational Approach 1: Development of Parameter Optimization Program .	50
4.1. Introduction.....	50
4.2. Parameter Optimization Scheme.....	53
4.3. Gaussian 09 Program Parameter Optimization.....	55
4.3.1. Role of Gaussian 09 in the Program	55
4.3.2. Input File of Gaussian 09.....	55
4.3.3. Output File of Gaussian 09	56
4.4. CONFLEX 7B Program and Parameter Optimization.....	58
4.4.1. Role of CONFLEX in the Program	58
4.4.2. Input Files of CONFLEX	58
4.4.3. Output Files of CONFLEX.....	59
4.4.4. Running CONFLEX from Python	60
4.5. Validation of the Program Using Model Structures	62
4.5.1. Computational Method	62
4.5.2. Optimization of Internal Coordinates	62
4.5.3. Optimization of Rotational and Vibrational Frequencies.....	64
4.5.4. Optimization of Conformational Energies	67
4.6. References	69
Chapter 5. Computational Approach 2: Parameter Optimization	70
5.1. Introduction.....	70
5.2. Choice of Quantum Mechanics Method	71
5.3. Computational Method	75
5.3.1. Optimization of Bond Charge Increments.....	75
5.3.2. Optimization of Van Der Waals Interactions	76
5.3.3. Optimization of Internal Coordinates, Rotational and Vibrational Frequencies, and Conformational Energies	78
5.4. Results of Parameter Optimization	84
5.4.1. Parameter Table	84
5.4.2. Internal Coordinates	87
5.4.3. Rotational and Vibrational Frequencies	96
5.4.4. Conformational Energies	98
5.5. Application of the Force Field to the Polydialkylsilane System.....	103
5.5.1. Effect of Conformation to p and D	103

5.5.2. Optimization of Two Body Structures.....	107
5.6. References.....	110
Chapter 6. Concluding remarks.....	111
Appendix.....	115
List of Publications.....	138
Presented Works.....	140
Acknowledgements.....	142

Part of this thesis is reprinted with permission from *J. Am. Chem. Soc.* **2013**, *135*, 13073–13079. Copyright 2013 American Chemical Society.

Chapter 1. General Introduction

1.1. Materials with Switching Ability

Designing switching ability is one of the attractive goals in materials science. Elaborating switchable substances are applicable to; sensing of physical environment or certain chemical substance¹⁻⁵; fast and intense information storage and processing^{6,7}; and fabrication of molecular machines^{8,9}. Those substances are required to have ‘bistability’, the two forms that can be interchanged by external physical/chemical stimuli.⁶ For instance, guanine and cytosine rich DNA is known to show transition from right handed B-helix to left handed Z-helix by increasing salt concentration or solution temperature, known as BZ-transition.^{10,11} In this example, the structures of DNA are interconverted by salt or temperature, thus the DNA has the bistability.

The stable forms of switchable substance can be characterized from two points of views: property and structure. Firstly, from the property point of view, there are optical states¹³⁻²⁴, redox states²⁶, magnetic states, and surface states.^{7,27} When one aims to design information storage, the optical states has advantage over the other states since it enables rapid read processing.⁶ Moreover, optical states have multiple dimensions of property including absorption, reflection, emission, wavelength, and optical activity to keep the information. Secondly, from the structural point of view, there are conformational, configurational, constitutional, and compositional states as categories (Table 1.1).²⁸ Those components can be divided into both molecular level and higher order level (supramolecular structure).

Conformational changes^{14-16,29,30} are common among molecules and polymers because it does not require breaking bonds of the structure. Contrary to conformational change, some reactions involve breaking bonds and undergo configurational, constitutional, and compositional change. Acid-base reaction is a typical example and hydrogen atoms change its connectivity during the reaction though majority of the chemical structure remains unchanged. This reaction enables to

control the electrostatic interaction and alter the supramolecular configuration of the molecule.^{22,26} Some metal complexes are able to change the connectivity similar in the manner as acid-base reaction by exchanging molecules.²³ Photoirradiation causes change in configuration of photochromic molecules, and those structures do not interconvert at room temperature.^{18,21,31} In multiple component system, controlling the conformational arrangement in higher order structure is also possible.^{19,20,32,33} Liquid crystal is a typical example and phase transitions take place depending on the temperature.³⁴⁻³⁶

The stimuli that trigger the switching are classified to be either chemical or physical. Whether to introduce those stimuli actively or passively could differ the resulting usage. If one wishes to store data in the molecule, it requires to actively or artificially inducing the physical stimuli to change the property of the system to write or erase information. On the other hand, if the purpose is sensing, the stimuli is induced passively or naturally, and the information of the stimuli is read by analyzing the state of the system. The typical physical stimuli are light absorption, temperature, pressure, magnetic field, and electric field. The chemical stimuli can be acid/base molecules, metals, and solvents.

Table 1.1. The concepts of composition, constitution, configuration, and conformation in molecular and supramolecular structure. Reprinted from Turro, N. J. *Proc. Natl. Acad. Sci.* **2005**, *102*, 10766 with permission from National Academy of Sciences, U.S.A. The Copyright (2005) National Academy of Sciences, U.S.A.

Structural feature	Mathematical level	Molecular structure	Supramolecular structure
Composition	Topological	Numbers and kinds of atoms in a molecular structure	Numbers and kinds of molecules in a supramolecular structure
Constitution	Topological	Connections between the atoms in a molecular composition	Connections between the molecules in a supramolecular composition
Configuration	Geometric	Orientation of neighboring atoms about a given atom in 3D space	Orientation of neighboring molecules about a given molecule in 3D space
Conformation	Geometric	Instantaneous global molecular shape of a structure in 3D space	Instantaneous global shape of a supramolecular structure in 3D space

1.2. Chirality, Optical Activity, and Switching

When chirality is introduced in the molecular geometry, the physical properties of the substance are affected, and it induces optical activity. Chirality is basically a concept in configuration level when the single molecule is assumed with averaged time, so switching chiral states normally means to use opposite enantiomer and designing 'chiral switchability' would thus be a difficult task. However, designing a molecule with switchable optical activity is possible since the optical activity is defined as a difference in absorption of left and right circularly polarized light, and inversion or change in the strength of the optical activity could be introduced by conformational change. Such conformational change is not limited in molecular level but also observed in supramolecular level.

A helix is one of the most striking examples of chiral structures and is seen not only in biomolecules^{37,38} but also in synthetic macromolecules³⁹⁻⁴⁵ and supramolecules.⁴⁶⁻⁵³ Using simple helical π - and σ -conjugating polymers^{17,54-61} permits the designing switchable molecules due to its relatively lower energy to interact with light at UV-Vis region (300 nm–400 nm).^{19,20,62-69}

1.3. Polysilane as switching molecule

Polysilane exhibits intense, narrow absorption, and emission bands due to one-dimensional exciton in the region 300–400 nm (i.e. a short-lived photoexcited electron-hole pair confined to one-dimensional semiconductor). Intense study has been carried out for one-dimensional polysilanes^{59,61,70-72}, dendrimers^{73,74}, ladder polysilanes⁷⁵. For the one-dimensional polysilanes, it is known to form 7_3 helix (i.e. 7/3 helix), trans planer, TGTG' and disordered conformation (Table 1.2). Due to conformational change in the Si-Si-Si-Si dihedral angle this kind of compounds show thermochromism, solvatochromism, ionochromism, and piezochromism, that

respond to external physical and chemical stimuli. Certain optically active dialkylpolysilane (**PSi2**) showed chiroptical switching in aggregated states,^{19,76} which could not be seen in homogeneous solution. Additionally, the dialkylpolysilanes are known to form liquid crystalline phase, and smectic phases in binary mixtures are studied.^{34,35}

Unlike *n*-butane which has *gauche* (G, dihedral angle $\omega \sim 60^\circ$), and *anti* (A, $\omega \sim 180^\circ$) as metastable and the most stable conformations, permethyltetrasilane have *gauche* (G, dihedral angle $\omega \sim 60^\circ$), *ortho* (O, $\omega \sim 90^\circ$), and *transoid* (T, $\omega \sim 165^\circ$) conformations as energy minima. When silicons at positions 2 and 3 bear four ethyl groups instead of methyl ($\text{Me}_3\text{Si-SiEt}_2\text{-SiEt}_2\text{-SiMe}_3$), deviant (D, $\omega \sim 150^\circ$) conformation will appear.⁷⁷

Table 1.2. Summary of the structural, UV absorption, and thermal properties of some polysilane derivatives in the solid state. Reprinted with permission from *Chem. Rev.*, **1989**, 89, 1359–1410. Copyright 1989 American Chemical Society.

$-(\text{R}^1\text{R}^2\text{Si})_n-$	polymer backbone	λ_{max}^a nm (film)	DSC transition temp, °C	ΔH_i^b kcal/mol
$\text{R}^1 = \text{R}^2 = n\text{-butyl}$	7/3 helix	313–315	83	0.36 backbone disordering
$\text{R}^1 = \text{R}^2 = n\text{-pentyl}$	7/3 helix	313–315	75	0.45 backbone disordering
$\text{R}^1 = \text{R}^2 = n\text{-hexyl}$	trans planar	375	42	5.0 side-chain melting backbone disordering
$\text{R}^1 = \text{R}^2 = n\text{-octyl}$	trans planar	375	47	4.7 side-chain melting backbone disordering
$\text{R}^1 = \text{R}^2 = n\text{-tetradecyl}$	TGTG'	345	55	8.4 side-chain melting backbone disordering
$\text{R}^1 = n\text{-hexyl}; \text{R}^2 = n\text{-octyl}$ (atactic)	?	354	-19	1.4 side-chain melting backbone disordering
$\text{R}^1 = \text{R}^2 = 4\text{-methylpentyl}$	disordered	316		

^a Absorption maximum below the transition temperature. ^b Enthalpy change of the thermal transition when observable.

1.4. Switchable Molecules in Solid State

When one designs a switchable molecular device, it is necessary to analyze the property not in solution states but also in solid states. In addition to the low cost, one of the advantages of the polymer is its processability as film. However, there are several obstacles to study the optical properties in the solid states: (1) anisotropy in solid state may result in variable chiroptical properties; (2) multiple crystalline phases^{78,79} coexist in the film states complicate the optical properties; and (3) most conjugating polymers and molecules have multiple chromophores and/or

show vibronic sidebands which complicate the UV and circular dichroism (CD) spectra. A way to overcome the problems (1) and (2) is to study samples in aggregate states where the problem anisotropy and crystallinity do not arise. Therefore, use of an ideal conjugated polymer with a single chromophore without vibronic side band solves the problem (3).

Dialkylpolysilane is an excellent polymer in this respect because the derivatives of the macromolecule feature a unique $\text{Si}\sigma\text{-Si}\sigma^*$ transition approximately at 300 nm without vibronic sidebands in the UV and CD spectra.

So far, several researchers have proposed that higher-order chiral structures are governed by the twisting ability of the main-chain helix,⁶² the helical parameter of individual polymers (cholesteric hard-core model),¹⁹ an alternation in the $\pi\text{-}\pi$ stacking motif,⁶³⁻⁶⁵ and a subtle balance between repulsive and attractive chiral interactions.⁶⁶ In this work we have applied the cholesteric hard-core model to dialkylpolysilane system.

1.5. Cholesteric Hard-Core Model

The cholesteric hard-core model correlates the chirality of individual helical polymer and higher order structure based on two helical variables, pitch (p) and diameter of the helix (D) (see Section 3.2). It predicts that the chirality in higher order structure invert at $p/D = \pi$. The interesting point of this model is that the inversion of the higher order structure does not depend only on the handedness of each polymer but also p and D . This model provides the structural design of the switching material in solid state by controlling the p and/or D . For example, if one could synthesize helical polymer with side chain that undergo cis-trans isomerism, the polymer has a chance to show chiroptical switching by photo-irradiation in solid state. This is because such structure change in the side chain will increase or decrease the length of the side chain and so as D . Similar result is expected for the main chain as well since change in the main chain conformation should affect p .

This model states two arguments: (1) knowing the p and D of the helix, one can decide the chirality of the higher order structure, and (2) the critical value that inverts the higher order structure is $p/D = \pi$. In the original reference by Gottarelli and Spada,¹² they applied the model to B-helix DNA⁹ but they admitted that the model was not applicable to the system because of the electrostatic charge. However, J. R. Koe's groups provided examples that fulfill the statement (2) based on **Poly-B2** (Figure 1.1 and Table 1.3), which do not suffer from large electrostatic effects.¹⁹ They modified the diameter of helical alkylphenylpolysilane by attaching different side chains. Yet, the correlation between the chiroptical properties and the sign of the CD spectra has been not clear for alkylphenylpolysilane derivatives (series of **Poly-As** and **Poly-Bs**) due to the complexity of the σ - π conjugation. Therefore, dialkylpolysilane system that does not suffer from the difficulty was adopted in this work.

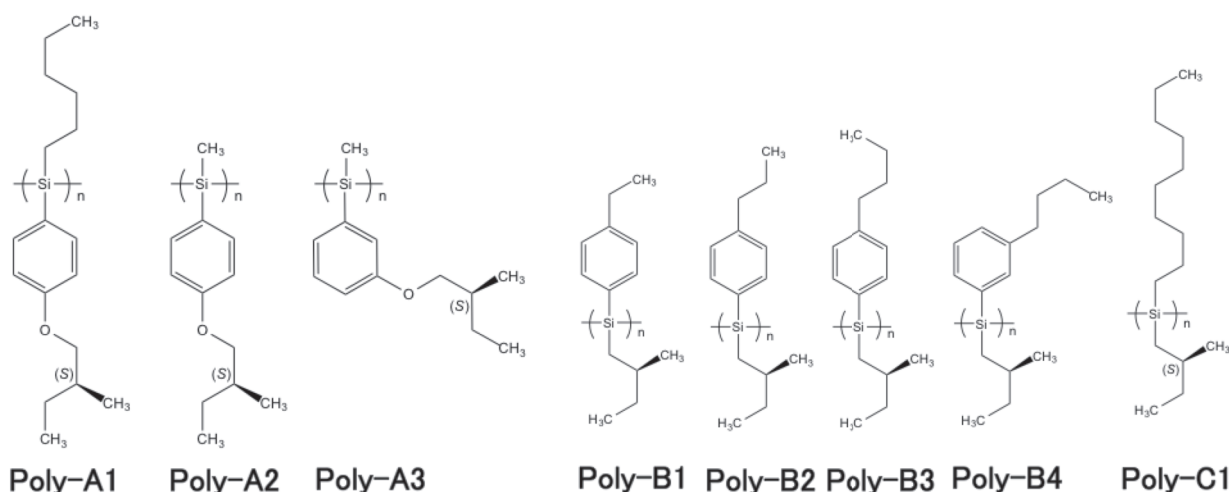


Figure 1.1. Example of polymers investigated.

Table 1.3. CD, helix sense, handedness of the structure, p and D values of polymers.

	Polymer		Higher order structure					Ref.
	CD ^a	Helix sense	CD ^a	Handedness	p [Å]	D [Å]	p/D	
DNA B-helix	–	right	–	left	34	20	1.7	9, 12
Poly-A1	– ^b	– ^c	(+)/(–)-bisign ^d	right/left ^e	–	–	–	25
Poly-A2	– ^b	– ^c	(–)-bisign	left ^e	–	–	–	25
Poly-A3	– ^b	– ^c	(–)-single sign	– ^f	–	–	–	25
Poly-B1	(+)-single sign	– ^c	(–)-bisign	left ^e	61.5 ^g	17.2 ^g	3.57 ^g	19
Poly-B2	(+)-single sign	– ^c	(+)-bisign ^h	right ^e	61.5 ^g	19.3 ^g	3.19 ^g	19
Poly-B3	(+)-single sign	– ^c	(+)-bisign	right ^e	61.5 ^g	21.9 ^g	2.81 ^g	19
Poly-B4	(+)-single sign	– ^c	(–)-bisign	left ^e	–	–	–	19
Poly-C1	(+)-single sign	Right ⁱ	(–)-bisign	left ^e	– ^j	– ^j	– ^j	67

^aCD at the longest wavelength.

^bNo detectable CD was observed.

^cHelix sense and optical activity correlation have not been established in the system due to the complexity of σ - π conjugation.

^dThe aggregate showed (+)-bisigned Cotton effect when dispersed in tetrahydrofuran/methanol cosolvent with relatively high amount of good solvent (tetrahydrofuran) but showed (–)-bisigned Cotton effect in that with relatively high amount of poor solvent (methanol).

^eElectric transition dipole moment along longitudinal axis was assumed and exciton chirality method (See section 3.3) was applied.

^fThe sign of the CD was not in bisigned shape, so the exciton chirality method was not applied.

^gEstimated using MM2.

^hIt was reported that this polymer shows chiroptical inversion but this could be transition from bisigned CD and trisigned CD as discussed in section 2.3.4.

ⁱ P -7₃ helix was assumed (see section 2.3.1).

^jIn this work, p , D , p/D were estimated as 27.4 Å, 10.5 Å, and 2.61 from WAXD. For estimation of p , 1.96 Å was used for the projection of Si-Si bond length to the longitudinal axis of the dialkylpolysilane with 7₃ helix (see section 3.5.1).

1.6. Purpose of This Research

The main purpose of this work is to establish and elucidate the switchability in higher-order chiral structures (supramolecular conformations in Table 1.1) of a helical polymer aggregates. To achieve this goal, the author took the following steps: (1) to find dialkylpolysilane system that shows chiroptical switching in solid states; (2) to establish a model to explain the phenomenon by combining the cholesteric hard-core model and the exciton chirality method; and (3) to build up molecular mechanics (MM) force field parameters for silicon, carbon, and hydrogen system for analyzing (1) and (2) utilizing the computational tool.

1.7. Outline of Each Chapter

This work can be divided into four main sections from Chapter 2 to Chapter 5. In Chapter 2, the experiment on the side chain length dependent and solvent dependent chiroptical inversion of dialkylpolysilane in aggregate state are presented. In Chapter 3, the author shows a cholesteric hard-core that can describe the higher order structures of helical polymer, and exciton chirality method to correlate between the structure and the optical activity. In Chapter 4, description of the parameter optimization program for MM is presented. In Chapter 5, the program was applied to the silicon, carbon, and hydrogen system. New parameters for MMFF94S force field were developed. In Chapter 6, each of the chapters was summarized and concludes the work.

1.8. References

- (1) Moonen, N. N. P.; Flood, A. H.; Fernández, J. M.; Stoddart, J. F. *Top. Curr. Chem.* **2005**, *262*, 99.
- (2) Koh, I.; Josephson, L. *Sensors* **2009**, *9*, 8130.
- (3) Canary, J. W.; Mortezaei, S.; Liang, J. *Coord. Chem. Rev.* **2010**, *254*, 2249.
- (4) Su, X.; Aprahamian, I. *Chem. Soc. Rev.* **2014**, *43*, 1963.
- (5) Bill, N. L.; Trukhina, O.; Sessler, J. L.; Torres, T. *Chem. Commun.* **2015**, *51*, 7781.
- (6) Feringa, B. L.; van Delden, R. A.; Koumura, N.; Geertsema, E. M. *Chem. Rev.* **2000**, *100*, 1789.
- (7) Ruben, M.; Rojo, J.; Romero-Salguero, F. J.; Uppadine, L. H.; Lehn, J.-M. *Angew. Chem. Int. Ed.* **2004**, *43*, 3644.
- (8) Coskun, A.; Banaszak, M.; Astumian, R. D.; Stoddart, J. F.; Grzybowski, B. A. *Chem. Soc. Rev.* **2012**, *41*, 19.
- (9) Rich, A.; Nordheim, A.; Wang, A. H. J. *Annu. Rev. Biochem.* **1984**, *53*, 791.
- (10) Rich, A.; Zhang, S. *Nat. Rev. Genet.* **2003**, *4*, 566.
- (11) Fuertes, M. A.; Cepeda, V.; Alonso, C.; Pérez, J. M. *Chem. Rev.* **2006**, *106*, 2045.
- (12) Gottarelli, G.; Spada, G. P. In *Circular dichroism : principles and applications*; 2nd ed.; Berova, N., Nakanishi, K., Woody, R., Eds.; Wiley-VCH: New York, 2000, p 547.
- (13) Tsivgoulis, G. M.; Lehn, J.-M. *Angew. Chem. Int. Ed. Engl.* **1995**, *34*, 1119.
- (14) Mao, C. D.; Sun, W. Q.; Shen, Z. Y.; Seeman, N. C. *Nature* **1999**, *397*, 144.
- (15) Fujiki, M.; Koe, J. R.; Motonaga, M.; Nakashima, H.; Terao, K.; Teramoto, A. *J. Am. Chem. Soc.* **2001**, *123*, 6253.
- (16) Fujiki, M. *J. Organomet. Chem.* **2003**, *685*, 15.
- (17) Dellaportas, P.; Jones, R. G.; Holder, S. J. *Macromol. Rapid Commun.* **2002**, *23*, 99.
- (18) van Delden, R. A.; Huck, N. P. M.; Piet, J. J.; Warman, J. M.; Meskers, S. C. J.; Dekkers, H. P. J. M.; Feringa, B. L. *J. Am. Chem. Soc.* **2003**, *125*, 15659.
- (19) Peng, W.; Motonaga, M.; Koe, J. R. *J. Am. Chem. Soc.* **2004**, *126*, 13822.
- (20) Pijper, D.; Jongejan, M. G. M.; Meetsmia, A.; Feringa, B. L. *J. Am. Chem. Soc.* **2008**, *130*, 4541.
- (21) Hayasaka, H.; Miyashita, T.; Tamura, K.; Akagi, K. *Adv. Funct. Mater.* **2010**, *20*, 1243.
- (22) Hmadeh, M.; Fang, L.; Trabolsi, A.; Elhabiri, M.; Albrecht-Gary, A. M.; Stoddart, J. F. *J. Mater. Chem.* **2010**, *20*, 3422.
- (23) Dai, Z.; Lee, J.; Zhang, W. *Molecules* **2012**, *17*, 1247.
- (24) Fujiki, M.; Yoshida, K.; Suzuki, N.; Zhang, J.; Zhang, W.; Zhu, X. *RSC Adv.* **2013**, *3*, 5213.
- (25) Nakashima, H.; Fujiki, M.; Koe, J. R.; Motonaga, M. *J. Am. Chem. Soc.* **2001**, *123*, 1963.

- (26) Nijhuis, C. A.; Ravoo, B. J.; Huskens, J.; Reinhoudt, D. N. *Coord. Chem. Rev.* **2007**, *251*, 1761.
- (27) Bunker, B. C. *Mater. Sci. Eng., R* **2008**, *62*, 157.
- (28) Turro, N. J. *Proc. Natl. Acad. Sci.* **2005**, *102*, 10766.
- (29) Koe, J. R.; Fujiki, M.; Nakashima, H. *J. Am. Chem. Soc.* **1999**, *121*, 9734.
- (30) Ha, J.-H.; Loh, S. N. *Chem.-Eur. J.* **2012**, *18*, 7984.
- (31) Irie, M.; Fukaminato, T.; Sasaki, T.; Tamai, N.; Kawai, T. *Nature* **2002**, *420*, 759.
- (32) Gibaud, T.; Barry, E.; Zakhary, M. J.; Henglin, M.; Ward, A.; Yang, Y.; Berciu, C.; Oldenbourg, R.; Hagan, M. F.; Nicastro, D.; Meyer, R. B.; Dogic, Z. *Nature* **2012**, *481*, 348.
- (33) Katsonis, N.; Lacaze, E.; Ferrarini, A. *J. Mater. Chem.* **2012**, *22*, 7088.
- (34) Okoshi, K.; Kamee, H.; Suzaki, G.; Tokita, M.; Fujiki, M.; Watanabe, J. *Macromolecules* **2002**, *35*, 4556.
- (35) Okoshi, K.; Watanabe, J. *Macromolecules* **2010**, *43*, 5177.
- (36) Wensink, H. H. *Europhys. Lett.* **2014**, *107*, 36001.
- (37) Pauling, L.; Corey, R. B.; Branson, H. R. *Proc. Natl. Acad. Sci.* **1951**, *37*, 205.
- (38) Watson, J. D.; Crick, F. H. *Nature* **1953**, *171*, 737.
- (39) van Beijnen, A. J. M.; Nolte, R. J. M.; Zwikker, J. W.; Drenth, W. *J. Mol. Catal.* **1978**, *4*, 427.
- (40) Rowan, A. E.; Nolte, R. J. M. *Angew. Chem. Int. Ed.* **1998**, *37*, 63.
- (41) Okamoto, Y.; Suzuki, K.; Ohta, K.; Hatada, K.; Yuki, H. *J. Am. Chem. Soc.* **1979**, *101*, 4763.
- (42) Green, M. M.; Peterson, N. C.; Sato, T.; Teramoto, A.; Cook, R.; Lifson, S. *Science* **1995**, *268*, 1860.
- (43) Yashima, E.; Maeda, Y.; Matsushima, T.; Okamoto, Y. *Chirality* **1997**, *9*, 593.
- (44) Inouye, M.; Waki, M.; Abe, H. *J. Am. Chem. Soc.* **2004**, *126*, 2022.
- (45) Schlitzer, D. S.; Novak, B. M. *J. Am. Chem. Soc.* **1998**, *120*, 2196.
- (46) Katagiri, H.; Miyagawa, T.; Furusho, Y.; Yashima, E. *Angew. Chem. Int. Ed.* **2006**, *45*, 1741.
- (47) Lehn, J. M. *Proc. Natl. Acad. Sci.* **2002**, *99*, 4763.
- (48) Lehn, J. M.; Rigault, A.; Siegel, J.; Harrowfield, J.; Chevrier, B.; Moras, D. *Proc. Natl. Acad. Sci. U.S.A.* **1987**, *84*, 2565.
- (49) Piguet, C.; Bernardinelli, G.; Hopfgartner, G. *Chem. Rev.* **1997**, *97*, 2005.
- (50) Prince, R. B.; Barnes, S. A.; Moore, J. S. *J. Am. Chem. Soc.* **2000**, *122*, 2758.
- (51) Yan, N.; He, G.; Zhang, H.; Ding, L.; Fang, Y. *Langmuir* **2010**, *26*, 5909.
- (52) Langeveld-Voss, B. M. W.; Christiaans, M. P. T.; Janssen, R. A. J.; Meijer, E. W. *Macromolecules* **1998**, *31*, 6702.

- (53) Palmans, A. R. A.; Meijer, E. W. *Angew. Chem. Int. Ed.* **2007**, *46*, 8948.
- (54) Babudri, F.; Farinola, G. M.; Naso, F.; Ragni, R. *Chem. Commun.* **2007**, 1003.
- (55) Barnes, M. D.; Baghar, M. *J. Polym. Sci., Part B: Polym. Phys.* **2012**, *50*, 1121.
- (56) Roncali, J. *Chem. Rev.* **1992**, *92*, 711.
- (57) Scherf, U.; List, E. J. W. *Adv. Mater.* **2002**, *14*, 477.
- (58) Becker, S.; Ego, C.; Grimsdale, A. C.; List, E. J. W.; Marsitzky, D.; Pogantsch, A.; Setayesh, S.; Leising, G.; Mullen, K. *Synth. Met.* **2001**, *125*, 73.
- (59) Miller, R. D.; Michl, J. *Chem. Rev.* **1989**, *89*, 1359.
- (60) Fujiki, M. *J. Am. Chem. Soc.* **1994**, *116*, 11976.
- (61) West, R. *J. Organomet. Chem.* **1986**, *300*, 327.
- (62) Ohira, A.; Okoshi, K.; Fujiki, M.; Kunitake, M.; Naito, M.; Hagihara, T. *Adv. Mater.* **2004**, *16*, 1645.
- (63) Goto, H.; Okamoto, Y.; Yashima, E. *Macromolecules* **2002**, *35*, 4590.
- (64) Satrijo, A.; Swager, T. M. *Macromolecules* **2005**, *38*, 4054.
- (65) Satrijo, A.; Meskers, S. C. J.; Swager, T. M. *J. Am. Chem. Soc.* **2006**, *128*, 9030.
- (66) Wu, L. B.; Sato, T. *Kobunshi Ronbunshu* **2006**, *63*, 505.
- (67) Nakano, Y.; Fujiki, M. *Macromolecules* **2011**, *44*, 7511.
- (68) Tabei, J.; Nomura, R.; Shiotsuki, M.; Sanda, F.; Masuda, T. *Macromol. Chem. Phys.* **2005**, *206*, 323.
- (69) Fujiki, M.; Koe, J. R.; Terao, K.; Sato, T.; Teramoto, A.; Watanabe, J. *Polym. J.* **2003**, *35*, 297.
- (70) Tsuji, H.; Fukazawa, A.; Yamaguchi, S.; Toshimitsu, A.; Tamao, K. *Organometallics* **2004**, *23*, 3375.
- (71) Tsuji, H.; Terada, M.; Toshimitsu, A.; Tamao, K. *J. Am. Chem. Soc.* **2003**, *125*, 7486.
- (72) Tsuji, H.; Michl, J.; Tamao, K. *J. Organomet. Chem.* **2003**, *685*, 9.
- (73) Sekiguchi, A.; Lee, V. Y.; Nanjo, M. *Coord. Chem. Rev.* **2000**, *210*, 11.
- (74) Krempner, C. *Polymers* **2012**, *4*, 408.
- (75) Sunada, Y.; Haige, R.; Otsuka, K.; Kyushin, S.; Nagashima, H. *Nat. Commun.* **2013**, *4*.
- (76) Suzuki, N.; Fujiki, M.; Kimpinde-Kalunga, R.; Koe, J. R. *J. Am. Chem. Soc.* **2013**, *135*, 13073.
- (77) Fogarty, H. A.; Ottosson, C.-H.; Michl, J. *J. Mol. Struct.* **2000**, *556*, 105.
- (78) Rizzo, P.; Beltrani, M.; Guerra, G. *Chirality* **2010**, *22*, E67.
- (79) Kyotani, H.; Shimomura, M.; Miyazaki, M.; Ueno, K. *Polymer* **1995**, *36*, 915.

Chapter 2. Experimental Approach: Chiroptical Inversion of Polysilane Aggregates

2.1. Introduction

In this chapter, chiroptical inversion of dialkylpolysilane is reported. Unlike alkylphenylsilane system, this system do not show complex CD spectra due to σ - π conjugation and thus the screw sense has been deduced from CD measurement¹, X-ray diffraction², and calculation based on H-(SiH₂)₁₃-H³ by Fujiki's group. Cholesteric hard-core model predicts that the diameter of the helix affects the handedness of the higher order structure, so various diameter of helix (D) was prepared by changing the side chain length of the dialkylpolysilane (see Section 2.2). The sign of the CD spectra of the polymers dispersed in solvent and in the form of aggregate were measured (see Section 2.3).

2.2. Experimental

2.2.1. Synthesis of Dialkylpolysilanes

A series of poly[alkyl-(*S*)-2-methylbutylsilane]s were prepared (Figure 2.1). **PSi2–4** were synthesized according to a previous work⁴. For **PSi1** and **PSi5**, previously reported samples were used.⁴ Synthesized polymers were re-precipitated to obtain fractions with various M_n and narrow polydispersity index (PDI).

2.2.2. Sample Preparation and CD Measurement in Solution State

Following polymer samples were prepared and put in hot toluene (80°C).

Poly[ethyl-(*S*)-2-methylbutylsilane] (**PSi1**)

Poly[*n*-propyl-(*S*)-2-methylbutylsilane] (**PSi2**)

Poly[*n*-butyl-(*S*)-2-methylbutylsilane] (**PSi3**)

Poly[*n*-pentyl-(*S*)-2-methylbutylsilane] (**PSi4**)

Poly[*n*-hexyl-(*S*)-2-methylbutylsilane] (**PSi5**)

The sample was covered with aluminum foil to prevent photodegradation by UV-light and used within two days. The sample concentrations was set to approximately 1.0×10^{-4} M.

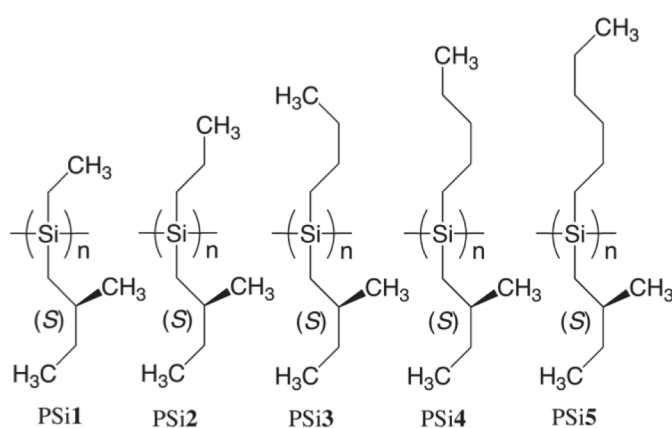


Figure 2.1. Chemical structures of **PSi1–5**.

2.2.3. Sample Preparation and CD Measurement in Aggregate States

To induce aggregation, various samples with toluene/methanol cosolvents were prepared by slowly adding a poor solvent ($\sim 0.1 \text{ mL min}^{-1}$) to the sample in toluene. Methanol was added dropwise (1 drop/sec $\sim 1 \text{ mL min}^{-1}$) using 100–1000 μL micro pipet stirring the content with 1000 rpm. After adding methanol, the sample was transferred from sample vial to 3 mL quartz cuvette. CD/UV measurements were initiated within 30 sec after the addition of the poor solvent. The amounts of methanol and toluene used for each fraction are summarized in Table 2.1.

Table 2.1. Volume fraction and corresponding amount of solvents used in this work.

Toluene/Methanol (Volume fraction)	Toluene/Methanol (mL)
1.0/0.0	3.0/0.0
0.9/0.1	2.7/0.3
0.8/0.2	2.4/0.6
0.7/0.3	2.1/0.9
0.6/0.4	1.8/1.2
0.5/0.5	1.5/1.5
0.4/0.6	1.2/1.8
0.3/0.7	0.9/2.1
0.2/0.8	0.6/2.4
0.1/0.9	0.3/2.7

2.3. Results and Discussion on Chiroptical Properties

2.3.1. Chiroptical Properties in Solution State

To obtain the structural information of the dialkylpolysilanes samples in solution, CD measurements of all **PSi1–5** in dilute toluene (a good solvent) were carried out. Those samples showed intense narrow UV and positive-signed CD bands at approximately at 315 nm (Kuhn's anisotropy, $g_{CD} = 1.95\text{--}2.28 \times 10^{-4}$) due to the $\text{Si}\sigma\text{--Si}\sigma^*$ transition (Figure 2.2). These chiroptical characteristics of the g_{CD} and the absorption wavelength ~ 315 nm indicate that the **PSi1–5** all revealed a right-handed $P\text{-}7_3$ -helical structure.¹⁻³

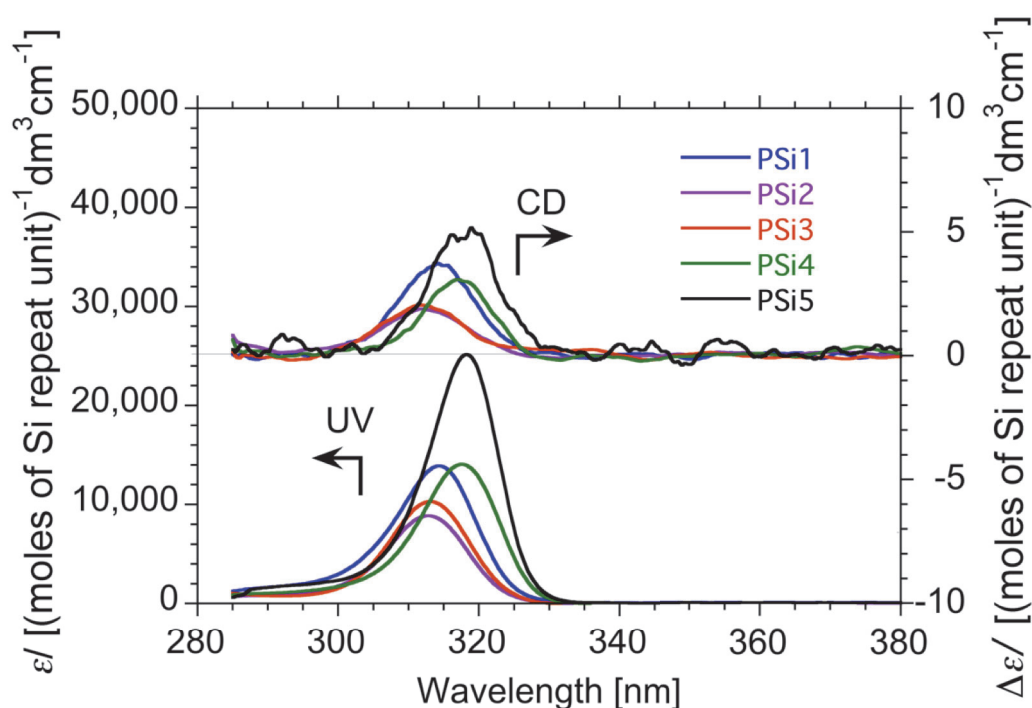


Figure 2.2. CD spectra of dialkylpolysilanes (**PSi1–5**) in toluene. **PSi1**: $M_n = 3.77 \times 10^3$, PDI = 1.22, **PSi2**: $M_n = 3.76 \times 10^3$, PDI = 1.17, **PSi3**: $M_n = 3.25 \times 10^3$, PDI = 1.11, **PSi4**: $M_n = 2.52 \times 10^3$, PDI = 1.12, **PSi5**: $M_n = 6.14 \times 10^3$, PDI = 1.60.

2.3.2. Chiroptical Properties in Aggregate States

By adding methanol (poor solvent) to dilute solutions of **PSi1–5**, corresponding aggregates were formed. In the aggregate form, UV λ_{\max} values were typically blue-shifted by *ca.* 10 nm (Fig. 2.3–Fig. 2.7), compared to those in the homogeneous solution state (Fig. 2.2). The spectra of the solution state described in previous section are also included as light blue lines. The shifted peak approximately at 300 nm corresponds to the aggregate and peak at \sim 315 nm corresponds to solution state determined by membrane filter experiment in Section 2.3.3. **PSi1–5** aggregates showed bisigned Cotton effects due to the exciton coupling arising from the interaction between the nearest neighbors. **PSi1** had a positive bisigned Cotton effect (Fig. 2.3, the sign is taken from the longer wavelength), while **PSi3** had a negative bisigned Cotton effect (Fig. 2.5). The sign of the bisigned Cotton effect did not change depending on the toluene/methanol ratio. Similarly, **PSi3**, **PSi4**, and **PSi5** also showed a negative bisigned CD signals (Table 2.2).

Interestingly, **PSi2** showed a noticeable cosolvent ratio-dependent chiroptical inversion. When the toluene ratio in the cosolvent was relatively high (toluene/methanol = 0.7/0.3–0.5/0.5), the aggregate showed a negative bisigned Cotton effect, but when the toluene ratio was lower (0.3/0.7–0.1/0.9), the chiroptical profile inverted to a positive bisigned Cotton effect (Fig. 2.4). Because the absolute value of the g_{CD} is relatively small compared to other **PSis** (Fig. 2.8), it indicates (1) structures that show positive bisigned Cotton effect and negative bisigned Cotton effect are mixed, leading to a cancelling their Cotton effects each other or (2) the optical activity of the structure is weak in this system.

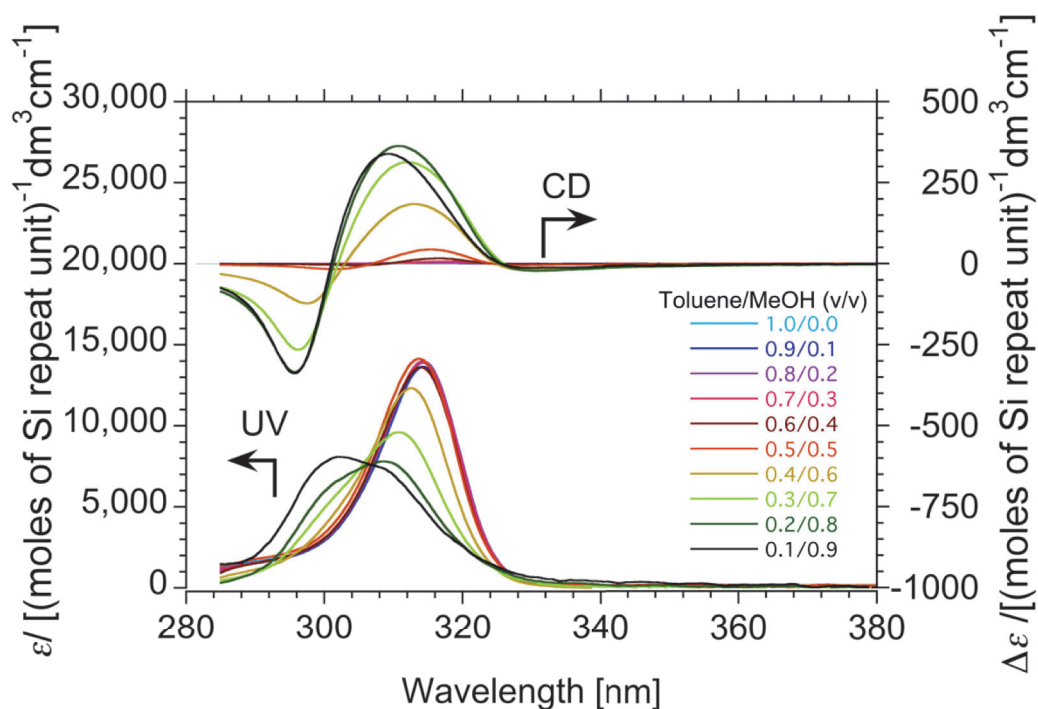


Figure 2.3. CD spectra of **PSi1** in various toluene/methanol cosolvents. The sample concentration is 1.0×10^{-4} M, $M_n = 3.77 \times 10^3$, and PDI = 1.22.

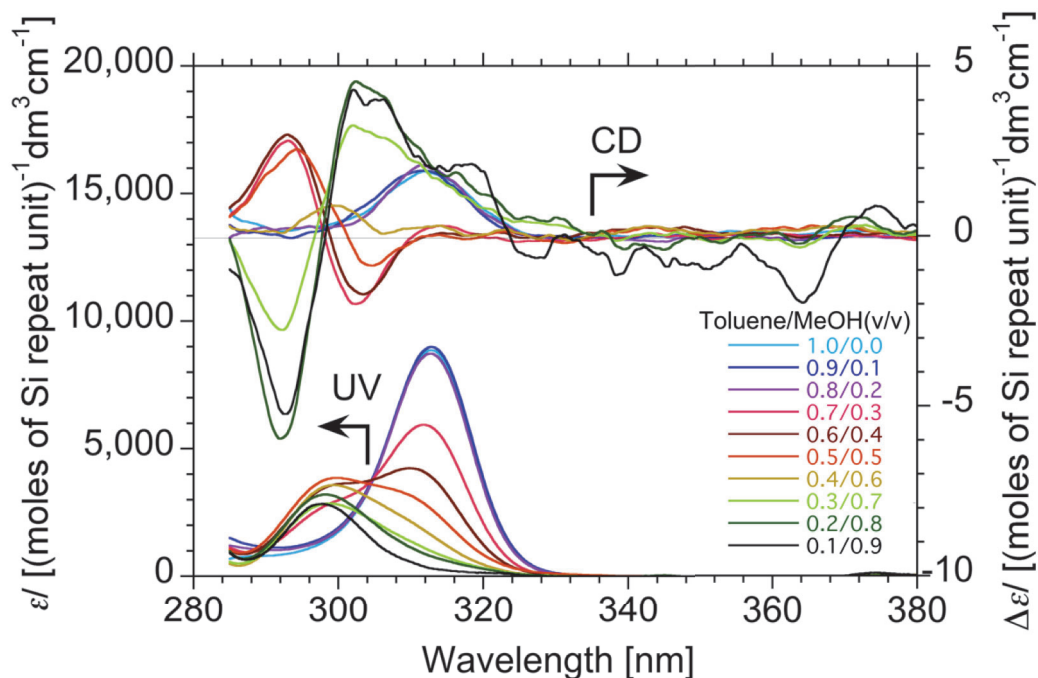


Figure 2.4. CD spectra of **PSi2** in various toluene/methanol cosolvents. The sample concentration is 1.4×10^{-4} M, $M_n = 3.76 \times 10^3$, and PDI = 1.17.

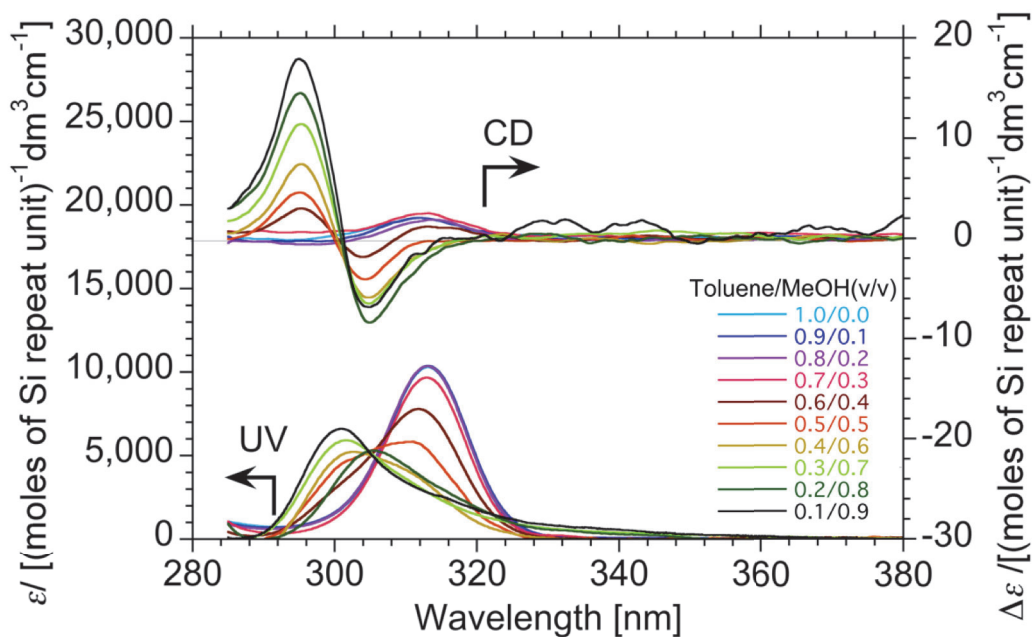


Figure 2.5. CD spectra of **PSi3** in various toluene/methanol cosolvents. The sample concentration is 1.4×10^{-4} M, $M_n = 3.25 \times 10^3$, and PDI = 1.11.

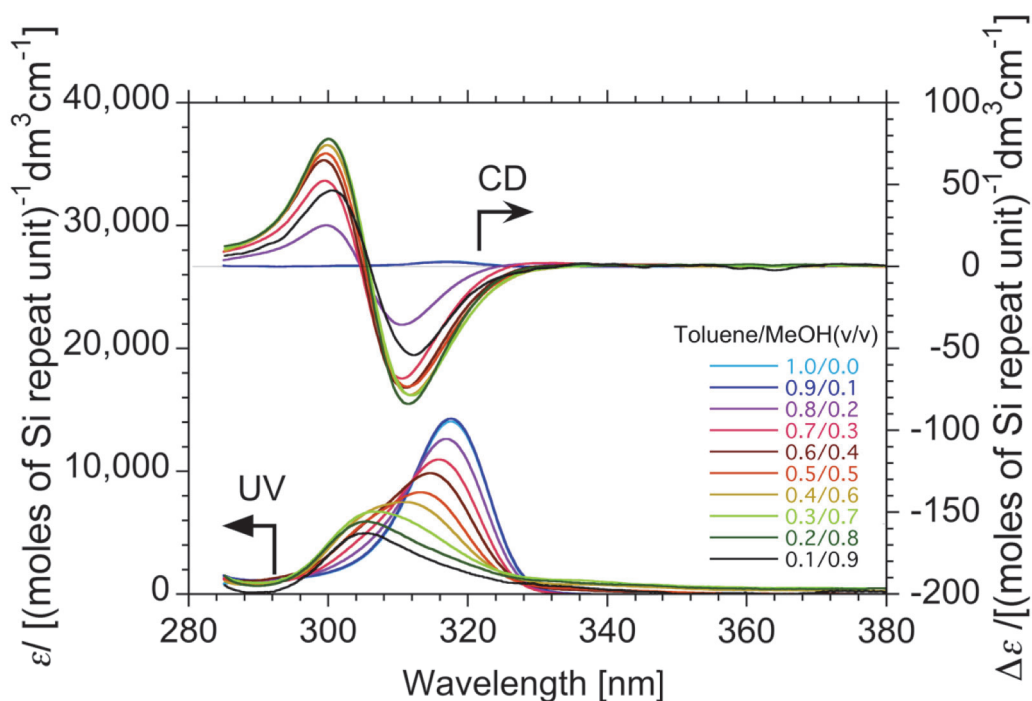


Figure 2.6. CD spectra of **PSi4** in various toluene/methanol cosolvents. The sample concentration is 7.1×10^{-5} M, $M_n = 2.52 \times 10^3$, and PDI = 1.12.

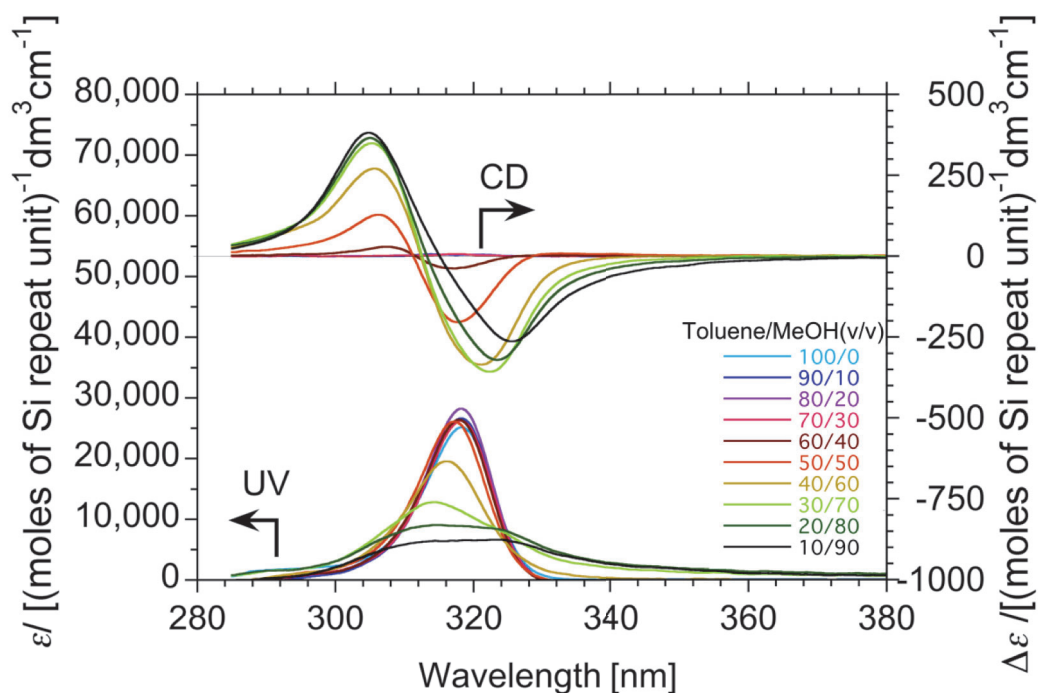


Figure 2.7. CD spectra of **PSi5** in various toluene/methanol cosolvents. The sample concentration is 1.0×10^{-4} M, $M_n = 6.14 \times 10^3$, and PDI = 1.60.

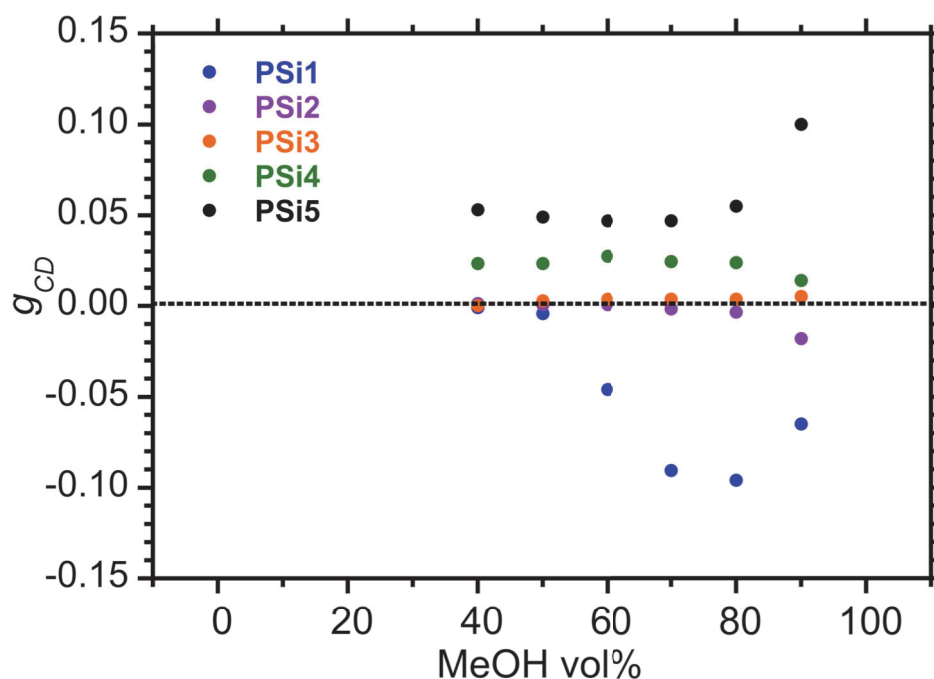


Figure 2.8. Kuhn's dissymmetry factors (g_{CD}) of the bisigned Cotton effect at longer wavelength region for each dialkylpolysilane in toluene/methanol cosolvent. Only methanol fractions above 40% are shown because bisigned CD was observed for all samples at this fraction.

Table 2.2. Summary of the signs of the Cotton effect in solution and aggregate states.

Polysilane	Sign of the Cotton effect	
	Solution (Toluene)	Aggregate (Toluene/Methanol)
PSi1	(+)-single sign	(+)-bisign
PSi2	(+)-single sign	(-)/(+)-bisign ^a
PSi3	(+)-single sign	(-)-bisign
PSi4	(+)-single sign	(-)-bisign
PSi5	(+)-single sign	(-)-bisign

^aThe aggregates showed (-)-bisigned Cotton effect when dispersed in toluene/methanol cosolvent with relatively high amount of good solvent (toluene) but showed (+)-bisigned Cotton effect in that with relatively high amount of poor solvent (methanol).

2.3.3. Membrane Filter Experiment of Aggregates

To test the origin of the bisigned CD and the peak shift at ~ 300 nm, the aggregates of **PSi3** (toluene/methanol = 0.5/0.5 (v/v)) were formed and filtered by polyvinylidene fluoride (PVDF) membrane filters (Fig. 2.9). The CD spectra of the filtrates were measured after the removal of the aggregates. Filters with 5.0, 0.65, 0.22, 0.10 μm pore size were used and one-time filtration with each pore size was applied to individual fresh sample. Sequential filtration of one sample was not operated because this procedure cannot distinguish whether the aggregates are selectively filtered or just adsorbed on the filter.

UV peak at ~ 300 nm was observed when the pore size is more than 0.22 μm but became unobservable when filtered with less or equal to 0.22 μm pore size. The bisigned Cotton effect disappeared by the filtration as well. This indicates that the peak at ~ 300 nm originate from aggregates and not from solution state. Therefore, the UV peak shift is not induced by conformational change of polymer in solution but by aggregation. Thus, the author concluded that the chiroptical anomaly of **PSi3** aggregates should be termed *aggregachromism* rather than *solvatochromism*.

Not only peak at 300 nm, but also peak at 312 nm was reduced almost by half when pore size is changed from 0.65 μm to 0.22 μm . This could be indicating that some polymers are weakly entangled in the region surrounding the particles and showing the peak at 312 nm that is identical to the peak in solution state.

The blue-shift in the UV spectra could be arose due to two factors: a decrease in the Si–Si–Si–Si dihedral angle^{3,5-7} and/or J- and H-aggregation, as proposed by Kasha.^{8,9} First, if the Si–Si–Si–Si dihedral angle diminishes from $\theta = 154^\circ$ ($P-7_3$ helix), it reduces the degree of σ -conjugation in the Si main chain, which thus induces the blue-shift. Placing the polymer in a poor solvent could decrease the dihedral angle, because the polymer should prefer a shorter pitch form ($\theta < 154^\circ$) rather than the more extended form ($\theta = 154^\circ$), thus reducing the surface area between solute and poor solvent. Second, the blue-shift could also be induced by the parallel orientation of transition dipole moments in the aggregate state, known as H-aggregation in the molecular exciton theory proposed by Kasha (Figure 2.10.a).^{8,9} In this theory, two different possible arrangements of two transition dipoles were proposed, one with a parallel arrangement (H-aggregate) that induces a blue-shift (Figure 2.10.a) and the other with a collinear arrangement (J-aggregate) giving rise to a red-shift (Figure 2.10.b). Since J-aggregates are less likely to be formed than H-aggregates when considering the solvophobic effect (see Section 3.2.3), the blue-shift of λ_{max} in H-aggregate is possible.

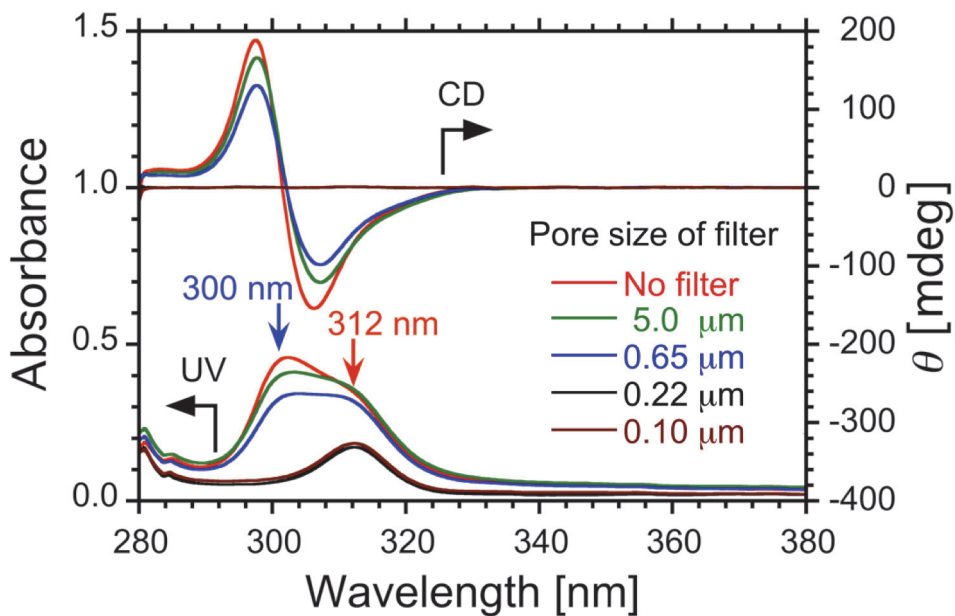


Figure 2.9. CD/UV spectra of **PSi3** in a toluene/methanol cosolvent (ratio = 0.5/0.5 (v/v)) filtered through various pore size of polyvinylidene fluoride (PVDF) membrane filters.

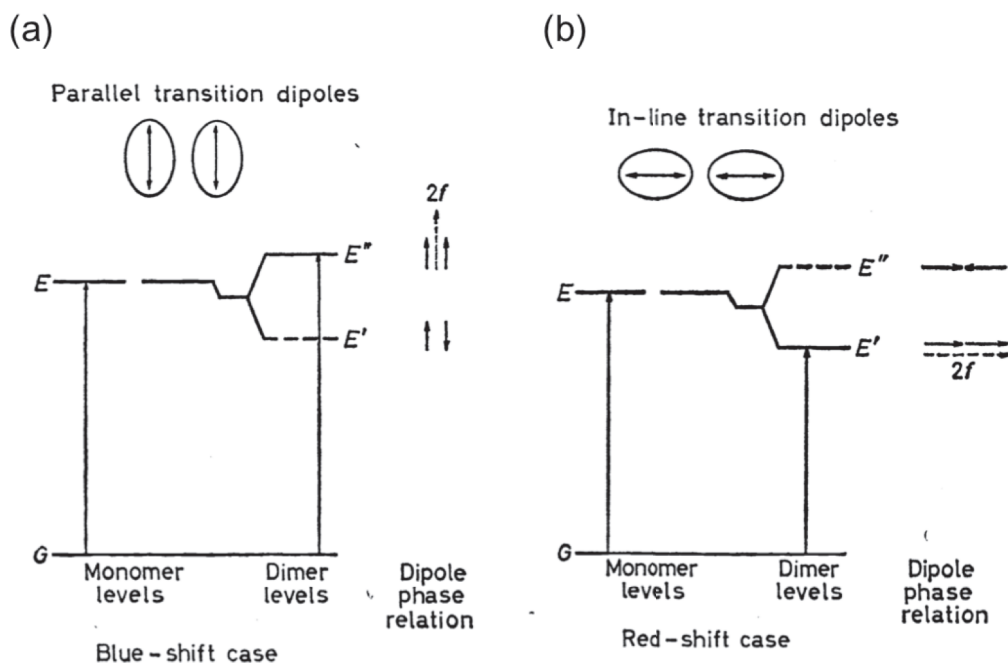


Figure 2.10. Exciton band energy diagram for a molecular dimer, or a double molecule. (a) With parallel transition dipoles. (b) With in-line transition dipoles. Reprinted from Pure and Applied Chemistry, Vol. 11, M. Kasha, H. R. Rawls, Ashraf El-Bayoumi, M. "The exciton model in molecular spectroscopy", pp. 371-392, 1965.

2.3.4. Molecular Weight Dependency of UV/CD Spectra

Interestingly, the CD spectrum with relatively higher molecular weight showed different CD profile from that with lower molecular weight. The CD spectra did not show bisigned but showed trisigned CD (Figure 2.11, Figure 2.12). The sign of the first Cotton band of high molecular weight was the opposite sign of low molecular weight sample. For example, **PSi1** with low molecular weight showed positive bisigned Cotton effect (indicating plus sign at long wavelength and minus sign at shorter wavelength) (Fig. 2.3) but high molecular weight sample showed minus trisigned Cotton effect (indicating minus sign at long wavelength, plus sign at the middle wavelength and minus sign at shorter wavelength) (Figure 2.11). The sign of the **PSi5** was opposite to that of **PSi1**.

Such change in CD shape could be understood by applying Frenkel exciton model to helical cylindrical aggregates.¹⁰⁻¹⁵ The assumed model and resulting CD and UV spectra are shown in Appendix Figure A.2.1 and A.2.2. However, this work lacks (i) experimental data to confirm the structure of the aggregate (the Frenkel exciton model assume cylinder aggregate) (ii) justification to see a single stranded conjugated polymer as J-aggregate, though their similarity is pointed out¹⁶.

W. Peng¹⁷ reports chiroptical inversion of **Poly-B2** in tetrahydrofuran(THF)/methanol cosolvent. However, the aggregates showed positive *bisigned* CD when the amount of THF is relatively high and changed to negative *trisigned* CD when the methanol ratio is high (See Fig. A.2.3.a). Thus this appearing inversion could be arisen from mixed property of high molecular weight and low molecular weight fraction described above. Actually, the PDI was 2.36 and broad spectrum of molecular weight sample could be mixed in this system. The M_n was 2.49×10^6 and the value is far above the M_n of high molecular weight **PSi5** (Figure 2.12) so it is not surprising to show trisigned CD. Therefore, it could be important to distinguish high molecular weight from low molecular weight to see the chiroptical inversion that is caused by the reorientation of higher order

structure. Yet in other words, mixing of two different molecular weight fractions could induce the chiroptical inversion.

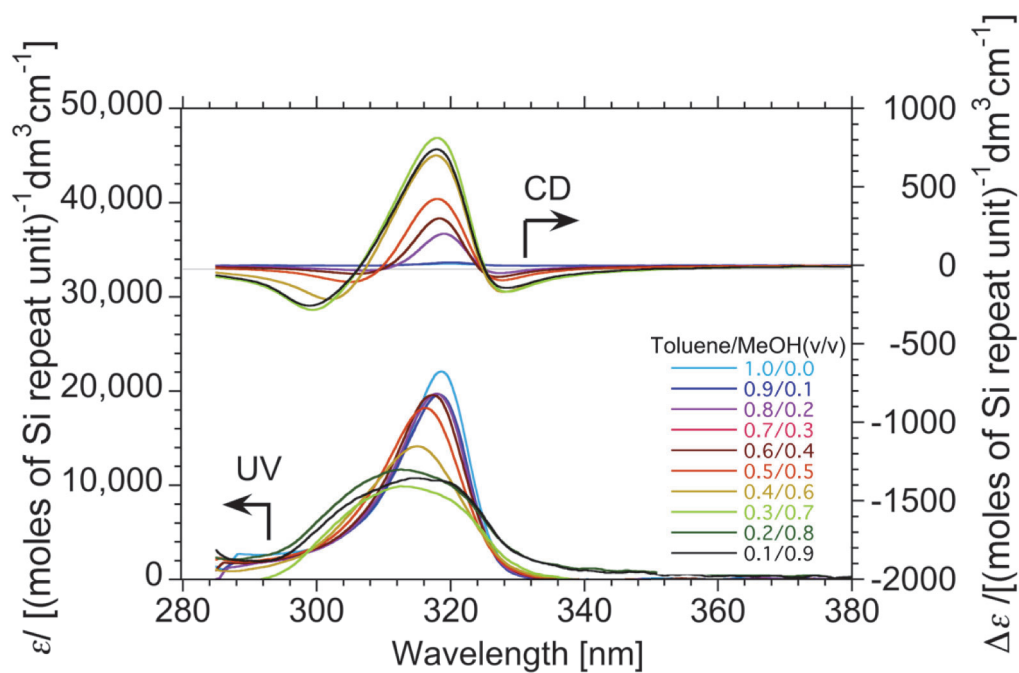


Figure 2.11. CD spectra of **PSi1** in various toluene/methanol cosolvent. **PSi1**: $M_n = 7.04 \times 10^3$, PDI = 1.90.

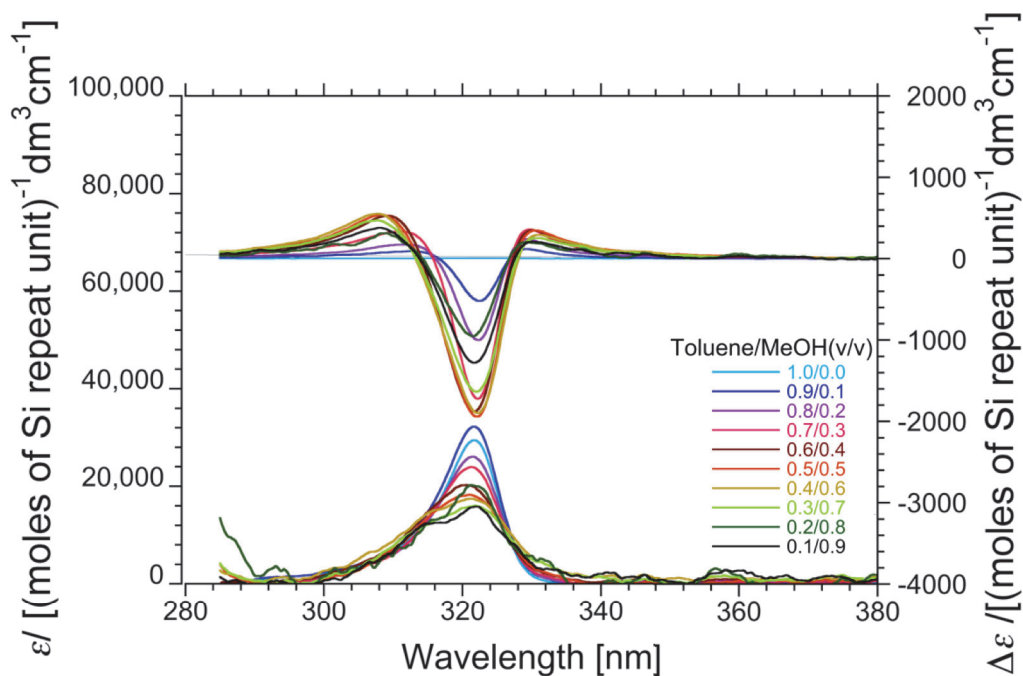


Figure 2.12. CD spectra of **PSi5** in various toluene/methanol cosolvent. **PSi5**: $M_n = 2.62 \times 10^4$, PDI = 5.93.

2.4. TEM Image of the Polymers

To determine the diameter of the polymers, observation of transmission electron microscope (TEM) images was attempted. **PSi1** and **PSi5** were dissolved in toluene with concentration 10^{-2} M casted on copper grid. Vapor annealing at room temperature was followed using chloroform as the solvent. The resulting film was heated at 140 °C for more than 5 minutes. Figure 2.13 and 2.14 represents the TEM image of **PSi1** and **PSi5**, respectively. Fiber-like aggregates were observed for both polymers but with different shape. For **PSi1**, aligned globular aggregates were observed. The diameter of one stranded polymer was not clear for this system. For **PSi5**, ordered structure was observed as black line (Figure 2.14.b). The M_n was 2.62×10^4 [g/mol] and it corresponds to 252 [(Number of polystyrene repeat unit)/mol]. Thus the length of the polymer was estimated to be ~ 50 nm assuming the polymer is rigid and forming 7_3 -helix. For the projection to the longitudinal axis of Si-Si bond length, 1.96 Å was used. Because the diameter of one stranded helix is expected to be around several nm, the black line in Figure 2.13(b) is thus too long to see as one stranded polymer. Therefore, aligned structure of polymers was assumed. Such alignment has also been observed for poly[*n*-decyl-2-methylpropylsilane].¹⁸ The helix sense and diameter of individual polymer as well as chirality of the aggregate were not observed from the TEM.

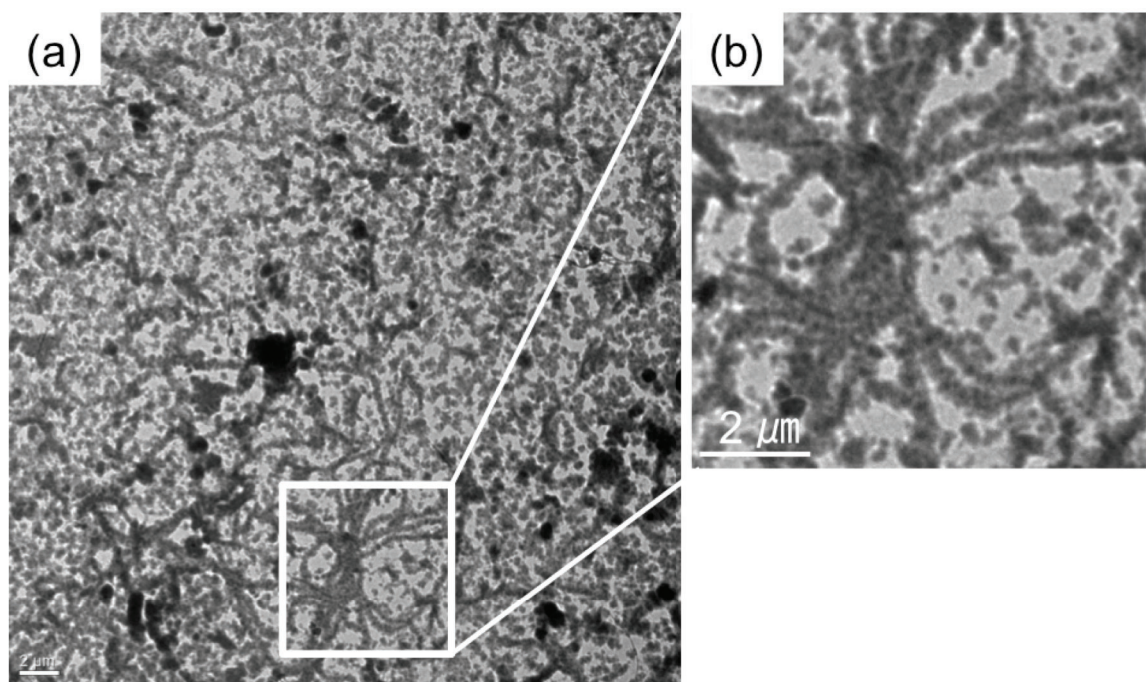


Figure 2.13. TEM image of **PSi1** ($M_n = 7.04 \times 10^3$, PDI = 1.90) casted on copper grid without any staining. (a) TEM image of **PSi1**. (b) Enlarged image.

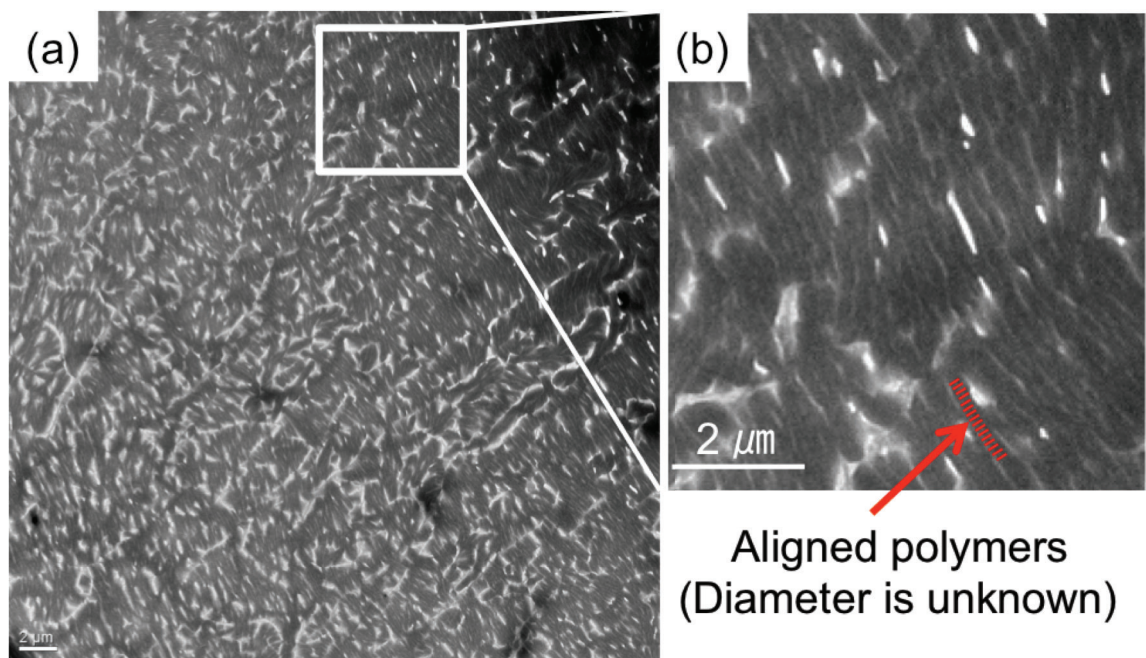


Figure 2.14. TEM image of **PSi5** ($M_n = 7.04 \times 10^3$, PDI = 1.90) casted on copper grid without any staining. (a) TEM image of **PSi5**. (b) Enlarged image.

2.5. References

- (1) Fujiki, M. *Appl. Phys. Lett.* **1994**, *65*, 3251.
- (2) Okoshi, K.; Kamee, H.; Suzaki, G.; Tokita, M.; Fujiki, M.; Watanabe, J. *Macromolecules* **2002**, *35*, 4556.
- (3) Fujiki, M. *Symmetry* **2010**, *2*, 1625.
- (4) Fujiki, M., (Kanagawa-ken, Japan). Organosilicon compounds. US Patent 5710301, Jan 20, 1998.
- (5) Tsuji, H.; Fukazawa, A.; Yamaguchi, S.; Toshimitsu, A.; Tamao, K. *Organometallics* **2004**, *23*, 3375.
- (6) Tsuji, H.; Terada, M.; Toshimitsu, A.; Tamao, K. *J. Am. Chem. Soc.* **2003**, *125*, 7486.
- (7) Tsuji, H.; Michl, J.; Tamao, K. *J. Organomet. Chem.* **2003**, 685, 9.
- (8) Kasha, M. *Radiat. Res.* **1963**, *20*, 55.
- (9) Kasha, M.; Rawls, H. R.; Ashraf El-Bayoumi, M. *Pure Appl. Chem.* **1965**, *11*, 371.
- (10) Bednarz, M.; Knoester, J. *J. Phys. Chem. B* **2001**, *105*, 12913.
- (11) Didraga, C.; Klugkist, J. A.; Knoester, J. *J. Phys. Chem. B* **2002**, *106*, 11474.
- (12) Lampoura, S. S.; Spitz, C.; Dähne, S.; Knoester, J.; Duppen, K. *J. Phys. Chem. B* **2002**, *106*, 3103.
- (13) Spitz, C.; Knoester, J.; Ouart, A.; Daehne, S. *Chem. Phys.* **2002**, *275*, 271.
- (14) Didraga, C.; Knoester, J. *J. Lumin.* **2003**, *102-103*, 60.
- (15) Didraga, C.; Knoester, J. *J. Lumin.* **2004**, *110*, 239.
- (16) Yamagata, H.; Spano, F. C. *J. Phys. Chem. Lett.* **2014**, *5*, 622.
- (17) Peng, W.; Motonaga, M.; Koe, J. R. *J. Am. Chem. Soc.* **2004**, *126*, 13822.
- (18) Okoshi, K.; Watanabe, J. *Macromolecules* **2010**, *43*, 5177.

Chapter 3. Theoretical Approach: Higher Order Structure and Chiroptical Activity

3.1. Introduction

To explain these unusual chiroptical inversion phenomena discussed in previous chapter, we constructed a new theoretical model by combining the cholesteric hard-core model of Straley¹⁻⁴ (see Section 3.2) and the exciton chirality method developed by Nakanishi (see Section 3.3).⁵⁻⁸ The former refers to a correlation between the chirality of individual helical polymer and the chirality of the most favorable higher order skew, based on the two helical variables, pitch (p) and diameter of the helix (D). On the other hand, the exciton chirality method predicts the sign of a CD spectrum due to exciton coupling between two interacting chiral chromophores in the photoexcited states. Those two methods were combined in Section 3.4 and applied to the dialkylpolysilane system in Section 3.5.

3.2. Cholesteric Hard-Core Model

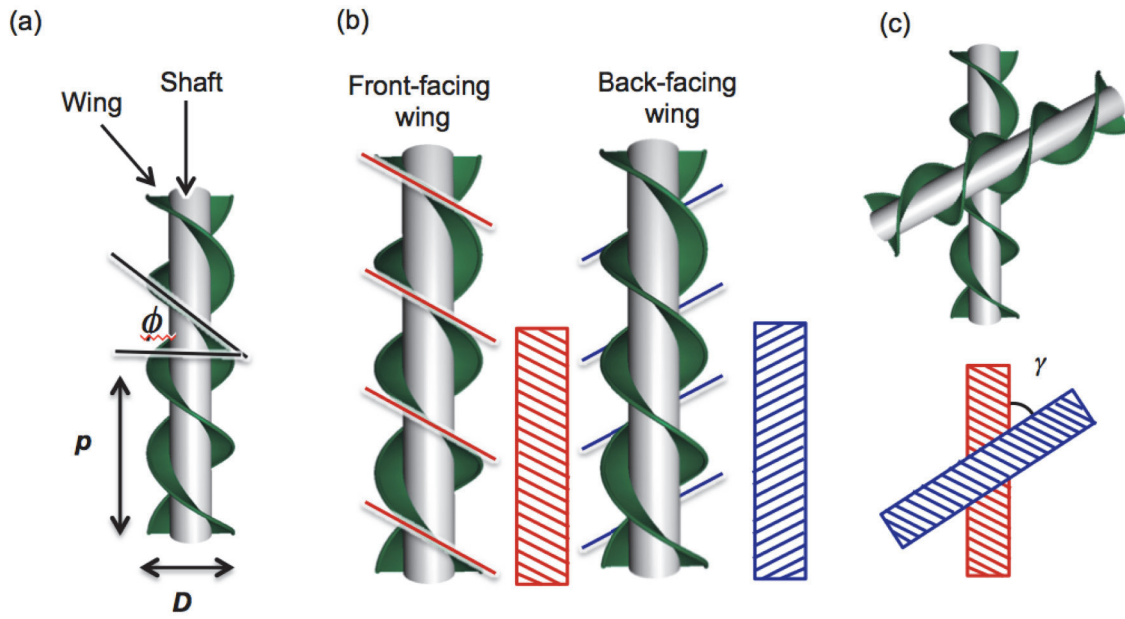
3.2.1. Qualitative Description of Cholesteric Hard-Core Model

According to the cholesteric hard-core model⁴, an individual helical polymer is characterized by the helical angle Φ defined by p and D (Figure 3.1.a). The value of p is defined as the minimum longitudinal distance between the start and end points of one full helical turn, and D is the diameter of the helix. The chiral skew of the higher order chiral structure is governed by the p/D ratio of the helix: for $p/D < \pi$ ($45^\circ > \Phi > 0^\circ$), a left-handed helix forms a left-handed skewed structure, while for $p/D > \pi$ ($90^\circ > \Phi > 45^\circ$), a left-handed helix leads to a right-handed skew, and vice versa.⁴

To explain how the structural inversion happens, the left-handed structure is depicted in Figure 3.1.a along with the definition of “wing” and “shaft”. Individual helix is represented as a simple two-dimensional (2D) model based on the cholesteric hard-core theory in Figure 3.1.b. The front-facing wings are represented by diagonal lines from the upper left to the lower right, while the back-facing wings of the helix are represented by diagonal lines from upper right to lower left. When one helical polymer is put in contact with another, i.e., one on top of the other with collinear transverse axes, the contacting surfaces exhibit a chiral skew with angle γ ($=2\Phi$), so that the front-facing wings of the helix in the back and back-facing wings of helix in front become parallel, with the wings aligning with the helical grooves. The p/D represents the slope of the slanted line: when the p/D value is high, the absolute value of the slope is large, and when the p/D value is low, the absolute value of the slope value becomes small.

The direction of higher order skew (looking from front helix to the back in Figure 3.1.d) inverts from left ($\gamma < 90^\circ$) to right ($\gamma > 90^\circ$) when p/D value increases from $p/D < \pi$ to $p/D > \pi$. This is because the slope of the slanted line increases as the p/D increase. The plus and minus sign in Figure 3.1.d will be explained by exciton chirality method in Section 3.3. In the next section, the

relations among p , D , Φ , and γ , are described in detail.



(d)

Side-chain Length	Long ←————→ Short						
p/D	Small ←———— π ————→ Large						
γ	0°	30°	60°	90°	120°	150°	180°
Schematic Drawing							

Figure 3.1. Helical structure and description of the cholesteric hard-core model. (a) Definition of the pitch p and diameter D . (b) Description of the front-facing and back-facing wings. (c) Assembled structure of the two helices. (d) Higher order structure dependency on p/D value.

3.2.2. Quantitative Description of Cholesteric Hard-Core Model

The explanation in the previous section sufficiently provides the key idea of the model, but it will be beneficial to quantitatively describe the relationship among p , D , Φ , for researchers to develop a more advanced and versatile model to numerical simulation. The quantitative description is simple and can be broken down into two steps including (1) correlation among p , D , and Φ , and (2) relation between Φ and γ . In the first step, when one traces the helix in Figure 3.2.b for one full turn, the traced line will form side AC of the triangle ABC. The length of the side BC corresponds to circumference of the cylindrical bottom with diameter D , thus the length is πD . Therefore, the relation between p/D and Φ can be described as follows.

$$\phi[\text{degree}] = \frac{180}{\pi} \arctan\left(\frac{p}{\pi D}\right) \quad (\text{Eq. 3.1})$$

The second step is to evaluate the relationship between Φ and γ . The triangle ABC in Figure 3.2.b is copied to the Figure 3.2.c. The angle BAC is obtained from the condition that the triangle ABC is a right triangle. The triangle ABC represents the front facing wing of the assembled helix in the back (red square with slanted line in Figure 3.2.a). Reversed congruent triangle ADC in Figure 3.2.c, which is back-facing wing of the assembled helix in the front (blue square with slanted line in Figure 3.2.a), can be put on the triangle ABC so that it shares the side AC. This condition comes from the fact that the slanted line of the red and blue square in Figure 3.2.a should be parallel to each other. By considering that the triangle AEC is an isosceles triangle and angle AEC is the angle γ , the angle γ is calculated as follows.

$$\gamma[^\circ] = 180^\circ - 2 \times (90^\circ - \phi) = 2\phi \quad (\text{Eq. 3.2})$$

From equations 1 and 2, the angle γ and p/D are deduced as follows.

$$\gamma[^\circ] = 2\phi = \frac{360}{\pi} \arctan\left(\frac{p}{\pi D}\right) \quad (\text{Eq. 3.3})$$

Figure 3.2.d pictorially describes the relation between the p/D and γ . By taking it into

account that the inversion of the assembled structure occurs at $\gamma = 90^\circ$, one can obtain the conditions of p/D and critical parameter π to invert the CD sign.

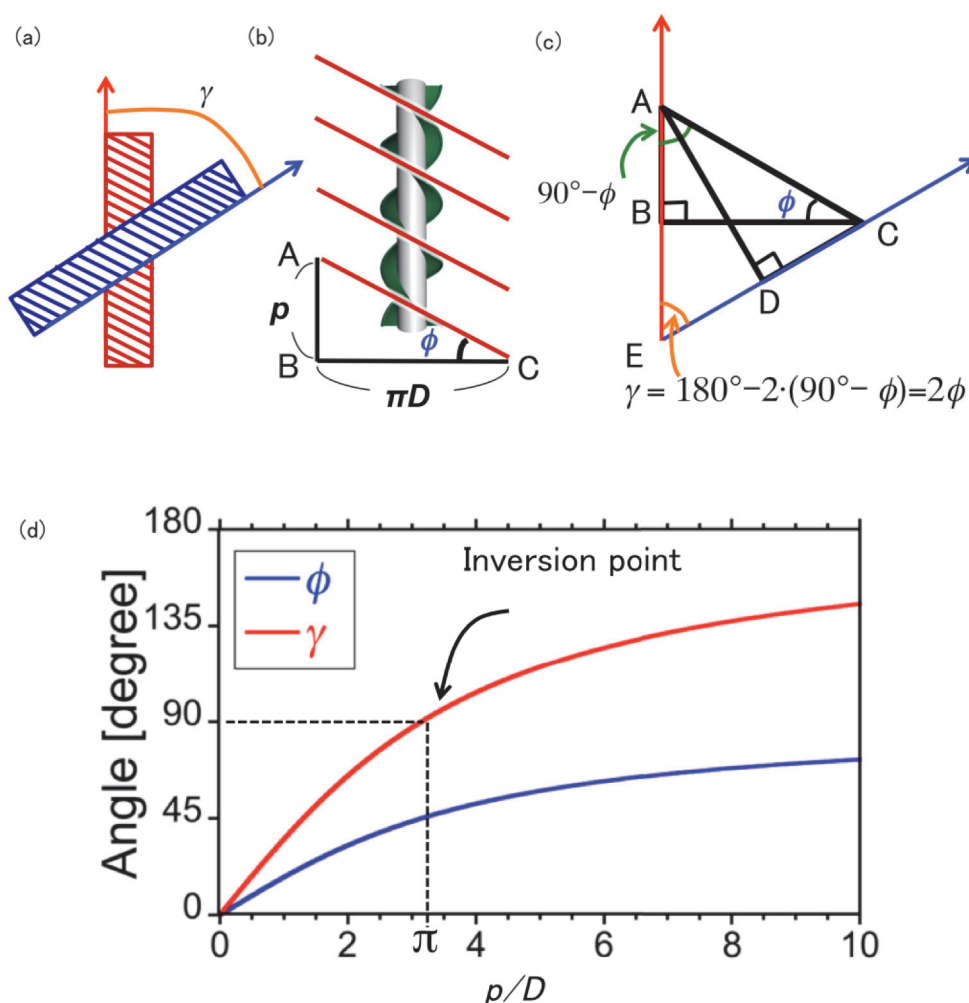


Figure 3.2. Geometrical figure showing the relationship among each parameters p , D , Φ , and γ . (a) Assembled helical structure. (b) The relationship among p , D , and Φ . (c) The relationship between Φ and γ . (d) A graph to show the relationship among p/D , Φ , and γ .

3.2.3. Consideration of Solvophobic Effects and Number of Molecules

The cholesteric hard-core model fully explains how the structural switching in the higher order structure could occur by considering the chiral steric hindrance (repulsive force) with simple assumption. However, the model does not include (i) solvophobic effects, and (ii) aggregates of more than two molecules. When two rod-like polymer molecules aggregate by the solvophobic

effect, the polymer prefers to form a parallel arrangement to minimize the surface in contact with the poor solvent rather than taking T-shaped aggregate or I-shaped aggregate (Figure 3.3). The author assumes aggregates form twisted pasta-like structure based on three key ideas: (i) the cholesteric hard-core model, (ii) solvent effect, and (iii) helices consisting of more than two molecules.

When $p/D = \pi$, the cholesteric hard-core model assumes that the higher order structure forms the crossed structure (angle $\gamma = 90^\circ$). However, this extreme case is unlikely to occur because the system prefers to minimize a contact surface with solvents, as discussed above. Thus, the main chains will form a parallel arrangement rather than crossed arrangement, enabling to reduce the surface area. As observed in Section 2.3.2, **PSi2** showed chiroptical inversion depending on the solvent ratio and the absolute value of the g_{CD} was small compared to the others (Figure 2.8). Two possibilities were suggested: (1) structures that show positive bisigned Cotton effect and negative bisigned Cotton effect are mixed or (2) the optical activity of the structure is weak in this system. The crossed arrangement that shows weak CD signal corresponds to the case (2), and it is unstable from the discussion above. Thus it is expected that the aggregates have the same possibility to form a left- or right-handed helically assembled motif that corresponds to the case (1).

Consideration of solvophobic effects and number of molecules could account for the discrepancy between experimental results and model predictions, and justify seeing real aggregates as an extension of the two-component aggregate. Increasing number of the components in the aggregate is directly connected to the volume fraction of poor solvent in the system. When the ratio of good solvent (toluene in the experiment described in Section 2.3.2) is relatively large, a relatively small number of the polymers would assemble as aggregate with a smaller size. Therefore, regardless of the toluene/methanol cosolvent ratio in **PSi1** and **PSi3–5** (Figure 2.3, 2.5–2.7), the maintenance of the bisignate Cotton CD band characteristics strongly supports the validity that the

dimer model proposed by the author in this thesis is extendable to several dialkylpolysilane aggregates.

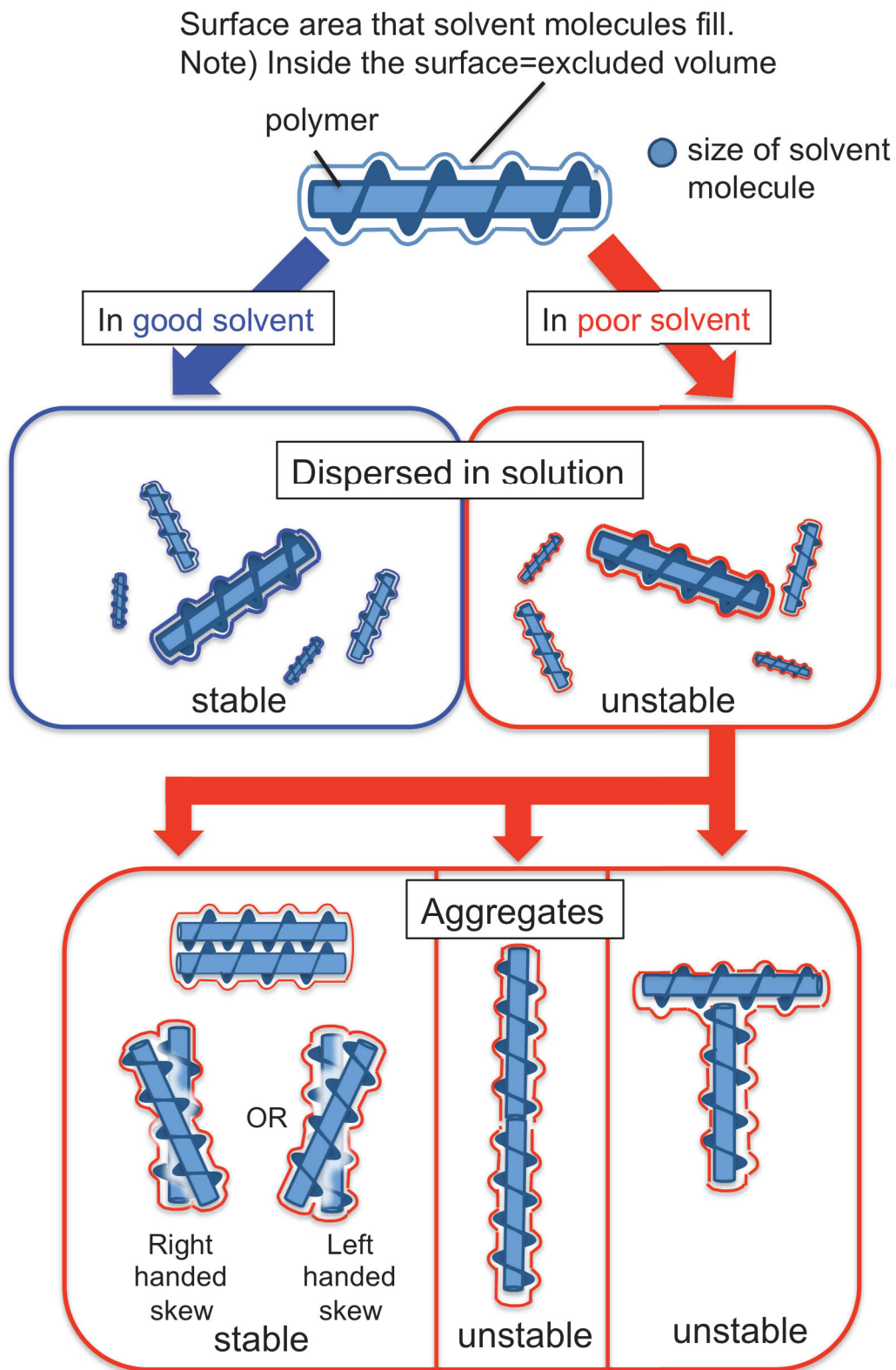


Figure 3.3. Schematic drawing of the solvent effect and aggregation.

3.3. Exciton Chirality Method

The exciton chirality method allows to semiempirically predict the signs of the split-type Cotton effect if the relative geometry of the two interacting electric transition dipole moments (hereafter, called transition dipole moment) is determined (Figure 3.4). The sign of the exciton chirality is derived as follows: *upon looking through the centers of the two dipoles, a negative sign is defined when an anticlockwise rotation by an acute angle brings the dipole in the front onto that in the back.*⁸ Since the magnitude of the aggregate transition dipole–transition dipole coupling is usually much greater than the inherent CD signal of an individual helical polymer molecule, the exciton couplet is assumed to dominate the CD of the higher order chiral structure. For dialkylpolysilanes, the $\text{Si}\sigma\text{--Si}\sigma^*$ transition moment at longest wavelength is known to be parallel to the main chain axis experimentally and theoretically (Figure 3.4.b).¹⁰

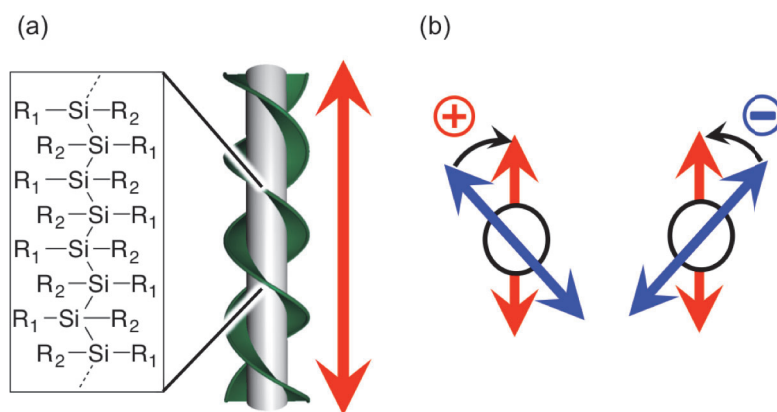


Figure 3.4. Application of exciton chirality method to dialkylpolysilane system. (a) Definition of each vector to describe exciton chirality method. Electric transition dipole moment of chromophore 1, that of chromophore 2, and (b) The direction of the electric transition dipole moment for dialkylsilane. (c) Schematic drawing of the exciton chirality method. Plus indicates positive bisigned CD (positive at longer wavelength and negative at shorter wavelength) and minus indicates negative bisigned CD.

The sign can be determined based on above description and it is based on the equation as follows.

$$\vec{\mu}_1 = \mu_1 \vec{e}_1 \quad (\text{Eq. 3.5})$$

$$\vec{\mu}_2 = \mu_2 \vec{e}_2 \quad (\text{Eq. 3.6})$$

$$\vec{r}_{12} = r \vec{e}_{12} \quad (\text{Eq. 3.7})$$

$$V_{12} = \frac{\mu_1 \mu_2}{r_{12}^3} [\vec{e}_1 \cdot \vec{e}_2 - 3(\vec{e}_1 \cdot \vec{e}_{12})(\vec{e}_2 \cdot \vec{e}_{12})] \quad (\text{Eq. 3.8})$$

$$\Delta\varepsilon(\lambda) \propto \pm \Gamma(\lambda, \lambda_0) V_{12} \vec{r}_{12} \cdot \vec{\mu}_1 \times \vec{\mu}_2 = \pm \Gamma(\lambda, \lambda_0) \frac{\mu_1^2 \mu_2^2}{r_{12}^2} [\vec{e}_1 \cdot \vec{e}_2 - 3(\vec{e}_1 \cdot \vec{e}_{12})(\vec{e}_2 \cdot \vec{e}_{12})] [\vec{e}_{12} \cdot \vec{e}_1 \times \vec{e}_2] \quad (\text{Eq. 3.8})$$

Where $\vec{\mu}_1$, $\vec{\mu}_2$, and \vec{r}_{12} are transition dipole moment of chromophore 1, that of chromophore 2, and mutual distance between the two transition dipole moment, respectively. The orientation of each vector is described in Figure 3.5.b. \vec{e}_1 , \vec{e}_2 , and \vec{e}_{12} are the unit vector of each vector of $\vec{\mu}_1$, $\vec{\mu}_2$, and \vec{r}_{12} , respectively. $2V_{12}$ is called Davydov splitting and it is the energy difference between the two coupled excited states (Figure 3.5.a) and thus can be correlated to the split in the CD and UV spectra (Figure 3.5.c, 3.5.d). $\Delta\varepsilon$ value represents the Cotton effect. $\Gamma(\lambda, \lambda_0)$ accounts for the couplet shape, typically, Gaussian distribution is assumed.⁶

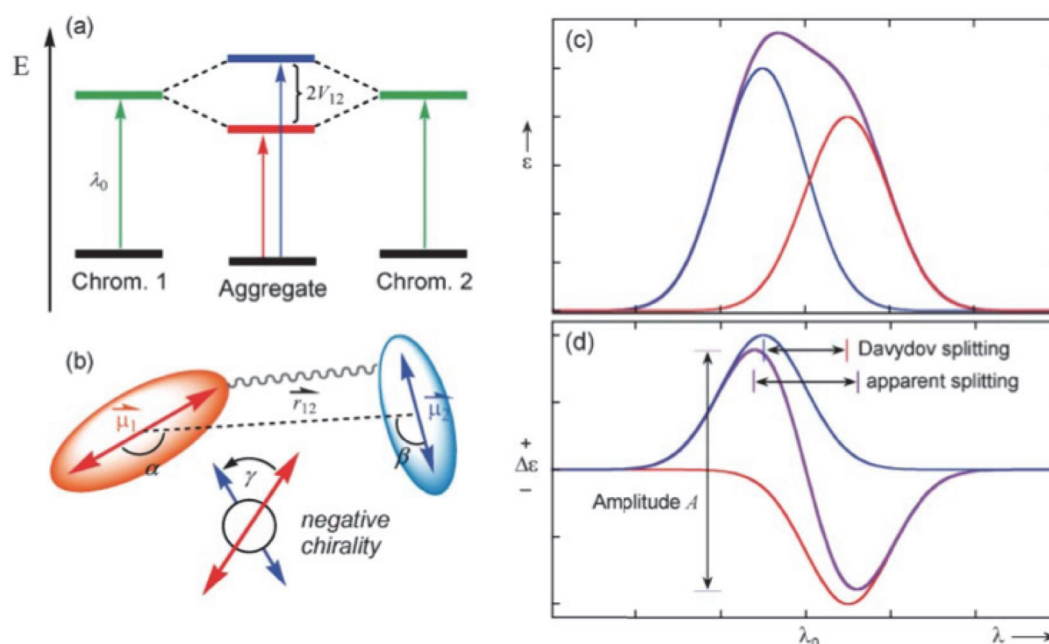


Figure 3.5. Description of the exciton chirality method. (a) Splitting of the excited states of two degenerate exciton-coupled chromophores linked by a chiral spacer. (b) Definition of geometrical parameters necessary for predicting CD sign and intensity through eq.. Expected absorption (c) and CD spectra (d) in case of exciton splitting as shown in (a): component spectra thin lines in blue/red, resultant spectra thick lines in violet. The distance between the peak and the trough of the split CD curve is called an amplitude or A . Reprinted from *Chemical Society Reviews*, Vol. 36, N. Berova, L. D. Bari, G. Pescitelli " Application of electronic circular dichroism in configurational and conformational analysis of organic compounds", pp. 914-931, Copyright (2003), with permission from Royal Society of Chemistry.

3.4. Combination of Cholesteric Hard-Core Model and Exciton Chirality Method

If one assumes that (i) two helices are assembled, and (ii) each helix has left-handed structure, the resulting structure and the corresponding bisigned Cotton effect can be illustrated as Figure 3.1.d.

Assuming that the helical pitch (p) is constant, the combination of the cholesteric hard-core model and exciton chirality method predict that interaction between left-handed helices with a sufficiently large D (i.e. $p/D < \pi$) leads to a negative bisigned CD profile. This is represented as minus sign in Figure 3.1.d for the case $\gamma = 30^\circ$ and 60° . Conversely, interaction of left-handed helices with a sufficiently small D (i.e. $p/D > \pi$) should result in a positive bisigned CD profile. This is represented as positive sign in Figure 3.1.d for the case $\gamma = 120^\circ$ and 150° .

3.5. Applying the Combined Model to Dialkylpolysilane System

3.5.1. Obtaining p and D values from PM3 model

To apply the combined model to the rodlike helical polymers used in our experiment, it is required to know the handedness of the individual chains. P - and M -helical senses in dialkylpolysilanes are defined solely by the Si–Si–Si–Si dihedral angle θ : a P - helix results for $0^\circ < \theta < 180^\circ$ and an M -helix results for $180^\circ < \theta < 360^\circ$.¹¹ However, this does not simply mean that the P - and M - helical senses appear as right- and left-handed helices, respectively. Actually, a P - 7_3 helix ($\theta \approx 155^\circ$) is predicted by Gaussian 03 calculations to form a left-handed helix.¹² To obtain the p and D values for **PSi1–5**, 12-mer oligomers were generated by setting the side chain to all-trans conformation and Si-Si-Si-Si and Si-Si-Si-H dihedral angles to 155° followed by optimization at semi-empirical parametric method 3 (PM3).¹³ The p/D ratios were calculated and summarized in Table 3.1 with the experimental result obtained from previous section (Table 2.2 in Section 2.3.2).

Table 3.1. Summary of the sign of Cotton effect in experiment and p , D and p/D values derived from PM3 model.

Polysilane	Sign of the Cotton effect		Helix parameters								
	Solution	Aggregate	PM3 ^a			MMFF ^b (CONFLEX)			WAXD (Extrapolated) ^c		
	(Toluene)	(Toluene/Methanol)	$p[\text{Å}]$	$D[\text{Å}]$	p/D	$p[\text{Å}]$	$D[\text{Å}]$	p/D	$p[\text{Å}]^d$	$D[\text{Å}]^e$	p/D
PSi1	(+)-single sign	(+)-bisign	28.3	14.4	2.0	28.6	9.3	3.1	27.4	8.3	3.3
PSi2	(+)-single sign	(-) and (+)-bisign [†]	28.5	14.4	2.0	28.3	9.2	3.1	27.4	8.6	3.2
PSi3	(+)-single sign	(-)-bisign	28.3	14.8	1.9	28.8	11.3	2.5	27.4	8.8	3.1
PSi4	(+)-single sign	(-)-bisign	28.6	16.8	1.7	28.8	13.3	2.2	27.4	9.1	3.0
PSi5	(+)-single sign	(-)-bisign	28.7	18.6	1.6	–	–	–	27.4	9.4	2.9

^aThe side chain conformation was set to all-trans and Si-Si-Si-Si and H-Si-Si-Si dihedral of the initial structure structure was set to 155°.

^bGeometry based on the most stable conformation found by CONFLEX search utilizing MMFF94S force field that was developed in Chapter 5 (See Section 5.5.1)

^cValues estimated by extrapolation from wide angle X-ray diffraction of poly[*n*-alkyl-(*S*)-2-methylbutylsilane]s.

^d1.96 Å was used for the projection of Si-Si bond length to the longitudinal axis of the dialkylpolysilane with 7₃-helix.

^eDiameter of the helix extrapolated from WAXD data of poly[*n*-alkyl-(*S*)-2-methylbutylsilane]s with longer side chains. See Table 3.2 and Figure 3.6.

[†]Showed (-)-bisigned Cotton effect when dispersed in cosolvent with relatively high amount of good solvent (toluene) but showed (+)-bisigned Cotton effect in that with relatively high amount of poor solvent (methanol).

3.5.1. Estimation of p and D values from WAXD data

In addition to computational estimation of p and D values, those values were also estimated from experimental data. Since the direct observation of the diameters and the pitches were not possible by using TEM. Also, liquid crystal form could not be observed for **PSi1–PSi5**, so estimation of the side chain diameter and the pitch from wide angle X-ray diffraction was not carried out for these systems. However, poly[*n*-alkyl-(*S*)-2-methylbutylsilane]s with longer side chains (number of carbon atoms in *n*-alkyl side chain = 10, 11, 12, 13, 14, 15, 16, and 18) were available from previous work by Hagiwara.⁹ Those compounds form monoclinic crystal or orthorhombic crystal and the lattice constants are summarized in Table 3.2.

Poly[*n*-alkyl-(*S*)-2-methylbutylsilane]s with relatively long achiral side chain (number of carbon atoms in *n*-alkyl side chain ≤ 15) showed coiled-coil structure (Figure 3.6). To estimate the diameter, the two lattice constants were divided by two for those coiled-coil structures. The

averaged diameter is also listed in the Table 3.2 and the estimated diameter of poly[*n*-decyl-(*S*)-2-methylbutylsilane]s was 10.5 Å and this value was within the standard deviation of the height of the cross sectional image measured by atomic force microscopy (AFM) (10±2 Å).¹⁴

The estimated diameters of the poly[*n*-alkyl-(*S*)-2-methylbutylsilane]s (number of carbon atoms in *n*-alkyl side chain = 10, 11, 12, 13, 14, and 15) were extrapolated to **PSi1–PSi5** assuming primary curve in Figure 3.7. By assuming that the side chain length linearly increase accord with carbon number, the adoption of the primary curve is justified by the consistency of the physical dimension between the alkyl group side chain length and diameter.

Table 3.2. The results of wide angle X-ray diffraction (WAXD) from reference 9 and estimated diameter of each polymer.

Number of Carbon ^a	M_w	PDI	a-axis ^b	b-axis ^c	coiled-coil ^d	D_a ^e	D_b ^f	Average ^g
10	18500	1.21	17.8	24.0	TRUE	8.9	12.0	10.5 ^h
11	27300	1.21	19.1	24.1	TRUE	9.6	12.1	10.8
12	12500	1.12	20.3	24.4	TRUE	10.2	12.2	11.2
13	14400	1.23	21.3	24.2	TRUE	10.7	12.1	11.4
14	14200	1.18	22.2	24.4	TRUE	11.1	12.2	11.7
15 ⁱ	14900	1.31	24.1	23.3	TRUE	12.1	11.7	11.9
15 ⁱ	14900	1.31	9.6	23.3	FALSE	9.6	23.3	16.5
16	15400	1.30	9.9	23.8	FALSE	9.9	23.8	16.9
18	16200	1.31	12.1	26.0	FALSE	12.1	26.0	19.1

^aNumber of carbon atoms for the achiral side chain of the poly[*n*-alkyl-(*S*)-2-methylbutylsilane].

^bLattice constant along a-axis

^cLattice constant along b-axis

^dWhether the structure has coiled-coil structure or not.

^eEstimated diameter along a-axis. The value was divided by two for coiled-coil structure.

^fEstimated diameter along b-axis. The value was divided by two for coiled-coil structure.

^gAveraged value of estimated diameter of the D_a and D_b .

^hAFM measurement of single stranded structure estimates this diameter as 10±2 Å.

ⁱFor this polymer, it showed mixture of two lattices. One of which was assumed to form coiled-coil structure and another does not.

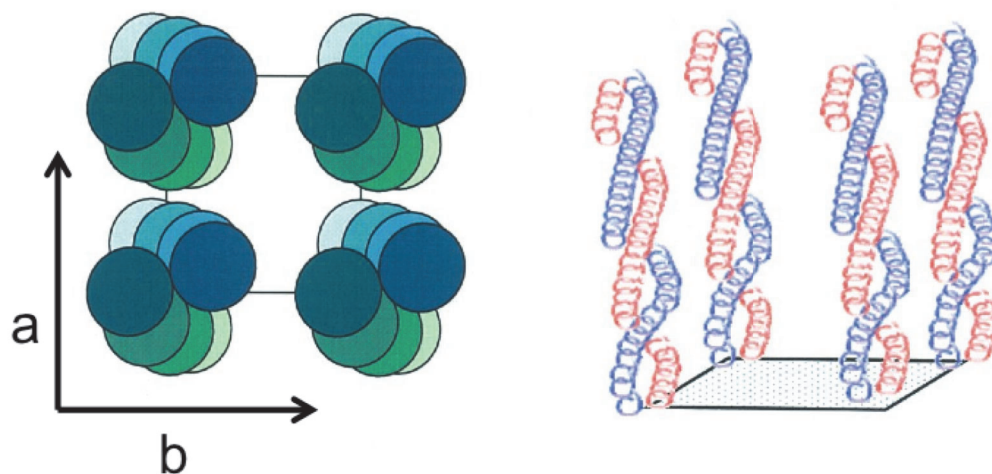


Figure 3.6. Schematic illustration of two-dimensional lattice with coiled-coil structure of poly[*n*-decyl-(*S*)-2-methylbutylsilane in columnar phase. Reprinted from reference 9.

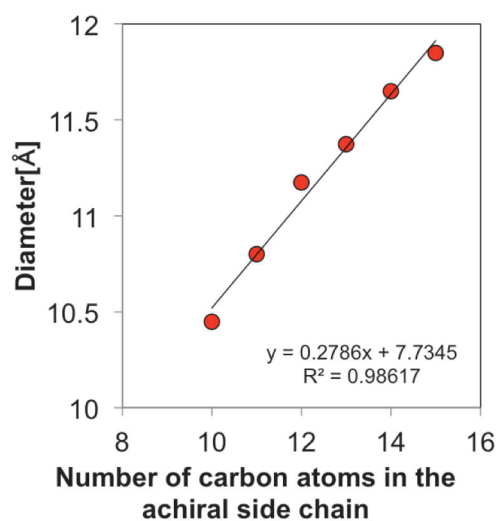


Figure 3.7. The relationship between the carbon number of the achiral side chain and the diameter estimated from WAXD.

3.5.2. Applying the Model to the Dialkylpolysilane System

For the PM3 and extrapolation of the WAXD result, the p/D values have the tendency of **PSi1** > **PSi 3** > **PSi 4** > **PSi 5**. In the cases of **PSi3–PSi5**, their side chains are sufficiently long and have a large D to induce negative bisigned Cotton effects, while for **PSi1**, with a short side chain and small D , a positive bisigned Cotton effect is evident. Thus the dependence of the sign of the Cotton effect on the p/D ratio was consistent with the experimental results.

For the critical value, there was a difference between PM3 and WAXD result. Interestingly, the p/D value of the **PSi2**, was 2.0 for the c PM3 model while experimental approach estimated this value as 3.2 that is close to π . Thus the experimental result matches with the cholesteric hard-core theory. For the PM3 model, the diameter of the **PSi2** should be 40 % smaller than the calculated value if p/D value is π . The discrepancy between the PM3 model and the cholesteric hard-core model could be arisen from (i) assumed all-trans conformation of the side chain (ii) calculation *in vacuo* rather than condensed phase and (iii) slight change in Si-Si-Si-Si dihedral angle from 155° (7_3 -helix) in solution state to smaller Si-Si-Si-Si dihedral angle resulting in shorter wavelength.

The author doubted the possibility of (i) rather than (ii) and (iii). Since the initial structure was arbitral structure and depend on the researcher who generates the structure. Even initial conformation is clearly defined as has been done for this work, the problem whether or not the initial conformation is stable or not remain unclear. Actually, the conformation search using CONFLEX method based on MMFF94s force field showed good agreement with WAXD result (Table3.1) (see Section 5.5.1).

For **PSi2** in toluene/methanol, the condition is slightly more complicated because it showed negative bisigned Cotton effect when the amount of the toluene is relatively high but it changed to positive bisigned CD signal when the amount of the methanol is relatively high (see

Section 2.3.2 for detail). The mechanism of the switching remains unknown. This kind of switching may be understood by introducing solvent effect to the combined model. The solvent-dependent chiroptical inversion of **PSi2** arises from the differing solvation effects on the polymer side chains by shrinking or stretching them. When the volume ratio of toluene (lower polarity, good solvent) is relatively high, the alkyl side chain is well solvated and stretches away from the polymer chain (i.e., when the D value is relatively large, it leads to a negative bisigned Cotton effect). However, as the methanol (higher polarity, poor solvent) ratio increases, a large difference in polarity between solute polymer and cosolvent results in poor solvation of the nonpolar alkyl side chains, leading to contraction of the side chains toward the polymer chain (i.e., when the D value is relatively small, it leads to a positive bisigned Cotton effect).

3.6. References

- (1) Peng, W.; Motonaga, M.; Koe, J. R. *J. Am. Chem. Soc.* **2004**, *126*, 13822.
- (2) Straley, J. *Phys. Rev. A* **1976**, *14*, 1835.
- (3) Harris, A. B.; Kamien, R. D.; Lubensky, T. C. *Rev. Mod. Phys.* **1999**, *71*, 1745.
- (4) Gottarelli, G.; Spada, G. P. In *Circular dichroism : principles and applications*; 2nd ed.; Berova, N., Nakanishi, K., Woody, R., Eds.; Wiley-VCH: New York, 2000, p 547.
- (5) Harada, N.; Nakanishi, K. *Acc. Chem. Res.* **1972**, *5*, 257.
- (6) Harada, N.; Chen, S.-M. L.; Nakanishi, K. *J. Am. Chem. Soc.* **1975**, *97*, 5345.
- (7) Berova, N.; Nakanishi, K. In *Circular dichroism : principles and applications*; 2nd ed.; Berova, N., Nakanishi, K., Woody, R., Eds.; Wiley-VCH: New York, 2000, p 337.
- (8) Berova, N.; Bari, L. D.; Pescitelli, G. *Chem. Soc. Rev.* **2007**, *36*, 914.
- (9) Hagiwara, T. Study of thermotropic liquid crystal phases of rigid-rod like polysilane. M.S. Thesis [Online], Nara Institute of Science and Technology, Ikoma, Nara, 2004/03/24. https://library.naist.jp/mylimedio/dllimedio/showpdf2.cgi/DLPDFR003104_P1-74 (accessed 2016/1/30)
- (10) Miller, R. D.; Michl, J. *Chem. Rev.* **1989**, *89*, 1359.
- (11) Fujiki, M. *J. Am. Chem. Soc.* **1994**, *116*, 11976.
- (12) Gaussian 03, Revision E.01, Frisch, M. J.; Trucks, G. W.; Schlegel, H. B.; Scuseria, G. E.; Robb, M. A.; Cheeseman, J. R.; Montgomery, J. A., Jr.; Vreven, T.; Kudin, K. N.; Burant, J. C.; Millam, J. M.; Iyengar, S. S.; Tomasi, J.; Barone, V.; Mennucci, B.; Cossi, M.; Scalmani, G.; Rega, N.; Petersson, G. A.; Nakatsuji, H.; Hada, M.; Ehara, M.; Toyota, K.; Fukuda, R.; Hasegawa, J.; Ishida, M.; Nakajima, T.; Honda, Y.; Kitao, O.; Nakai, H.; Klene, M.; Li, X.; Knox, J. E.; Hratchian, H. P.; Cross, J. B.; Bakken, V.; Adamo, C.; Jaramillo, J.; Gomperts, R.; Stratmann, R. E.; Yazyev, O.; Austin, A. J.; Cammi, R.; Pomelli, C.; Ochterski, J. W.; Ayala, P. Y.; Morokuma, K.; Voth, G. A.; Salvador, P.; Dannenberg, J. J.; Zakrzewski, V. G.; Dapprich, S.; Daniels, A. D.; Strain, M. C.; Farkas, O.; Malick, D. K.; Rabuck, A. D.; Raghavachari, K.; Foresman, J. B.; Ortiz, J. V.; Cui, Q.; Baboul, A. G.; Clifford, S.; Cioslowski, J.; Stefanov, B. B.; Liu, G.; Liashenko, A.; Piskorz, P.; Komaromi, I.; Martin, R. L.; Fox, D. J.; Keith, T.; Al-Laham, M. A.; Peng, C. Y.; Nanayakkara, A.; Challacombe, M.; Gill, P. M. W.; Johnson, B.; Chen, W.; Wong, M. W.; Gonzalez, C.; Pople, J. A., Gaussian, Inc., Wallingford, CT, 2004.
- (13) Stewart, J. J. P. *J. Comput. Chem.* **1989**, *10*, 209.
- (14) Ebihara, K.; Koshihara, S.-y.; Yoshimoto, M.; Maeda, T.; Ohnishi, T.; Koinuma, H.; Fujiki, M. *Jpn. J. Appl. Phys.* **1997**, *36*, L1211.

Chapter 4. Computational Approach 1: Development of Parameter Optimization Program

4.1. Introduction

If one have a molecular mechanics force field that is suitable for the target molecular/polymer system, it will be beneficial to understand switching mechanism the system have. In this work following questions could be answered by establishing highly reliable force field for polydialkylsilane system and applicable to condensed phase.

- (1) What is the stable conformation in solution state and solid state?
- (2) Can we quantitatively explain the blue-shift during the aggregation by calculation?
- (3) How much the energies differ between left handed and right handed chiral higher structure?

So far, the conformation in solution state and solid state has not been clearly observed though some structural information can be estimated from extrapolated WAXD information and AFM image of poly[*n*-decyl-(*S*)-2-methylbutylsilane] (see Section 3.5). Therefore, question (1) arises to search for clearer picture of the shape of component both in solution state and solid state. This information will support the concept of cholesteric hard-core model or leads to find new aspect that **PSi1–PSi5** have. Furthermore, there was a discrepancy between the PM3 model calculation and extrapolated WAXD data on the critical value of p/D (see Section 3.2). The optimized structure of PM3 models assuming all-trans side chain conformation and $P-7_3$ helix in the Si-Si main chain underestimated the critical $p/D = 2.0$ while extrapolated WAXD data based on poly[*n*-alkyl-(*S*)-2-methylbutylsilane]s predicts 3.2 which is close to π . It could be possible that the initial conformation that was used for PM3 models was not the stable conformation. The explanation of the discrepancy between the computational and experimental will lead to more reliable computational approach and/or experimental method. Furthermore, some previous work

relies on computational approach to decide p and D values (Table 1.3), so it is crucial to establish the reliable force field and method to estimate those values.

In Chapter 2, *aggregachromism* has been observed for **PSi1–PSi5** and two possibilities were suggested. One is Si-Si-Si-Si dihedral angle change during the aggregation and another is H-aggregate as proposed by Kasha (see Section 2.3.3). However, it is difficult to distinguish those two mechanisms from one to another through experiment and thus question (2) is posed.

The cholesteric hard-core model does explain the switching by simple description of the model but it cannot discuss the energy difference between the left handed and right handed higher order structure without further development of the theory. If one could answer question (3), then the quantitative estimation how much the effect is large can be discussed.

Not only for the switching phenomenon in aggregate states but also in solution states mentioned in Section 1.3 could be covered by establishing the reliable force field and the computational methods.

- (1) What factor is crucial to undergo chiroptical inversion in solution state dialkylpolysilane?
- (2) What is the conformational pathway to change the chiroptical inversion?

As introduced in Section 1.3, some dialkylsilane shows chiroptical inversion in solution state and it has been argued that this was caused by helix inversion. However, the relationship between the structure and the chiroptical property has not been clarified yet.

To obtain a reliable force fields for polydialkylsilane system, the author created the parameter optimization program, the “Paramfit” written in Python 2.7.9 programming language. This program fits parameters (bond stretching, angle bending, torsion, cross-terms of those parameters, bond charge increment, and non-bonded interaction) of molecular mechanics, specifically MMFF94S, to the model structures obtained by quantum mechanics calculation at

various levels (HF, MP2, MP4, DFT etc.). The program requires to interact with CONFLEX 7B program and to use output files of Gaussian 09 program as reference information. CONFLEX 7B is a molecular mechanics software package and it can optimize geometry, execute frequency calculation, and obtain internal coordinates and total energy based on given MMFF94S parameters. Gaussian 09 calculates reference structure, energy, and rotational and vibrational frequencies based on quantum mechanics.

To describe the program, each section describes (1) how the parameter optimization takes place in this program (Section 4.2), (2) minimum features of Gaussian 09 to understand the parameter optimization (Section 4.3) (3) minimum features of CONFLEX 7B necessary to understand the parameter optimization (Section 4.4), and (4) validation of the program using relatively simple model structures (Section 4.5).

4.2. Parameter Optimization Scheme

In Figure 4.1, each steps of parameter optimization is presented.

- (1) The program gets reference data (e.g. R'_{ij}) from Gaussian 09 log files.
- (2) Input MM parameter \mathbf{x} in CONFLEX to optimize each model structure and obtain $f(\mathbf{x})$. For CONFLEX, the modification of the parameter is possible by writing ‘.ini file’ that is an input file. See CONFLEX Manual (keyword option section) and Section 4.4.2 for the details.
- (3) Get gradient vector $\Delta\mathbf{x}$ (Eq. A.4.4). In this process, the favorable direction of parameter change is determined. For example, whether slight increase or decrease of one of the component x_n in \mathbf{x} (Eq. A.4.1) is more favorable to reduce $f(\mathbf{x})$. One will know how the parameter change of x_n is effective to reduce $f(\mathbf{x})$ by taking partial derivative of $f(\mathbf{x})$ with respect to x_n .
- (4) Multiply the step size (t_i) by certain value (the Paramfit uses 1.2) to increase the step size. This prevents t_i to be diminished too much and stops the optimization at (9).
- (5) Modify the parameter based on derived step size and gradient vector $\Delta\mathbf{x}$.
- (6) Similarly to (2), calculate $f(\mathbf{x})$.
- (7) Carry out one-dimension search. If t_i is too large and $f(\mathbf{x})$ obtained at (6) increase, reduce t_i in (8) and (9). If not, go to (10).
- (10) If the $f(\mathbf{x})$ difference is small between before and after the parameter modification or t_i is small enough, ends parameter fitting. If not, go to (3).

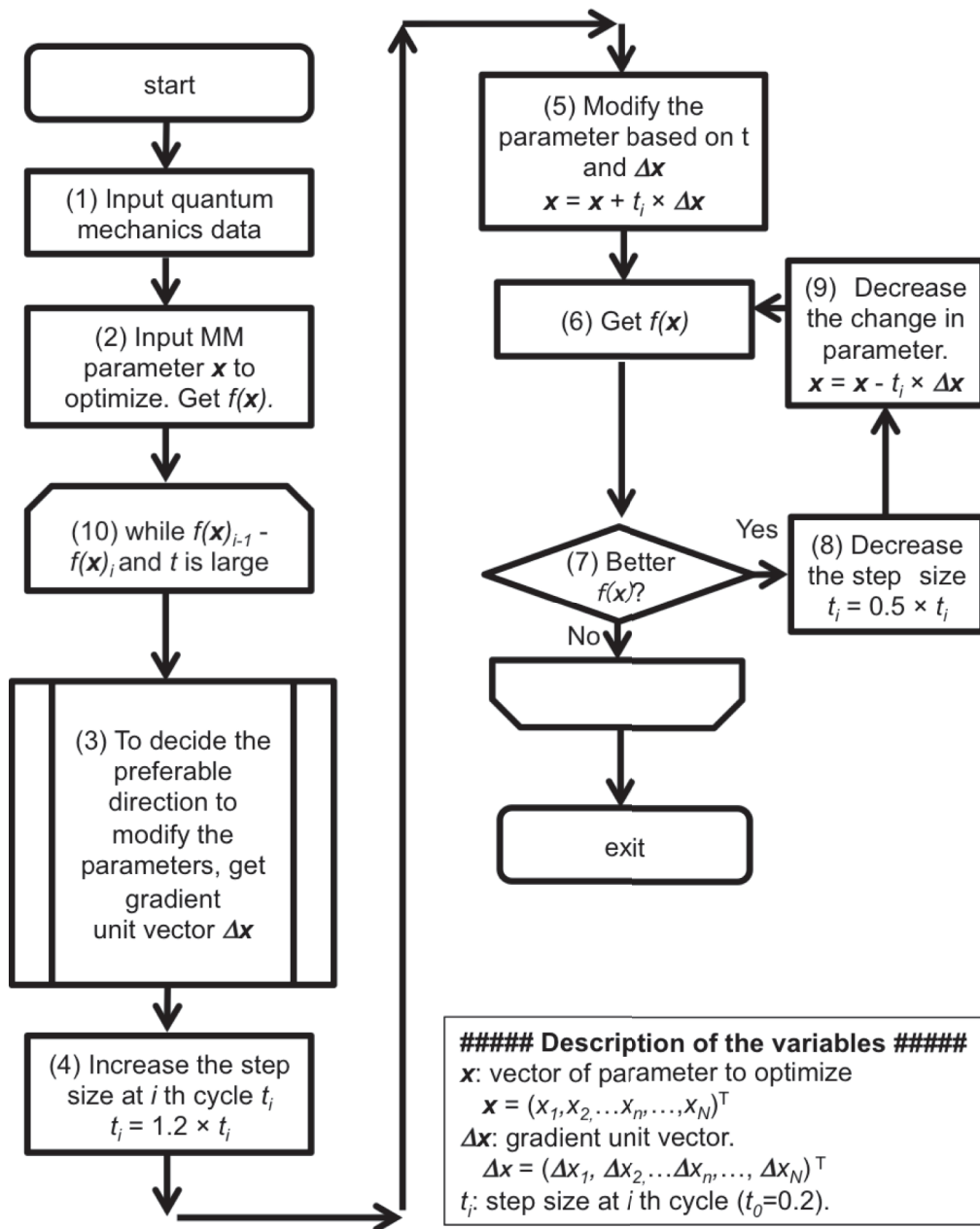


Figure 4.1. Flow chart of the parameter fitting process.

4.3. Gaussian 09 Program Parameter Optimization

4.3.1. Role of Gaussian 09 in the Program

The Paramfit utilize quantum mechanics data instead of experimental data as reference. Gaussian 09 provides the reference quantum mechanics data including geometry, vibrational frequency, eigenvectors, atom charge, and energies of the given geometry. The Paramfit reads those values except atom charge, and optimize MM parameters so that the resulting MM values reproduce the quantum mechanics data.

4.3.2. Input File of Gaussian 09

Basic information is well documented for the Gaussian 09 program¹ and that has user-friendly interface GaussView 5 which helps the user to work on. The Gaussian 09 program can carry out single point energy calculation, geometry optimization, frequency calculation, and charge distribution calculation based on quantum mechanics calculation valuable for parameter optimization as reference information. The input file (.com or .gjf file) with specific keywords at root section that starts with pound sign (#) can control calculations described above. The *ab initio* calculation is specified by the abbreviated name of the theory with the basis set (e.g. HF/6-31G(d), MP2/6-311G(d,p), B3LYP/cc-pVTZ). Geometry optimization, frequency calculation, and charge distribution calculation can be carried out by adding 'opt', 'freq', and 'pop', respectively. To obtain the potential surface at specific torsion angle, 'scan' or 'modredundant' keyword is used. For calculation of van der Waals parameters, 'counterpoise' keyword is used to avoid basis set basis set superposition error (BSSE).²⁻⁴

4.3.3. Output File of Gaussian 09

The program Paramfit reads the output files (.log file) of the Gaussian 09 with keywords above. When optimization without frequency calculation (with 'opt' but no 'freq' keyword) or single point energy calculation (without 'opt' and 'freq' keyword) is carried out, the program reads only electronic energy at the end of the log file.

The 'freq' keyword enables to carry out frequency calculation and resulting thermodynamics data are printed in the output file. The Paramfit reads not only the vibrational frequency but also the eigenvector of each normal mode. This is to attribute normal modes of quantum mechanics calculation to that of the molecular mechanics.⁵ When 'freq' keyword is included in the root section, Gaussian 09 outputs following information based on thermochemistry.

- Thermochemistry -	

Temperature	298.150 Kelvin. Pressure 1.00000 Atm.
...	
Zero-point correction=	0.062346 (Hartree/Particle) ...(1)
Thermal correction to Energy=	0.065859
Thermal correction to Enthalpy=	0.066804
Thermal correction to Gibbs Free Energy=	0.039019
Sum of electronic and zero-point Energies=	-330.515188 ...(2)
Sum of electronic and thermal Energies=	-330.511675
Sum of electronic and thermal Enthalpies=	-330.510730 ...(3)
Sum of electronic and thermal Free Energies=	-330.538515 ...(4)

The Paramfit reads four energies from the output file, which are (1) "Zero-point correction" (ΔE_{ZPE}), (2) "Sum of electronic and zero-point energies" (E_{ZPE}), (3) "Sum of electronic and thermal enthalpies" (E_H), (4) "Sum of electronic and thermal Free Energies" (E_G). Based on those energies, Electronic energy (E_e), entropy multiplied by room temperature at 298.15 K (E_{TS}) are calculated as follows.

$$E_e = E_{ZPE} - \Delta E_{ZPE} \text{ (Eq. 4.3.1)}$$

$$E_{TS} = E_H - E_G \text{ (Eq. 4.3.2)}$$

Thus, the program obtains five types of energy (E_e , E_{ZPE} , E_H , E_{TS} , and E_G) from the log file, facilitating to compare those values obtained from CONFLEX 7B. For the optimization, E_e is used as reference energy.

4.4. CONFLEX 7B Program and Parameter Optimization

4.4.1. Role of CONFLEX in the Program

The Paramfit utilizes the output file of the Gaussian 09 that does not interact dynamically with Paramfit. However, the Paramfit does dynamically send information, carry out calculation, reads the output file of the CONFLEX program. The main roles of the CONFLEX are as follows.

- (i) Read the CONFLEX input file (.ini file and .mol file) created by the Paramfit and optimize molecular structure based on the information.
- (ii) Calculate vibrational frequency.
- (iii) Print out bond, angle, torsion, steric energy, vibrational frequency, and eigenvector of the normal mode.

The Paramfit utilizes the above CONFLEX features as a routine and carries out the main part of the parameter fitting.

4.4.2. Input Files of CONFLEX

CONFLEX reads two independent files (.mol file and .ini file) as input. The .mol file contains the information of the molecular geometry, charges, and bond information. The .mol file is a general format and shared with other MM/QM software packages (such as Gaussian 09), and no special modification is necessary for the parameter fitting, thus the detail is omitted in this thesis. The .ini file can be viewed and edited with text editor and describes the keywords to specify method for CONFLEX. In the software, there are various attractive features including optimization options (e.g. fixing internal coordinates), conformation search, clustering, and crystal structure search but only important keywords related to parameter optimization are described as follows.

<p>MMFF94S ... (1) Force field</p> <p>STRETCH=(I,J,BORDER,FK,STD) ... (2) Bond stretching</p> <p>BEND=(I,J,K,RING,FK,STD) ... (3) Angle bending</p> <p>TORSION=(I,J,K,L,RING,V1,V2,V3) ... (4) Torsion</p> <p>OPLANE=(I,J,K,L,FK) ... (5) Out of plane</p> <p>STRBND=(I,J,K,FK_IJ,FK_KJ) ... (6) Stretch-bend</p> <p>VDWATOM=(I,DA,ALPHA,N,A,G) ... (7) van der Waals interaction</p> <p>BNDCHG=(I,J,BCI) ... (8) Bond charge increments</p> <p>OPTBY=GRADIENT ... (9) Minimize gradient of the energy (Minimize energy by default)</p> <p>ALLMODE ... (10) Output all vibration modes (Omits higher frequencies by default)</p> <p>NOOPT ... (11) Do not carry out geometry optimization</p>
--

The values of the parameters can be modified through the above input keywords (2)–(8) as well as parameter file (extension with .PAR). As long as the combinations of the atom type (I, J, K, L) are different, CONFLEX can treat multiple parameters in the same category of the interaction. Whether the parameters are read properly or not can be verified in .bso file that is one of the CONFLEX output files. When optimization of transition state is needed (e.g. to fit V_3 term of the torsion parameter), optimization by gradient (9) is necessary rather than optimizing energy itself. Otherwise, even the input structure is close to the transition state, the resulting structure is optimized to the ground state structure. For parameterizing van der Waals interaction without geometry optimization or printing out the internal coordinate of the reference file in .mol file, printing the .bso file without geometry optimization (11) will be necessary.

4.4.3. Output Files of CONFLEX

When geometry optimization is carried out, CONFLEX outputs .bso file. This file contains the following information.

(1) License information

- (2) Input parameters
- (3) Geometry of the molecule at initial structure
- (4) Steric energy and contribution of each interaction at initial structure
- (5) The optimization process
- (6) Geometry of the molecule at optimized structure
- (7) Steric energy and contribution of each interaction at optimized structure
- (8) Thermodynamic properties of optimized structure
- (9) Vibrational information of optimized structure

4.4.4. Running CONFLEX from Python

```

Macintosh:
$ export DYLD_LIBRARY_PATH=/Applications/CONFLEX.app/Contents/MacOS/lib:$DYLD_LIBRARY_PATH

$ /Applications/CONFLEX.app/Contents/MacOS/bin/flex7b3.Mac.exe -par /opt/local/conflex/par input
                (1)                                (2)      (3)      (4)

Windows:
$ C:\CONFLEX\bin\flex7b1x64.exe -par C:\CONFLEX\par input
                (1)      (2)      (3)      (4)

```

(1) Path to the CONFLEX executable file
(2) Option to specify the parameter file
(3) Path to the parameter file
(4) Path to the file (.mol and .ini file without the extension)

Since the CONFLEX can be executed on command line as described above, CONFLEX can be executed on python as well using the subprocess module. In this thesis, example program is written for Macintosh and use Python 2.7.9. Also, in this document, the environment setting starting ‘export’ is assumed to be set.

Assume that the user has .mol files (file1.mol and file2.mol below) and .ini files (file1.ini and file2.ini) in directory (‘/path/to/mol/’) and want to run CONFLEX sequentially. The user must know information (1)–(3) in the above box. One can define ‘s_path_conflex’ (string information of

path to conflex) and 'list_mol_filename' (list of path to mol file) in python script as follows.

```
s_path_conflex = '/Applications/CONFLEX.app/Contents/MacOS/bin/flex7b3.Mac.exe -par
                /Applications/CONFLEX.app/Contents/MacOS/par'
list_mol_filename = ['/path/to/mol/file1.mol', '/path/to/mol/file2.mol']
Run_CONFLEX(s_path_conflex, list_mol_filename)
exit()
```

One can define function 'Run_CONFLEX' to run CONFLEX for the entire file listed in list_mol_filename as follows.

```
def Run_CONFLEX(s_path_conflex, list_mol_filename):
    import subprocess
    # Run the molfiles in the list sequentially.
    for i in range(0,len(list_mol_filename)):
        # Delete given extension of the file name
        list_path_string = list_mol_filename[i].split('.')
        target_filename = ''.join(list_path_string[:-1])
        # Define the command as string
        s_command = (str(s_path_conflex) + ' ' + str(target_filename))
        # Execute CONFLEX calculation
        subprocess.Popen(s_command,shell=True).wait()
    return
```

4.5. Validation of the Program Using Model Structures

4.5.1. Computational Method

MMFF94S⁶⁻¹³ was chosen as molecular mechanics force field. To test the function of the program for optimizing geometry and vibration, methylsilane is used as model structure. The reference structure was optimized at MP2/6-311G(d,p), followed by frequency calculation. C-Si (1-19) and H-Si (5-19) for bond stretch and C-Si-H(1-19-5) and H-Si-H (5-19-5) for angle bending are optimized. The optimization of the bond stretching and angle bending was carried out separately. The rotational and vibrational frequencies of the quantum mechanics were scaled by 0.9496.¹⁴

To test the function of the program for torsion, *n*-propylsilane is used as a model structure. Four reference conformations (*anti*, *eclipsed*, *gauche*, and *syn*) were generated and optimized at MP2/6-311G(d,p) level. V_1 , V_2 , and V_3 term were optimized, which corresponds to the constant of $\cos\omega$, $-\cos2\omega$, and $\cos3\omega$ of the torsion, respectively.⁷

4.5.2. Optimization of Internal Coordinates

Bond stretching parameters (C-Si and H-Si) and angle bending parameters (C-Si-H and H-Si-H) of MMFF94S force field were optimized to reproduce the geometry at MP2/6-311G(d,p) level. Table 4.1 and Table 4.2 show the original and optimized parameters and Table 4.3 shows the resulting geometry of the molecule. The geometry with optimized parameter revealed closer values of the internal coordinates to the reference data. The errors for bond length and angle were within 0.002 Å and 0.003°, respectively. Those values are one and two magnitudes better than averaged RMSD for MMFF94S with respect to experiment data, which were 0.014 Å for bond length and 1.2° for angle, respectively.

Table 4.1. Bond stretching parameters before and after the optimization.

	Bond stretching			
	Original		Optimized	
	k_b	r_0	k_b	r_0
C-Si (1-19)	2.8660	1.8300	3.3038	1.8665
H-Si (5-19)	2.2540	1.4850	2.7547	1.4802

Table 4.2. Angle bending parameters before and after the optimization.

	Angle bending			
	Original		Optimized	
	k_a	θ_0	k_a	θ_0
C-Si-H (1-19-5)	0.3900	110.7900	0.3710	109.9877
H-Si-H (5-19-5)	0.2580	107.4500	0.4709	107.9847

Table 4.3. Geometry comparison of the methylsilane.

		MP2/6-311G(d,p)	MMFF94S	
			Original	Optimized
Bond length[Å]	C-Si	1.877	1.844	1.876
	H-Si	1.478	1.485	1.480
Angle[°]	C-Si-H	110.41	110.36	110.41
	H-Si-H	108.51	108.57	108.51

4.5.3. Optimization of Rotational and Vibrational Frequencies

During the optimization of the internal coordinates discussed in the previous section, the rotational and vibrational frequencies were also optimized to reproduce quantum mechanics data at MP2/6-311G(d,p) level. The reference and the result of the vibration frequencies are shown in Table 4.4. The final RMSD was 41 cm^{-1} which is better than vibrational frequency before the optimization (128 cm^{-1}) and the averaged RMDS for various molecules (61 cm^{-1}) using MMFF94S⁷, respectively.

The Paramfit automatically attributes the normal modes of the vibration because switching of the vibration order is expected to occur during the optimization.⁵ Actually, the order of the frequencies was not consistent between quantum mechanics and molecular mechanics calculation as shown in Table 4.4. For example, 5 th mode of MMFF94S revealed relatively lower frequency than that of 6th and 7th mode, while the quantum mechanics calculation showed the opposite tendency. To check whether the automated attribution is reasonable, the vibrational modes are illustrated in Figure 4.2. The figure shows the vibrational mode of methylsilane to compare the results obtained with the quantum mechanics and molecular mechanics calculations. The numbers of the normal modes in the figure corresponds to those labeled in Table 4.4. Several eigenvectors of MMFF94S points revealed the opposite direction of eigenvector of quantum mechanics (e.g. [QM mode, MM mode] = [3,3], [7,5], [8,9], [9,8], and [10,10]). However, the eigenvectors in the Figure 4.2 represents one of the two opposite directions of the vibration, which are equal so this case is not a serious problem. From those results, the automatic frequency correlation of methylsilane was confirmed to work well using the optimized parameters.

Table 4.4. Rotational and vibrational frequencies of methylsilane. Frequencies at MP2/6-311G(d,p) level and that of MMFF94S force field using the optimized parameters are shown. The vibrational frequencies in the same low are attributed as the same vibration mode.

MP2/6-311G(d,p)		MMFF94S(optimized)		Squared error
Mode	Frequency(cm ⁻¹)	Mode	Frequency(cm ⁻¹)	
1	187.8	1	215.4	759
2	498.2	2	530.6	1051
3	498.2	3	530.6	1051
4	682.2	4	712.9	943
5	862.8	6	839.6	538
6	862.8	7	839.6	538
7	939.5	5	837.1	10493
8	955.4	9	979.3	572
9	955.4	8	979.3	572
10	1254.3	10	1302.2	2295
11	1404.9	12	1428.1	538
12	1404.9	11	1428.1	538
13	2193.3	15	2205.8	156
14	2193.3	14	2205.8	156
15	2194.6	13	2169.4	638
16	2927.6	16	2863.5	4113
17	3018.3	17	2964.8	2866
18	3018.3	18	2964.8	2866
RMSD=				41.3

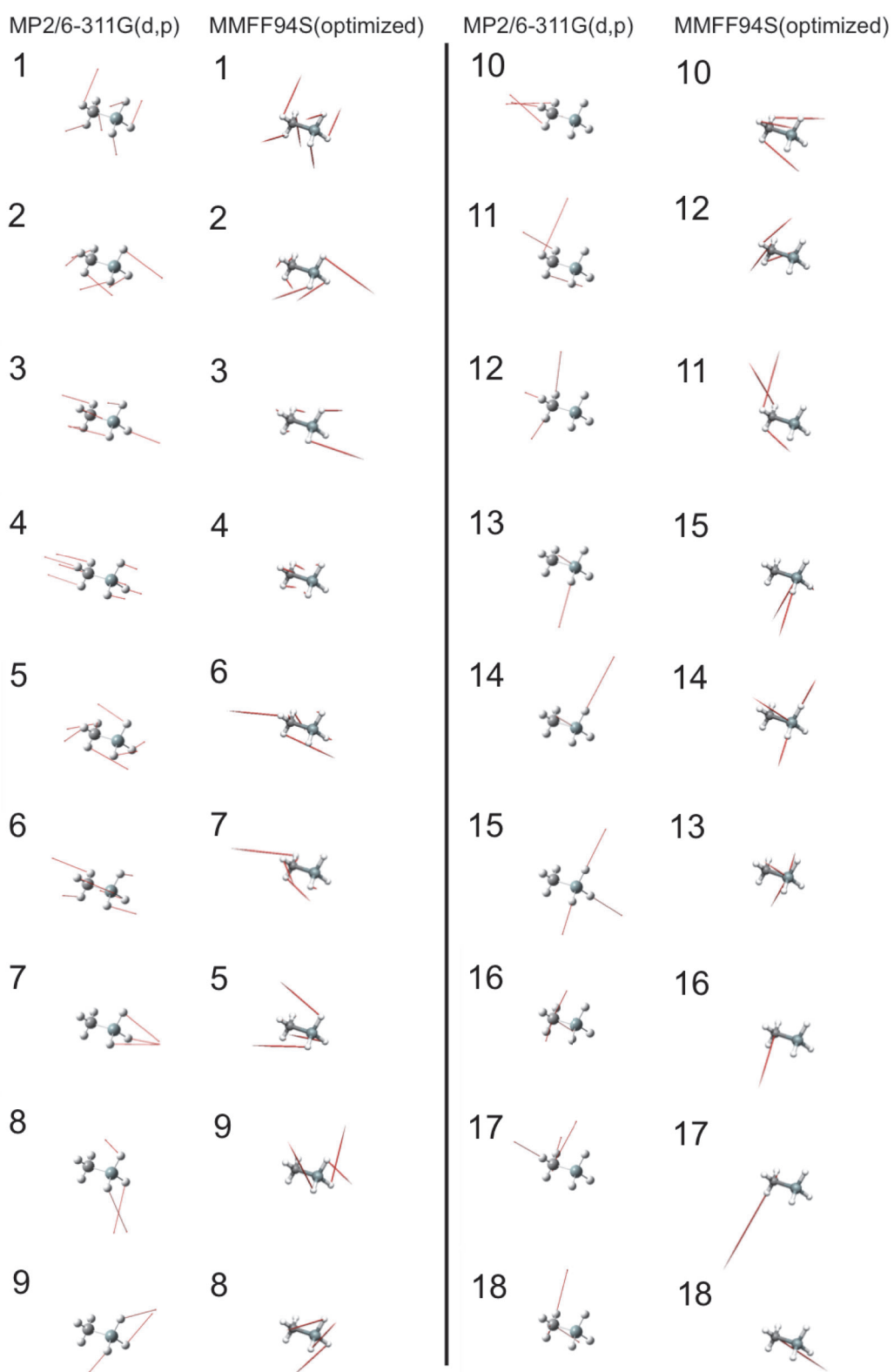


Figure 4.2. Result of automatic attribution of rotational and vibrational modes of methylsilane. The red lines represent the displacement of the rotation and vibration. The results of MP2/6-311G(d,p) are shown using GaussView and MMFF94S is shown using CONFLEX as visual interface.

4.5.4. Optimization of Conformational Energies

Figure 4.3 shows the potential energy of *n*-propylsilane. Four data points (*anti*, *eclipsed*, *gauche*, and *syn* conformations) used as references appear with green arrows and white open circles. The rest of the quantum mechanics data points with green filled dots were obtained by ‘scan’ keyword implemented in Gaussian 09 in which structures were not used as reference. The original MMFF94S torsion parameter of C-C-C-Si (atom type: 1-1-1-19) overestimates the transition energy by 2.40 kcal/mol at *syn* conformation and by 0.41 kcal/mol at *eclipsed* conformation. For comparison of the energy profile at *gauche* conformation, the figure is enlarged at upper right inset in Figure 4.3. The errors at *gauche* conformation using the original parameter are negligible but it still underestimates the energy by 0.07 kcal/mol.

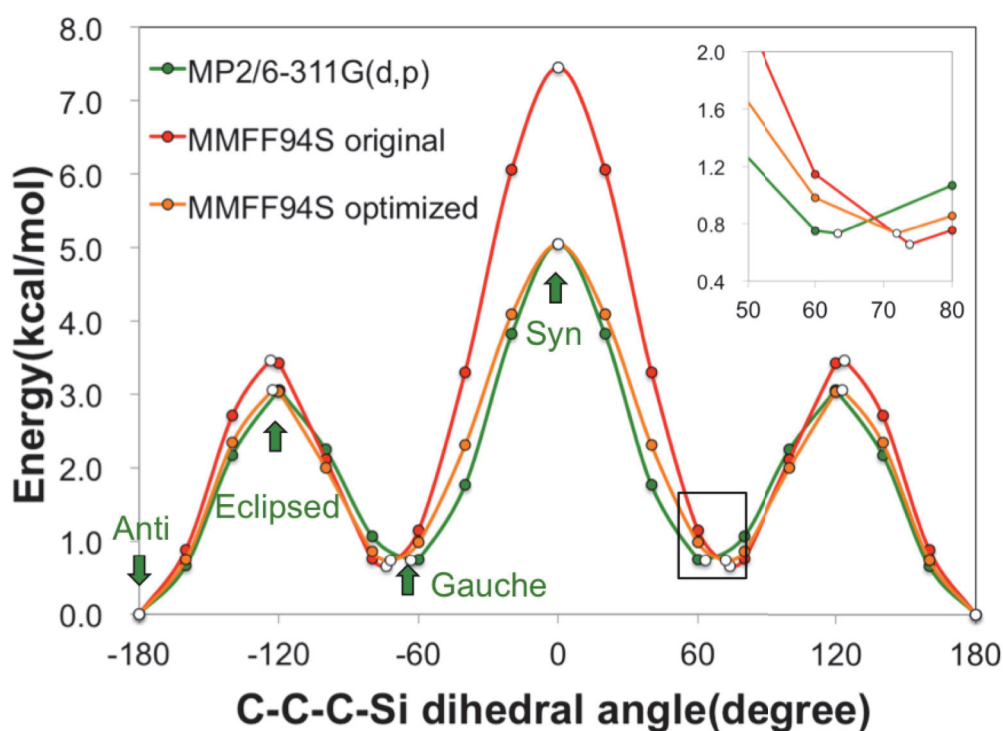


Figure 4.3. Potential energy of *n*-propylsilane. Notations with green arrow are data points used as reference data (the rest of the data were not used as reference). White circles are data point where the structure is optimized ground state or transition state without fixing the torsion angle.

Optimization of the C-C-C-Si torsion parameters took place. The resulting parameters

before and after the optimization are listed in Table 4.5. The potential energy curve after the optimization is shown in Figure 4.3 with orange line. Compared to the original parameters, the potential energies in the transition and the ground states became close to the reference quantum mechanics data. The error was within 0.001 kcal/mol and thus the accuracy of the program to fit the torsion energy is high enough.

Table 4.5. Original and optimized torsion parameters.

	Torsion					
	Original			Optimized		
	V_1	V_2	V_3	V_1	V_2	V_3
C-C-C-Si (1-1-1-19)	0.2730	0.6390	0.2640	-1.4563	-1.2288	-0.6480

4.6. References

- (1) Foresman, J. B.; Frisch, A.; Gaussian Inc. *Exploring chemistry with electronic structure methods*; 2nd ed.; Gaussian, Inc.: Pittsburgh, PA, 1996; pp. 1–297.
- (2) Bordner, A. J.; Cavasotto, C. N.; Abagyan, R. A. *J. Phys. Chem. B* **2003**, *107*, 9601.
- (3) Du, Q.-S.; Liu, P.-J.; Deng, J. *J. Chem. Theory Comput.* **2007**, *3*, 1665.
- (4) Mahlanen, R.; Pakkanen, T. A. *Chem. Phys.* **2011**, *382*, 121.
- (5) Vaiana, A. C.; Cournia, Z.; Costescu, I. B.; Smith, J. C. *Comput. Phys. Commun.* **2005**, *167*, 34.
- (6) Halgren, T. A. *J. Am. Chem. Soc.* **1992**, *114*, 7827.
- (7) Halgren, T. A. *J. Comput. Chem.* **1996**, *17*, 490.
- (8) Halgren, T. A. *J. Comput. Chem.* **1996**, *17*, 520.
- (9) Halgren, T. A. *J. Comput. Chem.* **1996**, *17*, 553.
- (10) Halgren, T. A. *J. Comput. Chem.* **1996**, *17*, 616.
- (11) Halgren, T. A.; Nachbar, R. B. *J. Comput. Chem.* **1996**, *17*, 587.
- (12) Halgren, T. A. *J. Comput. Chem.* **1999**, *20*, 720.
- (13) Halgren, T. A. *J. Comput. Chem.* **1999**, *20*, 730.
- (14) Scott, A. P.; Radom, L. *J. Phys. Chem.* **1996**, *100*, 16502.

Chapter 5. Computational Approach 2: Parameter Optimization

5.1. Introduction

In the previous chapter, the importance of development of the force field and the computational method was clarified (see Section 4.1) and the program Paramfit to optimize molecular mechanics force field was developed. Particular interests of the work in this thesis are: (1) to reproduce molecular geometry; (2) to develop MMFF force field¹⁻⁸ that is applicable for simulation in solution and solid states; (3) to reproduce conformational energy difference as well as transition state; and (4) to reproduce vibrational frequency that is comparable to MM3. In Section 5.2, the author chose the quantum mechanics method that reproduces the experimental result. Based on the result of quantum mechanics at MP4(sdq)/cc-pVTZ//MP2/6-311G(d,p) level, the MMFF parameters were optimized. The procedure to optimize the parameters of the MMFF force field was explained in Section 5.3. The resulting force field was evaluated in Section 5.4 based on the model structure that has been used for the optimization.

5.2. Choice of Quantum Mechanics Method

To decide the level of calculation suitable for the reference, disilane and permethyltetrasilane were tested as model compounds. The disilane is a well-studied compound due to its industrial application.⁹⁻¹³ Thus many experimental and theoretical data can be used as reference. Optimization at MP2 (frozen core) and MP4(sdq) levels with 6-311G(d,p), 6-311G++(2df,p), cc-pVTZ, aug-cc-pVTZ basis sets are carried out for the disilane (Table 5.1). The geometry and energy barrier are compared with CCSD(T)/cc-pVQZ and experiment. For the CCSD(T), the geometry and the energy are extrapolated to the valence correlation limit using uncontracted cc-pVTZ basis, the Martin–Taylor set.¹¹ Overall, the differences between each method and CCSD(T) was small: the errors were within 0.02 Å for Si-Si, 0.006 Å for Si-H bond length, 0.2° for Si-Si-H angle. Among these calculations, MP2/6-311G(d,p) showed the closest values with respect to CCSD(T) data and experiment values. Thus, the author thinks that MP2/6-311G(d,p) is a good choice for deriving geometry at this stage.

However, MP2/6-311G(d,p) overestimated energy barrier of the disilane by ~ 0.13 kcal/mol relative to CCSD(T) calculation though somehow close to experimental value (1.26 ± 0.03 kcal/mol). The other experiment, obtained indirectly from combination bands in the mid-infrared spectrum, indicates this energy barrier as ~ 1.0 kcal/mol which is consistent with CCSD(T) energy.¹³ Thus the CCSD was used as the reference in this work to compare with rather than the experiment. The torsion parameters that are derived in the MMFF94S force field use MP4(sdq) for estimation of energy. Though some lower level calculation showed closer energy values to experimental data than MP4(sdq)/cc-pVTZ//MP2/6-311G(d,p), the MP4(sdq)/cc-pVTZ//MP2/6-311G(d,p) level calculation provided reasonable value respect to the CCSD(T) data.

To confirm the accuracy of MP4(sdq)/cc-pVTZ//MP2/6-311G(d,p) for a larger structure, geometry optimization and frequency calculation at MP2/6-311G(d,p) was carried out for *gauche*, *ortho*, and *transoid* conformations of permethyltetrasilane (Table 5.1). Previous experimental work by Belyakov¹⁴ and theoretical work by Piqueras¹⁵ are also compared. They carried out optimization at MP2 level using cc-pVTZ for the silicon atoms, the 6-31G(d) for the carbon, and 6-31G basis sets for hydrogen atoms. MP2/6-311G(d,p) geometry reproduced Si-Si bond lengths at the edge of the molecule (Si(1)Si(2)) better than MP2/cc-pVTZ but slightly underestimates the other bond lengths, which leaves a room to consider to use MP2/cc-pVTZ for geometry optimization though the method overestimated the bond lengths of disilane compared to MP2/6-311G(d,p).

A comparison of the mole fraction at 340 K (χ_{340}) was made from frequency calculation for MP2/6-311G(d,p). The energy of *gauche* relative to *trans* conformation was slightly underestimated and resulted in a higher population. For previously reported MP2/cc-pVTZ calculation, vibrational analysis was carried out at HF/6-31G(d) level. The calculation overestimates resulting free energy at *gauche* conformation and slightly underestimated χ_{340} . Energy evaluated at MP4(sdq)/cc-pVTZ//MP2/6-311G(d,p) showed closer value with respect to the experiment data compared to MP2/6-311G(d,p) level. For *ortho* conformation, the relative energies to *transoid* conformation were close to the experiment data at all calculation level.

Because MP2/cc-pVTZ has much larger basis set compared to MP2/6-311G(d,p), the former basis set is considerably time-consuming to calculate vibrational frequency of permethyltetrasilane. Thus, MP4(sdq)/cc-pVTZ//MP2/6-311G(d,p) is used for this work although MP2/cc-pVTZ reproduced the geometry of permethyltetrasilane.

Table 5.1. Bond length [\AA], angles [$^\circ$], and relative total energy [kcal/mol] of disilane. The ΔE is a relative energy value of *syn* to *anti* conformation.

	Anti			Syn			ΔE
	r_{SiSi}	r_{SiH}	$\angle \text{SiSiH}$	r_{SiSi}	r_{SiH}	$\angle \text{SiSiH}$	
MP2/6-311G(d,p)//MP2/6-311G(d,p)	2.343	1.478	110.3	2.353	1.478	110.4	1.19
MP2/6-311G++(2df,p)//MP2/6-311G++(2df,p)	2.349	1.481	110.1	2.362	1.480	110.3	1.09
MP2/cc-pVTZ//MP2/cc-pVTZ	2.349	1.481	110.3	2.362	1.480	110.4	1.06
MP2/aug-cc-pVTZ//MP2/aug-cc-pVTZ	2.349	1.482	110.2	2.361	1.481	110.4	1.08
MP4/6-311G(d,p)//MP4/6-311G(d,p)	2.343	1.479	110.3	—	—	—	—
MP4/6-311G++(2df,p)//MP4/6-311G++(2df,p)	2.352	1.483	110.2	—	—	—	—
MP4/cc-pVTZ//MP4/cc-pVTZ	2.352	1.485	110.3	—	—	—	—
MP4/aug-cc-pVTZ//MP4/aug-cc-pVTZ	2.351	1.485	110.3	—	—	—	—
MP2/6-311G(d,p)//MP2/6-311G(d,p)	2.343	1.478	110.3	2.353	1.478	110.4	1.19
MP2/6-311G++(2df,p)//MP2/6-311G(d,p)	— ^b	— ^b	— ^b	— ^b	— ^b	— ^b	1.09
MP2/cc-pVTZ//MP2/6-311G(d,p)	— ^b	— ^b	— ^b	— ^b	— ^b	— ^b	1.07
MP2/aug-cc-pVTZ//MP2/6-311G(d,p)	— ^b	— ^b	— ^b	— ^b	— ^b	— ^b	1.08
MP4/6-311G(d,p)//MP2/6-311G(d,p)	— ^b	— ^b	— ^b	— ^b	— ^b	— ^b	1.17
MP4/6-311G(2df,p)//MP2/6-311G(d,p)	— ^b	— ^b	— ^b	— ^b	— ^b	— ^b	1.04
MP4/cc-pVTZ//MP2/6-311G(d,p)	— ^b	— ^b	— ^b	— ^b	— ^b	— ^b	1.02
MP4/aug-cc-pVTZ//MP2/6-311G(d,p)	— ^b	— ^b	— ^b	— ^b	— ^b	— ^b	1.03
CCSD(T)/cc-pVQZ//CCSD(T)/cc-pVQZ ^a	2.334	1.479	110.3	2.346	1.479	110.4	1.06
experiment	2.332(2) ^c	1.487(2) ^c	110.7(2) ^c	—	—	—	1.26(3) ^d

^aCCSD(T)/cc-pVQZ geometry and energy extrapolated using uncontracted cc-pVTZ basis set.¹¹ ^bThe same value as MP2/6-311G(d,p)//MP2/6-311G(d,p). ^cFrom Reference ¹². ^dFrom Reference ¹⁰. Reference ¹³ estimate this value as 1.0 kcal/mol obtained indirectly from combination bands in the mid-infrared spectrum.

Table 5.2. Bond length [\AA], angles [$^\circ$], and dihedral angles [$^\circ$], total energy and Gibbs' free energies relative to transoid (ΔE and ΔG_{340}) [kcal/mol], and mole fraction (χ_{340}), for *gauche*, *ortho*, and *transoid* conformers of permethylsilane obtained by *ab initio* calculation and experiment data.

		$r_{\text{Si}(1)\text{Si}(2)}$	$r_{\text{Si}(2)\text{Si}(3)}$	$r_{\text{Si}(1)\text{C}}$	$r_{\text{Si}(2)\text{C}}$	$\angle \text{SiSiSi}$	$\angle \text{SiSiSiSi}$	ΔE	ΔG_{340}	χ_{340}^c
Gauche	MP2/cc-pVTZ//MP2/cc-pVTZ ^a	2.354	2.353	1.889(2)	1.901(2)	114.1	54.5	0.270	0.63	0.23 ^d
	MP2/6-311G(d,p)//MP2/6-311G(d,p)	2.351	2.349	1.886(5)	1.889(1)	114.1	53.8	0.130	-0.05	0.43 ^e
	MP4(sdq)/cc-pVTZ//MP2/6-311G(d,p)							0.180	0.00	0.41 ^f
	exp. ^b	2.351(6)	2.354(6)	1.893(2)	1.900(1)	117.0(5)	–			0.32(8)
Ortho	MP2/cc-pVTZ//MP2/cc-pVTZ ^a	2.354	2.358	1.889(2)	1.900(1)	112.4	91.3	0.670	0.81	0.18 ^d
	MP2/6-311G(d,p)//MP2/6-311G(d,p)	2.351	2.354	1.888(1)	1.900(1)	112.8	89.9	0.460	0.53	0.18 ^e
	MP4(sdq)/cc-pVTZ//MP2/6-311G(d,p)							0.450	0.54	0.18 ^f
	exp. ^b	2.345(6)	2.359(6)	1.893(2)	1.903(2)	115.1(5)	–			0.17(14)
Transoid	MP2/cc-pVTZ//MP2/cc-pVTZ ^a	2.354	2.353	1.889(1)	1.899(0)	110.2	162.6	0.000	0.00	0.59 ^d
	MP2/6-311G(d,p)//MP2/6-311G(d,p)	2.351	2.350	1.889(1)	1.899(1)	110.7	162.8	0.000	0.00	0.40 ^e
	MP4(sdq)/cc-pVTZ//MP2/6-311G(d,p)							0.000	0.00	0.41 ^f
	exp. ^b	2.350(6)	2.354(6)	1.893(2)	1.901(2)	112.4(5)	163(8)			0.51(6)

^aOptimized at MP2 level using cc-pVTZ basis set for the silicon atoms, the 6-31G(d) for the carbon, and 6-31G for hydrogen atoms. ^bValues from Ref. ¹⁴. The values in parentheses are standard deviations in units of the last digit. ^cMole fractions at 340 K. ^dCalculated at HF/6-31G(d) level scaled by 0.9135. Values from Ref. ¹⁵. ^eCalculated at MP2/6-311G(d,p) level scaled by 0.9748. ^fFree energy correction was calculated at

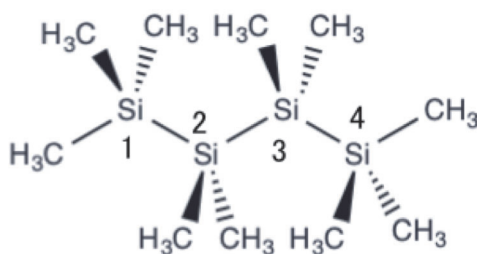


Figure 5.1. Chemical structure of permethyltetrasilane with numbered silicon.

5.3. Computational Method

5.3.1. Optimization of Bond Charge Increments

Bond charge increments (BCI) was utilized to estimate atomic charges, based on combination table of two atom types that form the bond.⁵ Atom type of silicon, sp^3 carbon, and hydrogen are defined as 19, 1, and 5 in MMFF94S, respectively. Original BCI parameters for C-Si (1-19) and H-Si (5-19) were 0.0805 and 0.2000 in electron unit, respectively.

Mulliken population analysis is one of the popular methods to estimate the charges by quantum mechanics calculation but it strongly depends on the basis set. As a result, the electrostatic moments are poorly described.¹⁶ To evaluate the original bond charge increment parameters, CHELPG method suited for parameterization of force field was chosen.^{5,17} As model molecules to decide the charge, several compounds containing one silicon atom (silane, methylsilane, trimethylsilane, and tetramethylsilane) and containing four silicon atoms (tetrasilane, 2,2-dimethyltetrasilane, 2,2,3,3-tetramethyltetrasilane, 1,1,1,4,4,4-hexamethyltetrasilane, 1,1,1,3,3-pentamethyltetrasilane, and permethyltetrasilane) were used. The calculated charges at MP4(sdq)/cc-pVTZ//MP2/6-311G(d,p) using CHELPG method are listed in Appendix (Figure A.5.1–A.5.11). To fit the BCI parameters, RMSD of atomic charges was calculated based on (1) temporal BCI charges and (2) MP4(sdq)/cc-pVTZ//MP2/6-311G(d,p) using CHELPG and the BCI charges were optimized using solver in Microsoft Excel for Mac 2011. The optimized charges of 1-19 and 5-19 were 0.1996 and 0.1452 in electron unit, respectively. The polarization tendency was opposite compared to that of the original parameters.

The optimized BCI parameters reproduced the charge at quantum mechanic with RMSD=0.06. For the molecules containing one Si atom, the derived BCI charges underestimate the absolute values of the atomic charges by 17%. Charges of the molecules containing four Si atoms overestimated approximately 39%, where Si atoms at the 1,4 position showed 2% smaller than the

reference, the Si atoms at 2,4 position revealed 71% larger value, and C atoms showed 43% larger value.

5.3.2. Optimization of Van Der Waals Interactions

To optimize van der Waals interaction parameters of silicon atom, silane molecule was chosen as a model. The geometry of the silane was optimized at MP2/6-311G(d,p) level and two silicon atoms were positioned and oriented as defined in Figure 5.2. The single point energy calculation was carried out for the two silane molecules at MP4(sdq)/aug-cc-pVTZ level. BSSE was corrected by counterpoise method.^{18,19}

During the parameterization of the van der Waals interaction parameters, geometry optimization process was omitted by using ‘NOOPT’ keyword (see Section 4.4.2). Inter Si-Si atomic distance (r_{SiSi}) was set to 4.20, 4.50, 4.60, 4.70, 4.80, 4.90, 5.00, 5.60, 6.00, 7.00, 8.00, 10.00, and 20.0 Å for the reference and the parameter optimization. Data points close to the minimum (r_{SiSi} = 4.60 Å) were adopted more frequently than data far from the minimum. The resulting parameter table and potential curve are shown in Table 5.3 and Figure 5.3. The potential curve based on the original MMFF94S parameter revealed shallower potential depth by ~ 0.04 kcal/mol and r_{SiSi} at minimum by ~ 0.40 Å compared to MP4(sdq)/aug-cc-pVTZ level. The optimized potential showed still slightly shallower (0.01–0.02 kcal/mol), but reproduced the r_{SiSi} at the minimum well.

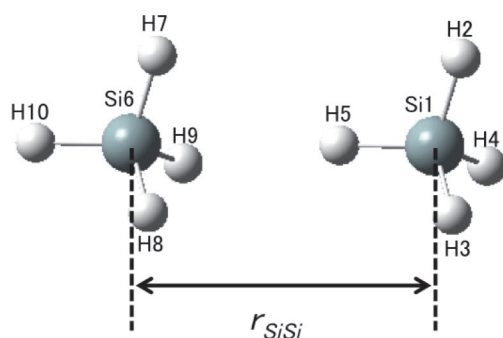


Figure 5.2. Defined orientation and inter Si-Si atom distance r_{SiSi} of two silanes to decide the van der Waals parameters. The positions of the atoms were defined so that angle H10-Si6-H5, Si6-H5-Si1, and dihedral angle H7-Si6-Si1-H2 become 0° .

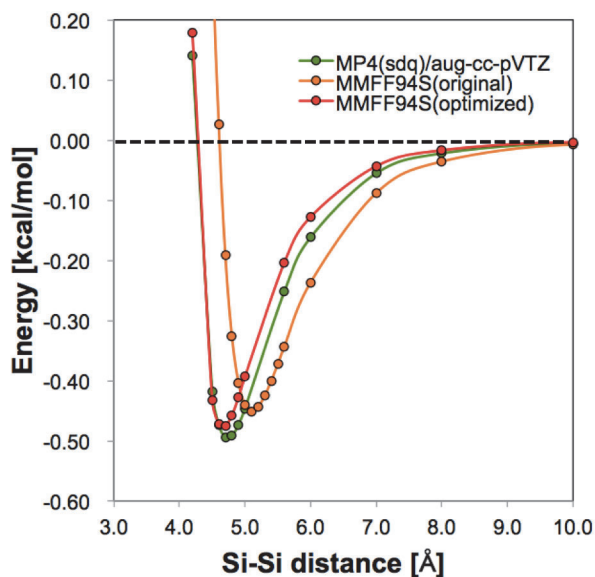


Figure 5.3. Potential energy of interacting two silane molecules. Energy at $r_{SiSi} = 20.0 \text{ \AA}$ (not shown) was set to 0.00 kcal/mol.

Table 5.3. Atomic polarizability (α), effective number of electrons (N), and two constants (A , G) of original and optimized MMFF94S.

	α	N	A	G
Original	4.5000	4.2000	3.3200	1.3450
Optimized	4.5000	4.2000	2.7568	0.8538

5.3.3. Optimization of Internal Coordinates, Rotational and Vibrational Frequencies, and Conformational Energies

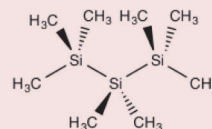
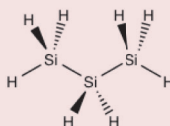
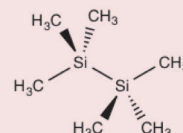
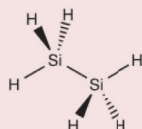
On the basis of the previous discussion, MP2/6-311G(d,p) was chosen as the default method to calculate geometry and vibrational frequency, and MP4(sdq)/cc-pVTZ for calculating single point energy (see, Section 5.2). GaussView 5.0 was used to generate an initial structure. Geometries at the ground and transition states were optimized at MP2/6-311G(d,p) level followed by vibrational analysis. For optimized structures at the ground and transition states, single point energy calculation was carried out at MP4(sdq)/cc-pVTZ level to estimate the energy at the ground state conformation and energy barrier at the transition state. The frequencies (cm^{-1}) calculated at MP2/6-31G(d,p) level were scaled by 0.9496.²⁰

The optimization steps for bonded interactions are divided into three major phases: parameterization of internal coordinates (phase 1, step 1–4, Fig. 5.4); parameterization of V_3 term (phase 2, step 5–7, Fig. 5.5); and parameterization of V_1 and V_2 terms (phase 3, step 8–13, Fig. 5.5). In steps 1 and 2, relatively simple structures and larger molecules (containing four silicon atoms) were used as reference structures because well description of their angle properties was crucial to reproduce their reference conformational energies. The rotational and vibrational frequencies were calculated only for molecules contain three silicon atoms or less in steps 1 and 2. Transition states of model structures in phase 2 possess relatively high symmetry compared to those listed in phase 3 so that those structure do not have more than one ground state conformation. It was possible to include transition structures of compounds in phase 3 that have two or three ground state conformations but those transition state structures were not used as references during the parameter optimization. This was to simplify the parameterization process of V_3 term by not using transition structures that depend on three parameters, V_1 , V_2 , and V_3 . The transition states of compounds in phase 3 were evaluated for the verification of the optimized parameters (see Section 5.4.4). In phase

3, the optimization of torsion parameters C-Si-Si-C, C-Si-Si-H, H-Si-Si-H, C-Si-Si-Si, H-Si-Si-Si, and Si-Si-Si-Si were repeated between steps 11 and 13. In step 11, model structures listed in step 13 were included as reference from the second cycle. This was because the conformational energies of the compounds listed in step 13 were not reproduced by optimization of V_1 and V_2 terms of Si-Si-Si-Si torsion.

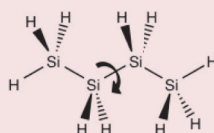
Step 1: Bond stretching

H-Si (5-19)
C-Si (1-19)
Si-Si (19-19)

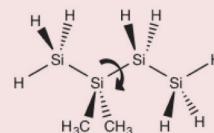


Step 2: Angle bending and stretch-bend

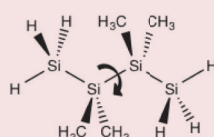
H-C-Si (5-1-19)
C-Si-C (1-19-1)
H-Si-H (5-19-5)
C-Si-Si (1-19-19)
H-Si-Si (5-19-19)
Si-Si-Si (19-19-19)



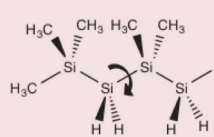
Si-Si-Si-Si = 60° and 180°



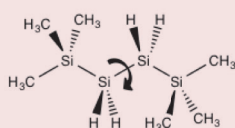
Si-Si-Si-Si = 60° and 180°



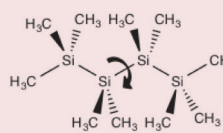
Si-Si-Si-Si = 60° and 180°



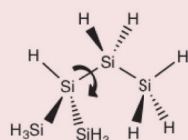
Si-Si-Si-Si = 60° and 180°



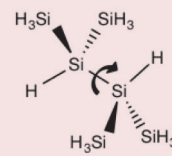
Si-Si-Si-Si = 60° and 180°



Si-Si-Si-Si = 60°, 100° and 180°



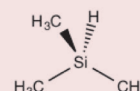
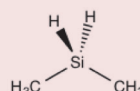
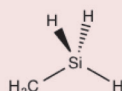
H-Si-Si-Si = 60° and 180°



H-Si-Si-H = 60° and 180°

Step 3:

C-Si-H (1-19-5)



Step 4

C-C-Si (1-1-19)

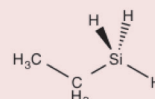
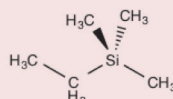
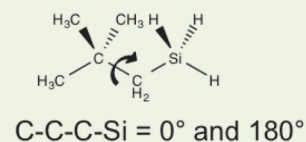
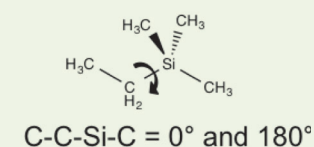
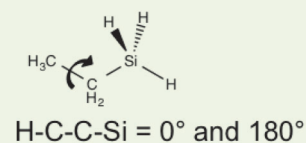
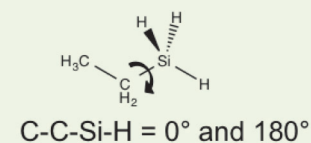
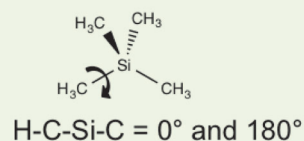
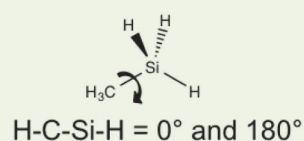


Fig. 5.4. The parameter optimization steps for the internal coordinates (Phase 1). Steps 1 and 2 share the same set of model structures. In steps 1 and 2, the vibration calculation was enabled only for molecules contain two and three Si atoms.

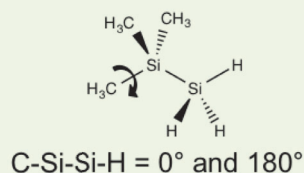
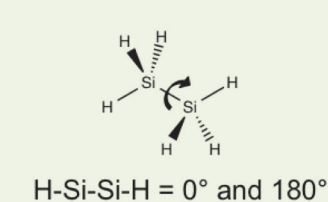
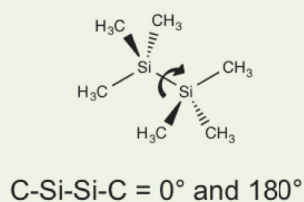
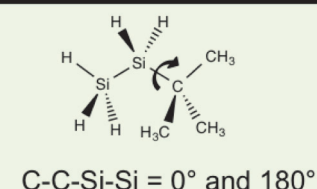
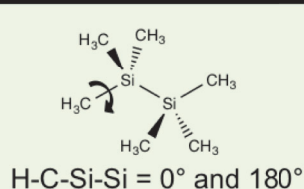
Step 5 : Torsion Interaction (V_3)

H-C-Si-H (5-1-19-5)
 H-C-Si-C (5-1-19-1)
 C-C-Si-H (1-1-19-5)
 C-C-Si-C (1-1-19-1)
 H-C-C-Si (5-1-1-19)
 C-C-C-Si (1-1-1-19)



Step 6

H-C-Si-Si (5-1-19-19)
 C-C-Si-Si (1-1-19-19)
 C-Si-Si-H (1-19-19-5)
 C-Si-Si-C (1-19-19-1)
 H-Si-Si-H (5-19-19-5)



Step 7

H-Si-Si-Si (5-19-19-19)
 C-Si-Si-Si (1-19-19-19)
 Si-Si-Si-Si (19-19-19-19)

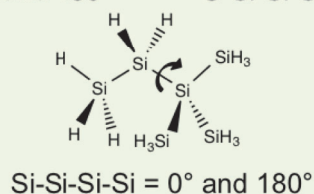
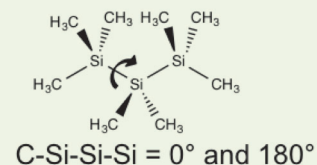
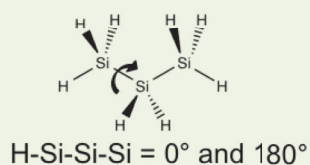
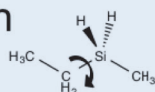


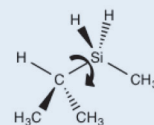
Fig. 5.5. The parameter optimization steps for V_3 term of the torsion parameter (Phase 2).

Step 8: Torsion interaction (V_1 and V_2)

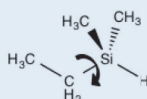
H-C-Si-H (5-1-19-5)
H-C-Si-C (5-1-19-1)
C-C-Si-H (1-1-19-5)
C-C-Si-C (1-1-19-1)



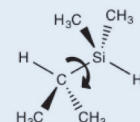
C-C-Si-C = 60° and 180°



H-C-Si-C = 60° and 180°



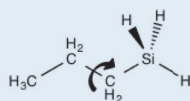
C-C-Si-H = 60° and 180°



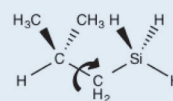
H-C-Si-H = 60° and 180°

Step 9

H-C-C-Si (5-1-1-19)
C-C-C-Si (1-1-1-19)



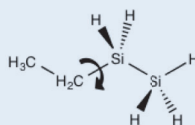
C-C-C-Si = 60° and 180°



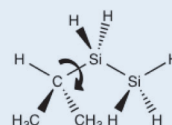
H-C-C-Si = 60° and 180°

Step 10

H-C-Si-Si (5-1-19-19)
C-C-Si-Si (1-1-19-19)



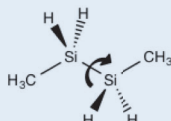
C-C-Si-Si = 60° and 180°



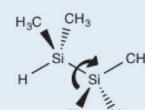
H-C-Si-Si = 60° and 180°

Step 11

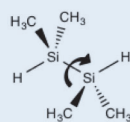
C-Si-Si-H (1-19-19-5)
C-Si-Si-C (1-19-19-1)
H-Si-Si-H (5-19-19-5)



C-Si-Si-C = 60° and 180°



H-Si-Si-C = 60° and 180°



H-Si-Si-H = 60° and 180°

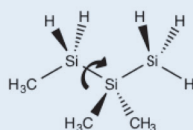
Fig. 5.6. The parameter optimization steps for V_1 and V_2 term of the torsion parameter (Phase 3).

Step 12: Torsion interaction

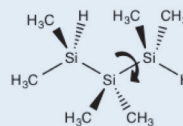
(V_1 and V_2)

H-Si-Si-Si (5-19-19-19)

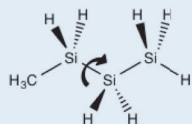
C-Si-Si-Si (1-19-19-19)



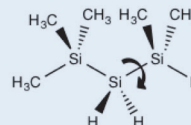
C-Si-Si-Si = 60° and 180°



H-Si-Si-Si = 60° and 180°



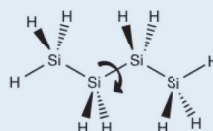
C-Si-Si-Si = 60° and 180°



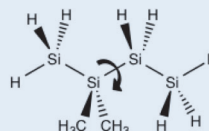
H-Si-Si-Si = 60° and 180°

Step 13

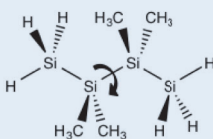
Si-Si-Si-Si (19-19-19-19)



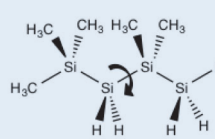
Si-Si-Si-Si = 60° and 180°



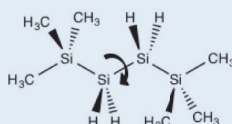
Si-Si-Si-Si = 60° and 180°



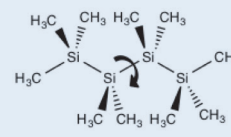
Si-Si-Si-Si = 60° and 180°



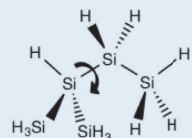
Si-Si-Si-Si = 60° and 180°



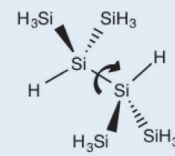
Si-Si-Si-Si = 60° and 180°



Si-Si-Si-Si = 60°,
100° and 180°



H-Si-Si-Si = 60° and 180°



H-Si-Si-H = 60° and 180°

Fig. 5.7. The parameter optimization steps for V_1 and V_2 term of the torsion parameter (Phase 3).

5.4. Results of Parameter Optimization

5.4.1. Parameter Table

Some silicon related parameters were optimized: 1-19 and 5-19 for bond stretching; 1-1-19, 1-19-1, 1-19-5, 5-1-19, and 5-19-5 for angle bending; 5-1-19-5 for torsion interaction. However, the rest of other parameter types are generated based on empirical rule and expected to reproduce the experimental value poorly (see Section 5.4.4).

All optimized parameters are listed in Table 5.4–5.7. In the list, parameters that already optimized in previous papers¹⁻⁸ were re-parameterized in this work because BCI and van der Waals parameters are basic parameters and subtle modifications of those parameters may alter optimal internal coordinates and torsion parameters dramatically.

Table 5.4. Optimized bond stretching parameters.

Bond stretching			
Atom types			
<i>I</i>	<i>J</i>	<i>k_b</i>	<i>r₀</i>
1	19	2.8034	1.8687
5	19	2.8043	1.4864
19	19	2.0611	2.3454

Table 5.5. Optimized angle bending parameters.

Angle bending				
Atom types				
<i>I</i>	<i>J</i>	<i>K</i>	<i>k_a</i>	<i>θ₀</i>
1	1	19	0.5915	111.4696
5	1	19	0.3554	113.3298
1	19	1	0.3387	112.6963
1	19	5	0.4992	110.7018
1	19	19	0.2852	114.3269
5	19	5	0.4312	109.5871
5	19	19	0.3624	111.1738
19	19	19	0.2702	120.0032

Table 5.6. Optimized stretch bending parameters.

Stretch bending				
Atom types				
<i>I</i>	<i>J</i>	<i>K</i>	k_{baJK}	k_{baKJI}
1	1	19	-0.3290	-0.6154
5	1	19	-0.1430	0.2320
1	19	1	0.0248	-0.0004
1	19	5	-0.0566	0.2828
1	19	19	0.2518	0.1048
5	19	5	0.0131	0.1000
5	19	19	0.0612	-0.0636
19	19	19	0.0176	-0.0025

Table 5.7. Optimized torsion parameters.

Torsion						
Atom types						
<i>I</i>	<i>J</i>	<i>K</i>	<i>L</i>	V_1	V_2	V_3
1	1	1	19	1.4531	1.1188	-0.0699
5	1	1	19	-0.3850	1.1378	0.0091
1	1	19	1	-0.1272	-0.3317	0.1967
1	1	19	5	-0.0676	0.0297	0.2230
1	1	19	19	-0.3086	-0.1983	0.0900
5	1	19	1	0.3497	0.2340	0.1398
5	1	19	5	-0.1941	-0.1775	0.1707
5	1	19	19	-0.4622	-0.2627	0.1854
1	19	19	1	-2.8293	-1.0790	0.0718
1	19	19	5	-1.5400	-0.3921	0.0945
1	19	19	19	-0.6549	-0.6248	0.0182
5	19	19	5	-0.3568	0.1528	0.1098
5	19	19	19	0.3502	-0.3341	0.0822
19	19	19	19	2.8224	-0.4435	0.1675

5.4.2. Internal Coordinates

Abbreviations of all model structures, bond length, and angle of the structures are shown in Table 5.8–5.14. The first number and Si in the ID represent the number of the silicon atoms in the compound and the following number specifies the structure in detail.

The RMSD of the bond stretching with respect to quantum mechanics data was 0.013 Å. The RMSD of bond length for 1-19, 5-19, and 19-19 were 0.020, 0.009, and 0.010, respectively. Several molecules that have 1-1-1-19 torsion, such as 1Si_15_neoPeSi, 1Si_10_PrSi, and 1Si_16_iBuSi showed specifically larger 1-19 bond length.

For the bond angle, the averaged RMSD was 0.6°. Each RMSD was 0.3° for 5-19-19 and 5-19-5, 0.4° for 1-19-5, 0.5° for 5-1-19, 1-19-1, and, 1-19-19, and 1.1° for 19-19-19, and 1.4° for 1-1-1-19. The error was large again for compounds with 1-1-1-19 torsion. Those results suggest that it is necessary to optimize the 1-1-19 angle bending and stretch-bend interaction parameter utilizing not only ethylsilane but also silane with longer alkyl side chains such as 1Si_10_PrSi, 1Si_15_neoPeSi, and 1Si_16_iBuSi as well.

The RMSD with respect to experimental data was also evaluated using silane, methylsilane, dimethylsilane, trimethylsilane, tetramethylsilane, ethylsilane, and ethylmethylsilane (see Table A.5.1–A.5.7 in appendix). The RMSD of the bond length compared to experimental data were 0.008 Å for MP2/6-311G(d,p), and 0.011 Å for MMFF94S based on the optimized parameter, respectively. The RMSD of the MMFF94S was slightly better than the average RMSD of MMFF94S, 0.012 Å², and it was comparable to RMSD of MM3²¹, which was 0.010 Å. For the angles, the RMSD were 0.9° for MP2/6-311G(d,p) and 1.1° for optimized MMFF94S, respectively. The RMSD of the MMFF94S was again, slightly better than the average RMSD of MMFF94S, 1.2°. The RMSD of MMFF94S was slightly worse than that of MM3 which was 0.7° but this comes from the discrepancy between the quantum mechanics data because the RMSD of MP2/6-311G(d,p) with

respect to experiment was larger than that of MM3. However, the emphasis should be made that there are various lacking experimental data especially for molecules with two or more silicon atoms and angle parameters such as, Si-Si-Si, C-Si-Si was covered by quantum mechanics data in this work.

Table 5.8. Structure ID, Symbol and the name of compounds.

ID	Symbol	Name
1Si_01	Si	silane
1Si_02	MeSi	methylsilane
1Si_03	diMeSi	dimethylsilane
1Si_04	trMeSi	trimethylsilane
1Si_05	teMeSi	tetramethylsilane
1Si_06	EtSi	ethylsilane
1Si_07	EttrMeSi	ethyltrimethylsilane
1Si_10	PrSi	propylsilane
1Si_11	EtMeSi	ethylmethylsilane
1Si_12	EtdiMeSi	ethyldimethylsilane
1Si_13	iPrMeSi	isopropylmethylsilane
1Si_14	iPrdiMeSi	isopropyldimethylsilane
1Si_15	neoPeSi	neopentylsilane
1Si_16	iBuSi	isobutylsilane
2Si_01	SiSi	disilane
2Si_04	trMeSiSi	1,1,1-trimethyldisilane
2Si_05	MeSiMeSi	1,2-dimethyldisilane
2Si_06	diMeSiMeSi	1,1,2-trimethyldisilane
2Si_09	trMeSiTrMeSi	1,1,1,2,2,2-hexamethyldisilane
2Si_10	diMeSidiMeSi	1,1,2,2-tetramethyldisilane
2Si_11	EtSiSi	ethyldisilane
2Si_15	iPrSiSi	isopropyldisilane
2Si_16	tButSiSi	tert-butylidisilane
3Si_01	SiSiSi	trisilane
3Si_08	trMeSidiMeSiTrMeSi	1,1,1,2,2,3,3,3-octamethyltrisilane
3Si_09	MeSiSiSi	1-methyltrisilane
3Si_12	MeSidiMeSiSi	1,2,2-trimethyltrisilane
3Si_15	trMeSiSidiMeSi	1,1,1,3,3-pentamethyltrisilane
3Si_17	diMeSidiMeSiTrMeSi	1,1,1,2,2,3,3-heptamethyltrisilane
4Si_01	SiSiSiSi	tetrasilane
4Si_02	SidiMeSiSiSi	2,2-dimethyltetrasilane
4Si_04	SidiMeSidiMeSiSi	2,2,3,3-tetramethyltetrasilane
4Si_07	trMeSiSiSiTrMeSi	1,1,1,4,4,4-hexamethyltetrasilane
4Si_09	trMeSiSidiMeSiSi	1,1,1,3,3-pentamethyltetrasilane
4Si_11	trMeSidiMeSidiMeSiTrMeSi	permethyltetrasilane
5Si_01	diSiSiSiSi	2-silyltetrasilane
6Si_01	SiSSidiSiSi	2,2-disilyltetrasilane
6Si_02	diSiSidiSiSi	2,3-disilyltetrasilane

Table 5.9. Bond lengths of MMFF94S based on optimized parameters (MM) and reference structure optimized at MP2/6-311G(d,p) level (QM).

ID ^a	Conformation		GS/TS ^d	Bond length [Å]					
	Type ^b	[deg] ^c		H-Si (5-19)		C-Si(1-19)		Si-Si (19-19)	
				MM	QM	MM	QM	MM	QM
1Si_01	No conf.		GS	1.486	1.475	-----	-----	-----	-----
1Si_02	No conf.		GS	1.488	1.470	1.877	1.940	-----	-----
1Si_03	No conf.		GS	1.491	1.481	1.878	1.878	-----	-----
1Si_04	No conf.		GS	1.497	1.485	1.879	1.879	-----	-----
1Si_05	HCSiC	0	TS	-----	-----	1.883	1.884	-----	-----
		180	GS	-----	-----	1.882	1.881	-----	-----
1Si_06	CCSiH	0	TS	1.487	1.479	1.895	1.894	-----	-----
	HCCSi	0	TS	1.487	1.479	1.903	1.881	-----	-----
	All	180	GS	1.488	1.479	1.891	1.883	-----	-----
1Si_07	CCSiC	0	TS	-----	-----	1.892	1.887	-----	-----
		180	GS	-----	-----	1.889	1.884	-----	-----
1Si_10	CCCSi	0	TS	1.487	1.479	1.972	1.889	-----	-----
		60	GS	1.487	1.479	1.910	1.887	-----	-----
		120	TS	1.487	1.479	1.906	1.881	-----	-----
		180	GS	1.488	1.479	1.893	1.884	-----	-----
1Si_11	CCSiC	0	TS	1.493	1.482	1.894	1.890	-----	-----
		60	GS	1.492	1.483	1.888	1.882	-----	-----
		120	TS	1.491	1.483	1.887	1.887	-----	-----
		180	GS	1.491	1.483	1.884	1.881	-----	-----
1Si_12	CCSiH	0	TS	1.498	1.487	1.886	1.886	-----	-----
		60	GS	1.499	1.487	1.886	1.882	-----	-----
		120	TS	1.501	1.486	1.891	1.887	-----	-----
		180	GS	1.498	1.486	1.888	1.883	-----	-----
1Si_13	HCSiC	0	TS	1.491	1.484	1.887	1.891	-----	-----
		60	GS	1.492	1.484	1.886	1.885	-----	-----
		120	TS	1.493	1.484	1.894	1.894	-----	-----
		180	GS	1.492	1.483	1.887	1.886	-----	-----
1Si_14	HCSiH	0	TS	1.504	1.487	1.898	1.893	-----	-----
		60	GS	1.500	1.487	1.889	1.885	-----	-----
		120	TS	1.501	1.487	1.891	1.890	-----	-----
		180	GS	1.500	1.489	1.888	1.885	-----	-----
1Si_15	CCCSi	0	TS	1.487	1.479	1.992	1.889	-----	-----
		180	GS	1.487	1.479	1.953	1.890	-----	-----
1Si_16	HCCSi	0	TS	1.487	1.480	1.909	1.881	-----	-----
		60	GS	1.487	1.479	1.916	1.887	-----	-----
		120	TS	1.487	1.479	1.982	1.889	-----	-----
		180	GS	1.487	1.479	1.941	1.891	-----	-----
2Si_01	HSiSiH	0	TS	1.488	1.478	-----	-----	2.353	2.353
		180	GS	1.488	1.478	-----	-----	2.353	2.343
2Si_04	CSiSiH	0	TS	1.488	1.482	1.891	1.884	2.368	2.360
		180	GS	1.488	1.482	1.891	1.884	2.368	2.350
2Si_05	CSiSiC	0	TS	1.492	1.482	1.882	1.886	2.356	2.358
		60	GS	1.492	1.482	1.883	1.886	2.357	2.346
		120	TS	1.492	1.483	1.883	1.885	2.357	2.356
		180	GS	1.492	1.483	1.882	1.885	2.355	2.346
2Si_06	HSiSiC	0	TS	1.494	1.485	1.886	1.885	2.363	2.358
		60	GS	1.494	1.485	1.885	1.886	2.361	2.347
		120	TS	1.494	1.484	1.885	1.886	2.362	2.359
		180	GS	1.494	1.484	1.886	1.887	2.363	2.348
2Si_09	HCSiSi	0	TS	-----	-----	1.891	1.889	2.386	2.364
	CSiSiC	0	TS	-----	-----	1.892	1.891	2.385	2.351
	All	180	GS	-----	-----	1.891	1.889	2.383	2.352
2Si_10	HSiSiH	0	TS	1.499	1.486	1.886	1.888	2.367	2.362
		60	GS	1.497	1.487	1.887	1.888	2.368	2.349
		120	TS	1.498	1.488	1.887	1.887	2.368	2.360
		180	GS	1.500	1.488	1.886	1.887	2.366	2.349
2Si_11	CCSiSi	0	TS	1.490	1.481	1.908	1.902	2.355	2.349
		60	GS	1.490	1.481	1.901	1.890	2.355	2.346
		120	TS	1.490	1.481	1.905	1.901	2.355	2.345
		180	GS	1.490	1.481	1.902	1.889	2.355	2.345

Table 5.10. Bond lengths of various structures based on MM and QM.

ID ^a	Conformation		GS/TS ^d	Bond length [Å]					
	Type ^b	[deg] ^c		H-Si (5-19)		C-Si(1-19)		Si-Si (19-19)	
				MM	QM	MM	QM	MM	QM
2Si_15	HCSiSi	0	TS	1.489	1.481	1.907	1.909	2.355	2.345
		60	GS	1.490	1.481	1.898	1.895	2.355	2.347
		120	TS	1.490	1.481	1.908	1.910	2.355	2.349
		180	GS	1.490	1.481	1.898	1.896	2.355	2.349
2Si_16	CCSiSi	0	TS	1.490	1.481	1.877	1.920	2.353	2.349
		180	GS	1.490	1.481	1.869	1.903	2.354	2.348
3Si_01	HSiSiSi	0	TS	1.489	1.479	-----	-----	2.343	2.347
		180	GS	1.489	1.479	-----	-----	2.343	2.343
3Si_08	CSiSiSi	0	TS	-----	-----	1.894	1.891	2.370	2.358
		180	GS	-----	-----	1.893	1.891	2.366	2.350
3Si_09	CSiSiSi	0	TS	1.489	1.480	1.882	1.883	2.344	2.350
		60	GS	1.490	1.480	1.883	1.883	2.343	2.344
		120	TS	1.490	1.480	1.882	1.883	2.344	2.348
		180	GS	1.490	1.481	1.882	1.883	2.343	2.344
3Si_12	CSiSiSi	0	TS	1.489	1.483	1.896	1.889	2.356	2.353
		60	GS	1.489	1.483	1.896	1.890	2.355	2.347
		120	TS	1.489	1.482	1.896	1.890	2.356	2.352
		180	GS	1.489	1.482	1.896	1.891	2.355	2.346
3Si_15	HSiSiSi	0	TS	1.492	1.487	1.889	1.884	2.350	2.353
		60	GS	1.493	1.487	1.888	1.885	2.350	2.350
		120	TS	1.494	1.486	1.887	1.885	2.351	2.356
		180	GS	1.493	1.486	1.888	1.886	2.350	2.351
3Si_17	HSiSiSi	0	TS	1.496	1.489	1.892	1.891	2.361	2.354
		60	GS	1.495	1.488	1.892	1.891	2.361	2.349
		120	TS	1.499	1.489	1.893	1.891	2.365	2.357
		180	GS	1.499	1.490	1.892	1.891	2.362	2.350
4Si_01	SiSiSiSi	0	TS	1.489	1.479	-----	-----	2.342	2.348
		60	GS	1.489	1.479	-----	-----	2.342	2.343
		120	TS	1.489	1.479	-----	-----	2.342	2.345
		180	GS	1.489	1.480	-----	-----	2.342	2.342
4Si_02	SiSiSiSi	0	TS	1.488	1.481	1.901	1.889	2.349	2.350
		60	GS	1.488	1.481	1.902	1.889	2.348	2.346
		120	TS	1.488	1.481	1.903	1.889	2.349	2.349
		180	GS	1.488	1.481	1.903	1.890	2.349	2.345
4Si_04	SiSiSiSi	0	TS	1.487	1.482	1.901	1.893	2.356	2.352
		60	GS	1.487	1.482	1.900	1.893	2.354	2.347
		120	TS	1.488	1.482	1.902	1.892	2.357	2.352
		180	GS	1.488	1.482	1.902	1.892	2.356	2.348
4Si_07	SiSiSiSi	0	TS	1.492	1.486	1.889	1.885	2.350	2.357
		60	GS	1.490	1.486	1.890	1.885	2.350	2.351
		120	TS	1.490	1.486	1.890	1.884	2.348	2.350
		180	GS	1.490	1.486	1.890	1.884	2.349	2.349
4Si_09	SiSiSiSi	0	TS	1.488	1.484	1.896	1.887	2.355	2.353
		60	GS	1.488	1.484	1.894	1.887	2.353	2.350
		120	TS	1.489	1.484	1.894	1.887	2.353	2.352
		180	GS	1.489	1.484	1.895	1.888	2.353	2.349
4Si_11	SiSiSiSi	0	TS	-----	-----	1.898	1.893	2.376	2.358
		60	GS	-----	-----	1.895	1.893	2.367	2.351
		100	GS	-----	-----	1.895	1.893	2.367	2.352
		120	TS	-----	-----	1.896	1.893	2.370	2.357
		160	GS	-----	-----	1.895	1.892	2.365	2.350
5Si_01	HSiSiSi	0	TS	1.488	1.480	-----	-----	2.338	2.343
		60	GS	1.488	1.479	-----	-----	2.338	2.342
		120	TS	1.488	1.480	-----	-----	2.338	2.346
		180	GS	1.488	1.479	-----	-----	2.337	2.343
6Si_01	SiSiSiSi	0	TS	1.487	1.479	-----	-----	2.334	2.343
		180	GS	1.487	1.479	-----	-----	2.333	2.341
6Si_02	HSiSiH	0	TS	1.488	1.479	-----	-----	2.336	2.347
		60	GS	1.488	1.480	-----	-----	2.336	2.342
		120	TS	1.488	1.480	-----	-----	2.337	2.344
		180	GS	1.488	1.479	-----	-----	2.336	2.343

Table 5.12. Angles of various structures based on MM and QM.

ID ^a	Conformation		GS/TS ^d	Angle [deg]							
	Type ^b	[deg] ^c		C-C-Si(1-1-19)		C-Si-Si(1-19-19)		H-Si-Si(5-19-19)		Si-Si-Si(19-19-19)	
				MM	QM	MM	QM	MM	QM	MM	QM
1Si_01	No conf.		GS	----	----	----	----	----	----	----	----
1Si_02	No conf.		GS	----	----	----	----	----	----	----	----
1Si_03	No conf.		GS	----	----	----	----	----	----	----	----
1Si_04	No conf.		GS	----	----	----	----	----	----	----	----
1Si_05	HCSiC	0	TS	----	----	----	----	----	----	----	----
		180	GS	----	----	----	----	----	----	----	----
1Si_06	CCSiH	0	TS	113.5	113.7	----	----	----	----	----	----
	HCCSi	0	TS	114.9	113.0	----	----	----	----	----	----
	All	180	GS	113.0	113.2	----	----	----	----	----	----
1Si_07	CCSiC	0	TS	115.9	115.6	----	----	----	----	----	----
		180	GS	114.9	114.5	----	----	----	----	----	----
1Si_10	CCCSi	0	TS	123.5	119.9	----	----	----	----	----	----
		60	GS	115.6	115.3	----	----	----	----	----	----
		120	TS	114.9	112.8	----	----	----	----	----	----
		180	GS	113.1	113.7	----	----	----	----	----	----
1Si_11	CCSiC	0	TS	115.4	115.1	----	----	----	----	----	----
		60	GS	113.9	113.5	----	----	----	----	----	----
		120	TS	113.5	114.0	----	----	----	----	----	----
		180	GS	112.8	113.5	----	----	----	----	----	----
1Si_12	CCSiH	0	TS	113.5	114.1	----	----	----	----	----	----
		60	GS	113.9	114.0	----	----	----	----	----	----
		120	TS	115.6	115.4	----	----	----	----	----	----
		180	GS	114.7	114.0	----	----	----	----	----	----
1Si_13	HCSiC	0	TS	112.0	112.1	----	----	----	----	----	----
		60	GS	111.9	111.4	----	----	----	----	----	----
		120	TS	113.1	112.3	----	----	----	----	----	----
		180	GS	112.2	111.8	----	----	----	----	----	----
1Si_14	HCSiH	0	TS	114.4	112.9	----	----	----	----	----	----
		60	GS	112.7	112.0	----	----	----	----	----	----
		120	TS	113.1	112.5	----	----	----	----	----	----
		180	GS	112.4	111.6	----	----	----	----	----	----
1Si_15	CCCSi	0	TS	124.7	120.5	----	----	----	----	----	----
		180	GS	120.8	119.4	----	----	----	----	----	----
1Si_16	HCCSi	0	TS	115.0	112.3	----	----	----	----	----	----
		60	GS	116.2	115.9	----	----	----	----	----	----
		120	TS	124.1	120.3	----	----	----	----	----	----
		180	GS	119.7	118.4	----	----	----	----	----	----
2Si_01	HSiSiH	0	TS	----	----	----	----	110.7	110.4	----	----
		180	GS	----	----	----	----	110.7	110.2	----	----
2Si_04	CSiSiH	0	TS	----	----	109.9	109.6	110.9	111.1	----	----
		180	GS	----	----	109.9	109.6	110.8	111.0	----	----
2Si_05	CSiSiC	0	TS	----	----	112.2	110.8	109.8	110.1	----	----
		60	GS	----	----	111.6	110.8	110.0	109.8	----	----
		120	TS	----	----	111.9	111.4	109.9	109.6	----	----
		180	GS	----	----	112.4	112.0	109.7	109.1	----	----
2Si_06	HSiSiC	0	TS	----	----	111.1	111.2	109.8	109.1	----	----
		60	GS	----	----	111.3	110.9	109.6	109.3	----	----
		120	TS	----	----	111.3	110.7	109.6	109.8	----	----
		180	GS	----	----	110.7	110.3	110.0	109.9	----	----
2Si_09	CSiSiC	0	TS	----	----	110.1	110.5	----	----	----	----
	HCSiSi	0	TS	----	----	109.7	110.2	----	----	----	----
	All	180	GS	----	----	109.8	110.2	----	----	----	----
2Si_10	HSiSiH	0	TS	----	----	111.1	110.5	109.1	109.9	----	----
		60	GS	----	----	110.6	110.4	109.6	109.6	----	----
		120	TS	----	----	110.8	110.9	109.4	108.8	----	----
		180	GS	----	----	111.0	110.9	108.9	108.4	----	----
2Si_11	CCSiSi	0	TS	114.9	115.2	113.4	113.1	110.2	109.6	----	----
		60	GS	113.6	113.6	111.7	111.5	110.4	110.0	----	----
		120	TS	113.9	113.2	111.3	111.8	110.4	110.0	----	----
		180	GS	113.6	113.2	111.0	111.6	110.4	110.1	----	----

Table 5.11. Angles of various structures based on MM and QM.

ID ^a	Conformation		GS/TS ^d	Angle [deg]					
	Type ^b	[deg] ^c		H-Si-H(5-19-5)		C-Si-H(1-19-5)		H-C-Si(5-1-19)	
				MM	QM	MM	QM	MM	QM
1Si_01	No conf.		GS	109.5	109.5	-----	-----	-----	-----
1Si_02	No conf.		GS	108.9	109.5	110.1	109.5	111.2	109.5
1Si_03	No conf.		GS	108.3	107.8	109.4	109.5	111.2	111.0
1Si_04	No conf.		GS	-----	-----	108.6	108.8	111.2	111.1
1Si_05	HCSiC	0	TS	-----	-----	-----	-----	111.2	111.2
		180	GS	-----	-----	-----	-----	111.2	111.2
1Si_06	CCSiH	0	TS	108.7	108.3	110.2	110.6	109.1	108.8
	HCCSi	0	TS	108.8	108.7	110.2	110.2	108.5	108.4
	All	180	GS	108.8	108.7	110.1	110.3	109.3	108.7
1Si_07	CCSiC	0	TS	-----	-----	-----	-----	110.7	110.7
		180	GS	-----	-----	-----	-----	110.7	110.7
1Si_10	CCCSi	0	TS	108.5	108.4	110.4	110.5	105.3	105.8
		60	GS	108.7	108.5	110.3	110.4	108.1	108.1
		120	TS	108.8	108.7	110.2	110.2	107.8	108.7
		180	GS	108.8	108.6	110.1	110.3	108.8	108.9
1Si_11	CCSiC	0	TS	107.7	107.3	108.8	109.3	110.1	110.0
		60	GS	108.0	108.0	109.2	109.4	110.3	110.1
		120	TS	107.9	107.6	109.4	109.5	110.4	110.1
		180	GS	108.4	107.6	109.4	109.4	110.5	110.1
1Si_12	CCSiH	0	TS	-----	-----	108.7	108.5	110.7	110.5
		60	GS	-----	-----	108.5	108.6	110.7	110.5
		120	TS	-----	-----	108.1	108.6	110.5	110.4
		180	GS	-----	-----	108.5	108.8	110.6	110.5
1Si_13	HCSiC	0	TS	107.7	107.7	109.5	109.5	110.2	109.8
		60	GS	108.1	107.9	109.1	109.3	110.2	110.0
		120	TS	107.5	107.5	108.8	109.1	109.9	109.9
		180	GS	107.7	108.1	109.1	109.4	110.1	109.9
1Si_14	HCSiH	0	TS	-----	-----	107.6	108.2	110.3	110.4
		60	GS	-----	-----	108.2	108.6	110.5	110.4
		120	TS	-----	-----	108.1	108.3	110.5	110.4
		180	GS	-----	-----	108.2	108.5	110.6	110.5
1Si_15	CCCSi	0	TS	108.4	108.4	110.5	110.5	103.4	105.8
		180	GS	108.5	108.3	110.5	110.6	105.5	106.9
1Si_16	HCCSi	0	TS	108.8	108.7	110.2	110.2	107.1	108.9
		60	GS	108.6	108.5	110.3	110.4	107.4	108.2
		120	TS	108.5	108.4	110.5	110.5	104.4	105.8
		180	GS	108.5	108.3	110.4	110.6	106.5	106.9
2Si_01	HSiSiH	0	TS	108.2	108.5	-----	-----	-----	-----
		180	GS	108.2	108.7	-----	-----	-----	-----
2Si_04	CSiSiH	0	TS	108.0	107.8	-----	-----	111.1	111.1
		180	GS	108.1	107.9	-----	-----	111.1	111.1
2Si_05	CSiSiC	0	TS	107.5	107.4	108.7	109.2	111.1	111.0
		60	GS	107.9	107.6	108.6	109.4	111.1	111.0
		120	TS	107.6	107.3	108.7	109.4	111.1	111.0
		180	GS	106.9	107.3	109.0	109.6	111.1	110.9
2Si_06	HSiSiC	0	TS	107.5	107.0	108.5	108.8	111.1	111.0
		60	GS	107.2	107.1	108.4	108.9	111.1	111.0
		120	TS	107.5	107.1	108.4	108.8	111.1	111.1
		180	GS	108.3	107.4	108.6	108.9	111.1	111.1
2Si_09	CSiSiC	0	TS	-----	-----	-----	-----	111.1	111.2
	HCSiSi	0	TS	-----	-----	-----	-----	111.1	111.2
	All	180	GS	-----	-----	-----	-----	111.0	111.2
2Si_10	HSiSiH	0	TS	-----	-----	108.0	108.2	111.1	111.1
		60	GS	-----	-----	108.4	108.5	111.1	111.1
		120	TS	-----	-----	108.1	108.2	111.1	111.1
		180	GS	-----	-----	107.8	108.3	111.1	111.1
2Si_11	CCSiSi	0	TS	108.0	108.1	108.6	110.1	108.5	108.1
		60	GS	108.0	108.3	108.9	109.5	109.0	108.5
		120	TS	108.0	108.2	109.2	109.6	108.9	109.1
		180	GS	108.1	108.2	109.1	109.2	108.9	108.7

Table 5.13. Angles of various structures based on MM and QM.

ID ^a	Conformation			Angle [deg]							
	Type ^b	[deg] ^c	GS/TS ^d	H-Si-H(5-19-5)		C-Si-H(1-19-5)		H-C-Si(5-1-19)		C-Si-C(1-19-1)	
				MM	QM	MM	QM	MM	QM	MM	QM
2Si_15	HCSiSi	0	TS	108.0	108.2	109.5	109.5	106.5	107.7	-----	-----
		60	GS	108.0	108.3	109.0	109.0	106.9	107.1	-----	-----
		120	TS	107.9	108.1	108.8	109.6	106.0	106.1	-----	-----
2Si_16	CCSiSi	0	TS	107.8	108.1	108.8	109.4	-----	-----	-----	-----
		180	GS	108.0	108.3	108.9	109.3	106.8	105.8	-----	-----
		180	GS	108.0	108.3	108.7	108.8	-----	-----	-----	-----
3Si_01	HSiSiSi	0	TS	108.3	108.5	-----	-----	-----	-----	-----	-----
		180	GS	108.3	108.6	-----	-----	-----	-----	-----	-----
3Si_08	CSiSiSi	0	TS	-----	-----	-----	-----	111.0	111.1	108.6	108.3
		180	GS	-----	-----	-----	-----	111.0	111.1	109.1	108.6
3Si_09	CSiSiSi	0	TS	108.0	108.2	109.2	109.5	111.1	111.0	-----	-----
		60	GS	108.2	108.3	109.0	109.7	111.1	111.0	-----	-----
		120	TS	108.1	108.2	108.9	109.8	111.1	110.9	-----	-----
		180	GS	107.9	108.2	109.0	109.8	111.1	110.9	-----	-----
3Si_12	CSiSiSi	0	TS	108.1	107.9	109.1	109.2	110.9	111.0	108.6	109.2
		60	GS	108.2	107.9	109.1	109.5	110.9	111.0	109.2	109.4
		120	TS	108.3	107.9	108.7	109.3	111.0	111.0	108.5	109.0
		180	GS	108.3	108.0	108.7	109.4	111.0	111.0	107.9	108.9
3Si_15	HSiSiSi	0	TS	107.5	107.0	108.6	108.1	111.1	111.0	109.4	109.5
		60	GS	107.0	107.0	108.4	108.5	111.1	111.0	109.3	109.4
		120	TS	106.8	106.6	107.8	108.4	111.1	111.1	109.0	109.1
		180	GS	107.9	107.2	108.1	108.5	111.1	111.1	109.3	109.2
3Si_17	HSiSiSi	0	TS	-----	-----	108.4	107.7	111.0	111.1	109.3	109.0
		60	GS	-----	-----	108.7	108.2	111.0	111.1	109.1	108.8
		120	TS	-----	-----	107.8	107.9	111.0	111.1	108.8	108.6
		180	GS	-----	-----	107.7	108.1	111.0	111.1	109.5	108.9
4Si_01	SiSiSiSi	0	TS	108.2	108.5	-----	-----	-----	-----	-----	-----
		60	GS	108.3	108.6	-----	-----	-----	-----	-----	-----
		120	TS	108.2	108.5	-----	-----	-----	-----	-----	-----
		180	GS	108.1	108.6	-----	-----	-----	-----	-----	-----
4Si_02	SiSiSiSi	0	TS	108.3	108.3	-----	-----	110.9	111.0	108.4	109.6
		60	GS	108.3	108.4	-----	-----	110.9	111.0	108.9	109.4
		120	TS	108.3	108.3	-----	-----	110.9	111.0	108.9	109.1
		180	GS	108.4	108.3	-----	-----	110.9	111.1	108.9	109.3
4Si_04	SiSiSiSi	0	TS	108.5	108.2	-----	-----	110.9	111.1	108.3	108.9
		60	GS	108.5	108.1	-----	-----	110.9	111.1	108.5	109.1
		120	TS	108.4	108.1	-----	-----	110.9	111.1	108.7	108.7
		180	GS	108.4	108.0	-----	-----	110.9	111.1	109.9	109.4
4Si_07	SiSiSiSi	0	TS	105.7	106.6	-----	-----	111.1	111.1	108.8	109.0
		60	GS	107.4	107.2	-----	-----	111.1	111.1	109.3	109.1
		120	TS	107.7	106.8	-----	-----	111.1	111.1	109.4	109.4
		180	GS	107.3	106.9	-----	-----	111.1	111.1	109.4	109.4
4Si_09	SiSiSiSi	0	TS	107.8	107.6	-----	-----	111.0	111.0	108.8	109.2
		60	GS	108.1	107.8	-----	-----	111.0	111.0	109.0	109.1
		120	TS	108.1	107.8	-----	-----	111.0	111.1	108.9	108.9
		180	GS	108.2	107.9	-----	-----	111.0	111.1	109.1	109.1
4Si_11	SiSiSiSi	0	TS	-----	-----	-----	-----	111.0	111.1	108.3	108.2
		60	GS	-----	-----	-----	-----	111.0	111.1	108.7	108.4
		100	GS	-----	-----	-----	-----	111.0	111.1	108.7	108.3
		120	TS	-----	-----	-----	-----	111.0	111.1	108.7	108.3
		160	GS	-----	-----	-----	-----	111.0	111.1	109.3	108.6
5Si_01	HSiSiSi	0	TS	108.5	108.7	-----	-----	-----	-----	-----	-----
		60	GS	108.5	108.7	-----	-----	-----	-----	-----	-----
		120	TS	108.5	108.7	-----	-----	-----	-----	-----	-----
		180	GS	108.6	108.7	-----	-----	-----	-----	-----	-----
6Si_01	SiSiSiSi	0	TS	108.7	108.7	-----	-----	-----	-----	-----	-----
		180	GS	108.8	108.8	-----	-----	-----	-----	-----	-----
6Si_02	HSiSiH	0	TS	108.8	108.8	-----	-----	-----	-----	-----	-----
		60	GS	108.8	108.8	-----	-----	-----	-----	-----	-----
		120	TS	108.8	108.8	-----	-----	-----	-----	-----	-----
		180	GS	108.8	108.8	-----	-----	-----	-----	-----	-----

Table 5.14. Angles of various structures based on MM and QM.

ID ^a	Conformation		GS/TS ^d	Angle [deg]							
				C-C-Si(1-1-19)		C-Si-Si(1-19-19)		H-Si-Si(5-19-19)		Si-Si-Si(19-19-19)	
	Type ^b	[deg] ^c		MM	QM	MM	QM	MM	QM	MM	QM
2Si_15	HCSiSi	0	TS	112.4	111.4	111.1	111.4	110.3	110.0	-----	-----
		60	GS	112.0	111.3	112.0	112.1	110.3	110.1	-----	-----
		120	TS	112.8	112.1	113.7	113.6	110.1	109.6	-----	-----
		180	GS	112.0	111.8	112.1	112.0	110.3	109.9	-----	-----
2Si_16	CCSiSi	0	TS	110.1	110.0	115.4	113.8	109.8	109.6	-----	-----
		180	GS	109.7	109.7	113.7	112.8	110.1	110.0	-----	-----
3Si_01	HSiSiSi	0	TS	-----	-----	-----	-----	110.0	110.0	112.3	111.0
		180	GS	-----	-----	-----	-----	110.0	109.8	112.3	111.8
3Si_08	CSiSiSi	0	TS	-----	-----	109.7	109.8	-----	-----	112.7	114.0
		180	GS	-----	-----	109.7	109.9	-----	-----	109.7	111.2
3Si_09	CSiSiSi	0	TS	-----	-----	111.9	111.0	109.8	109.7	112.0	111.6
		60	GS	-----	-----	111.5	110.8	109.8	109.7	111.5	111.4
		120	TS	-----	-----	111.9	110.6	109.8	109.7	111.9	111.7
		180	GS	-----	-----	112.2	112.0	109.8	109.5	112.3	112.4
3Si_12	CSiSiSi	0	TS	-----	-----	109.9	110.0	110.2	110.2	110.6	109.9
		60	GS	-----	-----	109.8	109.8	110.2	110.3	110.0	109.7
		120	TS	-----	-----	110.0	109.8	110.2	110.4	110.3	110.1
		180	GS	-----	-----	109.9	109.6	110.3	110.4	110.8	110.8
3Si_15	HSiSiSi	0	TS	-----	-----	110.0	110.2	109.8	109.4	109.2	111.0
		60	GS	-----	-----	110.1	110.2	109.6	109.2	110.4	112.0
		120	TS	-----	-----	110.7	110.4	108.8	108.6	114.0	115.4
		180	GS	-----	-----	110.3	110.0	109.3	109.5	110.8	111.8
3Si_17	HSiSiSi	0	TS	-----	-----	110.1	110.1	108.7	109.5	107.6	109.7
		60	GS	-----	-----	110.0	109.9	109.2	109.3	108.9	110.9
		120	TS	-----	-----	109.9	109.9	108.5	108.3	112.8	113.8
		180	GS	-----	-----	109.9	110.0	108.3	109.3	109.5	110.4
4Si_01	SiSiSiSi	0	TS	-----	-----	-----	-----	109.9	109.4	111.5	113.7
		60	GS	-----	-----	-----	-----	109.8	109.6	111.7	111.6
		120	TS	-----	-----	-----	-----	109.7	109.8	112.8	110.7
		180	GS	-----	-----	-----	-----	109.7	109.6	113.3	112.0
4Si_02	SiSiSiSi	0	TS	-----	-----	109.6	108.8	110.1	109.7	110.5	113.3
		60	GS	-----	-----	109.4	109.4	110.1	110.0	110.5	110.9
		120	TS	-----	-----	109.2	109.6	110.0	110.0	111.7	110.5
		180	GS	-----	-----	109.0	109.4	110.0	110.1	111.7	110.5
4Si_04	SiSiSiSi	0	TS	-----	-----	109.8	108.8	110.4	110.8	109.4	112.8
		60	GS	-----	-----	109.8	109.3	110.4	110.8	109.2	110.4
		120	TS	-----	-----	109.3	109.5	110.5	110.8	110.8	110.0
		180	GS	-----	-----	109.2	109.6	110.5	110.9	110.3	109.1
4Si_07	SiSiSiSi	0	TS	-----	-----	110.1	109.9	107.5	107.4	120.1	120.0
		60	GS	-----	-----	109.7	109.8	109.2	109.0	112.4	113.4
		120	TS	-----	-----	109.5	109.5	109.5	109.8	111.0	110.6
		180	GS	-----	-----	109.6	109.5	109.4	109.4	111.7	112.3
4Si_09	SiSiSiSi	0	TS	-----	-----	109.0	108.9	109.6	109.2	114.9	116.1
		60	GS	-----	-----	109.5	109.5	110.0	109.8	111.1	112.1
		120	TS	-----	-----	109.7	109.9	109.5	109.5	112.6	112.1
		180	GS	-----	-----	109.4	109.5	109.8	110.0	111.6	111.2
4Si_11	SiSiSiSi	0	TS	-----	-----	108.7	108.7	-----	-----	118.7	119.3
		60	GS	-----	-----	109.3	109.4	-----	-----	113.2	114.1
		100	GS	-----	-----	109.5	109.6	-----	-----	112.2	112.8
		120	TS	-----	-----	109.3	109.6	-----	-----	113.3	113.4
		160	GS	-----	-----	109.4	109.8	-----	-----	110.3	110.7
5Si_01	HSiSiSi	0	TS	-----	-----	-----	-----	109.6	109.7	111.3	110.3
		60	GS	-----	-----	-----	-----	109.6	109.6	111.3	110.8
		120	TS	-----	-----	-----	-----	109.6	109.5	111.2	111.4
		180	GS	-----	-----	-----	-----	109.7	109.6	110.7	110.7
6Si_01	SiSiSiSi	0	TS	-----	-----	-----	-----	109.8	109.8	109.9	110.0
		180	GS	-----	-----	-----	-----	109.9	109.9	109.8	109.8
6Si_02	HSiSiH	0	TS	-----	-----	-----	-----	109.4	109.3	111.0	111.3
		60	GS	-----	-----	-----	-----	109.5	109.6	110.6	110.2
		120	TS	-----	-----	-----	-----	109.5	109.4	110.9	110.7
		180	GS	-----	-----	-----	-----	109.4	109.5	110.9	110.7

5.4.3. Rotational and Vibrational Frequencies

The rotational and vibrational frequencies of various molecules and RMSD with respect to quantum mechanics data are listed in Table 5.15. The rotational and vibrational frequencies were attributed automatically. The structures with relatively high RMSD were 4Si_02_SidiMeSiSiSi (Si-Si-Si-Si = 60°), 4Si_11_trMeSidiMeSidiMeSitrMeSi (Si-Si-Si-Si = 60°), and 3Si_17_diMeSidiMeSitrMeSi (H-Si-Si-Si = 60° and 180°). In those compounds, the two frequencies at 130–190 cm⁻¹ and 700–1400 cm⁻¹ were switched. This was responsible for the raise in RMSD. After manually correcting the attribution, the averaged RMSD became less than 40 cm⁻¹.

The RMSD with respect to experimental data are calculated for silane, methylsilane, dimethylsilane, trimethylsilane, and disilane (see Fig A.5.8–5.12 in appendix). The RMSD of the vibrational frequency of MP2/6-311G(d,p) data scaled by 0.9496²⁰ was 32 cm⁻¹. The scaling factor was optimized to find the best match between the experimental and the MP2/6-311G(d,p) data, and the value was 0.9426 and minimum RMSD was 30 cm⁻¹, which showed very close value to the proposed scaling factor of 0.9496 by Scott and Radom. The RMSD of optimized MMFF94S was 51 cm⁻¹, which is slightly better than 61 cm⁻¹, the averaged value of MMFF94S. The value is comparable to RMSD of MM3, which is 47 cm⁻¹.

Table 5.15. RMSD of rotational and vibrational frequency for various molecular structure and conformations. Basically, the normal modes were attributed automatically but rotational and vibrational frequencies of some large molecules were misattributed and correction was necessary.

ID+Symbol	Conformation		Vibrational frequency (auto) [cm-1]	Vibrational frequency (corrected)	
	Type	[deg]		[cm-1]	
1Si_01_Si	No conf.		48		---
1Si_02_MeSi	No conf.		63		---
1Si_03_diMeSi	No conf.		52		---
1Si_04_trMeSi	No conf.		46		---
1Si_05_teMeSi	HCSiC	180	33		---
1Si_06_EtSi	All	180	36		---
1Si_07_EttrMeSi	CCSiC	180	34		---
1Si_10_ProSi	CCCSi	60	40		---
1Si_10_ProSi	CCCSi	180	35		---
1Si_11_EtMeSi	CCSiC	60	47		---
1Si_11_EtMeSi	CCSiC	180	46		---
1Si_12_EtdiMeSi	CCSiH	60	41		---
1Si_12_EtdiMeSi	CCSiH	180	40		---
1Si_13_iPrMeSi	HCSiC	60	48		---
1Si_13_iPrMeSi	HCSiC	180	48		---
1Si_14_iPrdiMeSi	HCSiH	60	49		---
1Si_14_iPrdiMeSi	HCSiH	180	50		---
1Si_16_diMeetSi	HCCSi	60	44		---
1Si_16_diMeetSi	HCCSi	180	48		---
2Si_11_EtSiSi	CCSiSi	60	34		---
2Si_11_EtSiSi	CCSiSi	180	50		---
2Si_15_iPrSiSi	HCSiSi	60	44		---
2Si_15_iPrSiSi	HCSiSi	180	48		---
2Si_16_tButSiSi	CCSiSi	180	51		---
2Si_01_SiSi	HSiSiH	180	53		---
2Si_04_trMeSiSi	CSiSiH	180	26		---
2Si_05_MeSiMeSi	CSiSiC	60	46		---
2Si_05_MeSiMeSi	CSiSiC	180	48		---
2Si_06_diMeSiMeSi	HSiSiC	60	45		---
2Si_06_diMeSiMeSi	HSiSiC	180	44		---
2Si_09_trMeSitrMeSi	All	180	29		---
2Si_09_trMeSitrMeSi	All	180	29		---
2Si_10_diMeSidiMeSi	HSiSiH	60	43		---
2Si_10_diMeSidiMeSi	HSiSiH	180	43		---
3Si_01_SiSiSi	HSiSiSi	180	38		---
3Si_08_trMeSidiMeSitrMeSi	CSiSiSi	180	27		---
3Si_09_MeSiSiSi	CSiSiSi	60	47		---
3Si_09_MeSiSiSi	CSiSiSi	180	46		---
3Si_12_MeSidiMeSiSi	CSiSiSi	60	35		---
3Si_12_MeSidiMeSiSi	CSiSiSi	180	33		---
3Si_15_trMeSiSidiMeSi	HSiSiSi	60	36		---
3Si_15_trMeSiSidiMeSi	HSiSiSi	180	33		---
3Si_17_trMeSidiMeSitrMeSi	HSiSiSi	60	86		34
3Si_17_trMeSidiMeSitrMeSi	HSiSiSi	180	84		33
4Si_01_SiSiSiSi	SiSiSiSi	60	33		---
4Si_01_SiSiSiSi	SiSiSiSi	180	34		---
4Si_02_SidiMeSiSiSi	SiSiSiSi	60	107		30
4Si_02_SidiMeSiSiSi	SiSiSiSi	180	32		---
4Si_04_SidiMeSidiMeSiSi	SiSiSiSi	60	28		---
4Si_04_SidiMeSidiMeSiSi	SiSiSiSi	180	28		---
4Si_07_trMeSiSiSitrMeSi	SiSiSiSi	60	33		---
4Si_07_trMeSiSiSitrMeSi	SiSiSiSi	180	34		---
4Si_09_trMeSiSidiMeSiSi	SiSiSiSi	60	32		---
4Si_09_trMeSiSidiMeSiSi	SiSiSiSi	180	32		---
4Si_11_trMeSidiMeSidiMeSitrMeSi	SiSiSiSi	60	157		28
4Si_11_trMeSidiMeSidiMeSitrMeSi	SiSiSiSi	100	73		27
4Si_11_trMeSidiMeSidiMeSitrMeSi	SiSiSiSi	160	27		---
5Si_01_diSiSiSiSi	HSiSiSi	60	30		---
6Si_02_diSiSiSiSiSi	HSiSiH	60	30		---
AVERAGE:			45		39

5.4.4. Conformational Energies

Conformational energies based on original parameter were summarized in Figure 5.8 and 5.9. The main purpose of the parameter optimization was to adjust the conformational energy of the oligosilane to reproduce the high-level quantum mechanics data. Actually, the conformational energies based on the original MMFF94S parameter showed large errors for oligosilanes with more than three silicon atoms and thus the optimization of the parameters was required. The large error was caused by (1) poor description of the original BCI parameters for 1-19 and 5-19 (Section 5.3.1), and (2) limited optimized torsion parameters and low accuracy of the potential derived from empirical rule that compensate the lacking torsion parameters. The effect of the latter is evident but the former also could be responsible. This is because the conformational energy especially for 4Si could not be reproduced without the re-parameterization of the BCI. The error in transition states was also large especially for 4Si and 5Si groups.

The energies based on the optimized parameters were compared with MP4(sdq)/cc-pVTZ//MP2/6-311G(d,p) in Figures 5.10 and 5.11. Overall, the averaged RMSD for ground and transition states were 0.17 and 0.30 kcal/mol, respectively. The 4Si_07 at *gauche* conformation showed relatively large error (0.71 kcal/mol) compared to the other structures. The 4Si_07 increases the RMSD dramatically and RMSD without this molecule was 0.06 kcal/mol.

A comparison of energy barrier with the experimental data was made in Table A.5.13. Methylsilane, dimethylsilane, trimethylsilane, tetramethylsilane, ethylsilane, propylsilane, and ethylmethylsilane were used as the model compounds. The steric energy and electronic energy were used for MMFF94S and MP4(sdq)/cc-pVTZ, and the RMSD were 0.25 and 0.26, respectively. The error for MM3 was 0.09 kcal/mol.

Figure 5.8. Evaluation of the conformational energy based on original parameters. The graphs summarize energy differences between MMFF94S (with original parameters) and MP4(sdq)/cc-pVTZ//MP2/6-311G(d,p) level of conformations relative to the most stable conformation. The data points include all model structures listed in Figure 5.4–5.7. The 4Si_11 written with red has two conformations that are Si-Si-Si-Si $\sim 60^\circ$ (4Si_11_60) and $\sim 100^\circ$ (4Si_11_100).

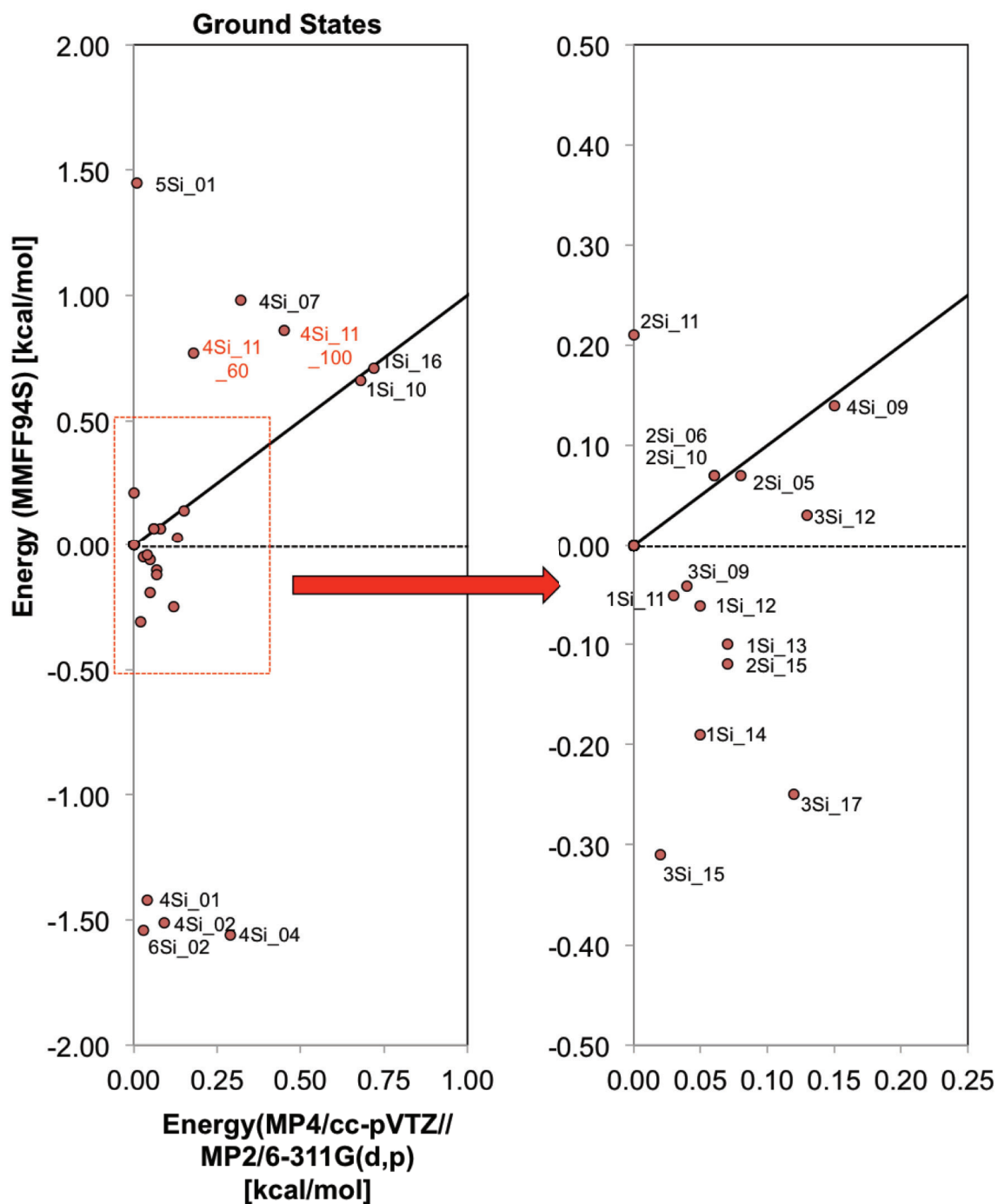


Figure 5.9. Evaluation of the transition energy based on original parameters. The graph summarize energy differences between MMFF94S (with original parameters) and MP4(sdq)/cc-pVTZ//MP2/6-311G(d,p) level of conformations relative to the most stable conformation. The data points include transition states of all model structures listed in Figure 5.4–5.7.

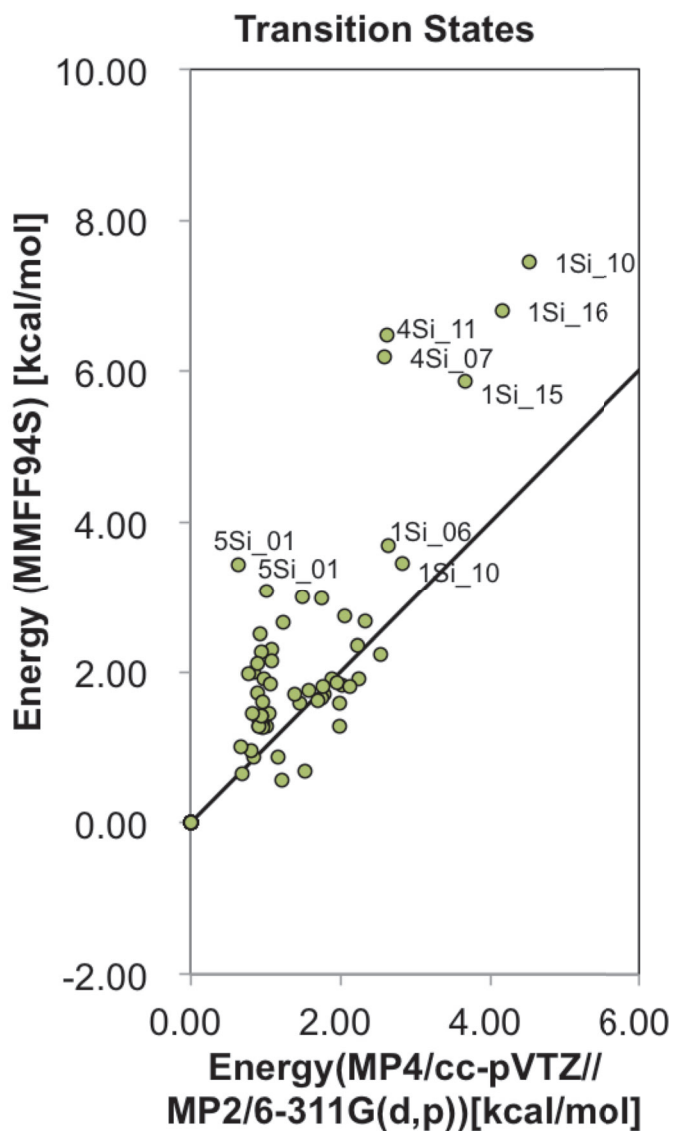


Figure 5.10. Evaluation of the conformational energy based on optimized parameters. See Figure 5.8 for detail.

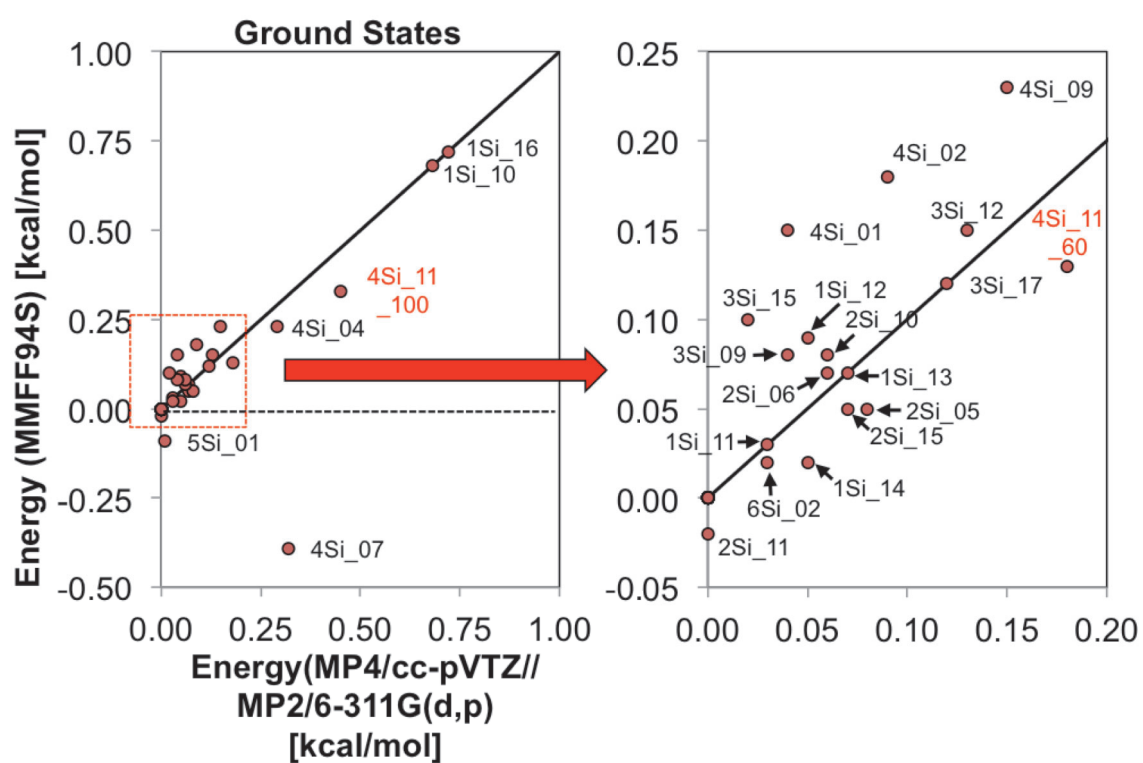
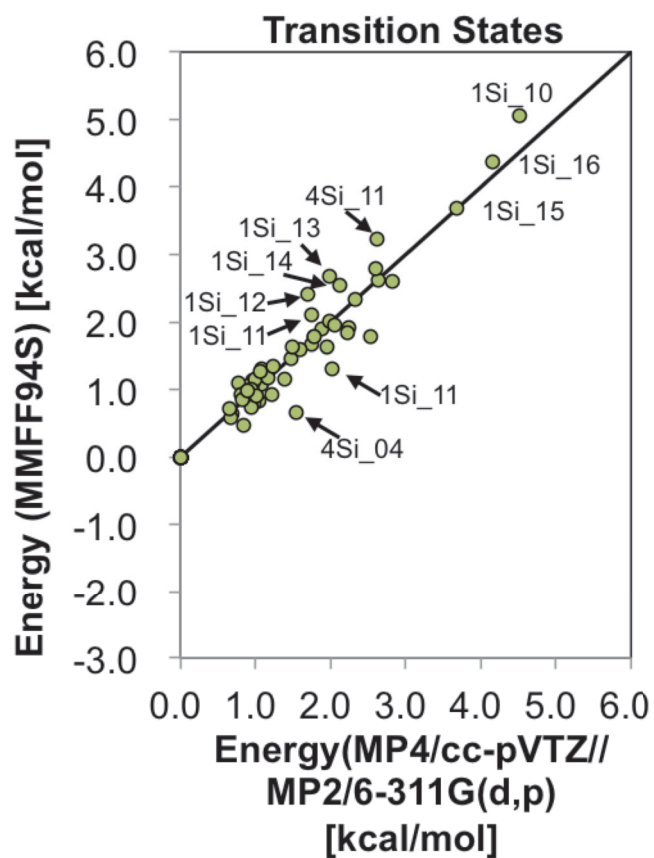


Figure 5.11. Evaluation of the transition energy based on optimized parameters. See Figure 5.9 for detail.



5.5. Application of the Force Field to the Polydialkylsilane System

5.5.1. Effect of Conformation to p and D

Questions were arisen in Section 4.1: (1) What is the stable conformation in solution state and solid state?; (2) Can we quantitatively explain the blue-shift during the aggregation by calculation?; and (3) How much the energies differ between left handed and right handed chiral higher structure? Answering to the question (2) require quantum mechanics calculation such as TD-DFT to obtain the UV spectra and thus takes more time to answer compared to questions (1) and (3). Therefore, calculations to answer questions (1) and (3) were carried out in this work. Particular interest for (1) is how does the conformation search make the difference to the estimated pitch (p) and diameter (D) of the helix. As discussed in Section 3.5.2, the PM3 did not reproduce the p/D value compared to extrapolated WAXD result. One of the possibilities was the absence of conformation search and initial geometry could be far from the optimum conformation.

To take conformation in account, conformation search of **PSi1–PSi4** was carried out based on the force field developed in the previous sections. The Si-H was assumes as their end group. As has been assumed for alkylphenylpolysilanes (**PolyB1–PolyB4**), following assumptions were made.

- (a) The Si-Si-Si-Si main chain can be estimated from CD and UV.
- (b) No solution effect was taken into account.
- (c) Variation of the tacticity will not affect the geometry of helix.

Based on assumption (a), Si-Si-Si-Si and H-Si-Si-Si dihedral angles were set to $+155^\circ$ assuming P -7₃ helix. No conformation search was done for those dihedral angles (i.e. only the low energy side chain conformation was searched). Based on the assumption (c), the isotactic geometry was assumed. CONFLEX method (Osawa method) was used as systematic conformation search setting searching energy limit was set to 1.0 kcal/mol.

Figure 5.12 shows the geometry of **PSi1–PSi4**. Most of the structure maintained the H-Si-Si-Si and Si-Si-Si-Si dihedral angle around $+155^\circ$, but those angle close to the end group some time flipped to *anti* ($\sim 180^\circ$) conformation (Table 5.16). For both chiral and achiral side chains, the dihedral angles were close to *anti* conformation when it is far from the main chain (two bonds away) but showed *gauche* ($\sim \pm 60^\circ$) or *trans* ($\sim \pm 150^\circ$) conformation.

Helical parameters, p and D , of the most stable conformation of **PSi1–PSi4** were measured (Figure 3.1). The p/D value was close to π , which was similar result as values by extrapolated WAXD. This indicates that the conformation search was crucial to estimate the diameter of the helix when such flexibility is involved in the system.

In the case of **PolyB1–PolyB4** (Table 1.3), the conformation search was not carried out to estimate p and D but the calculated p/D well explained the chiroptical inversion around π . This could be because the side chain that determines D contained phenyl group with alkyl group at the *para*-position (Figure 1.1). Thus the diameter was not affected by the conformational freedom of the side chain.

Figure 5.12. Obtained most stable structure after the conformation search.

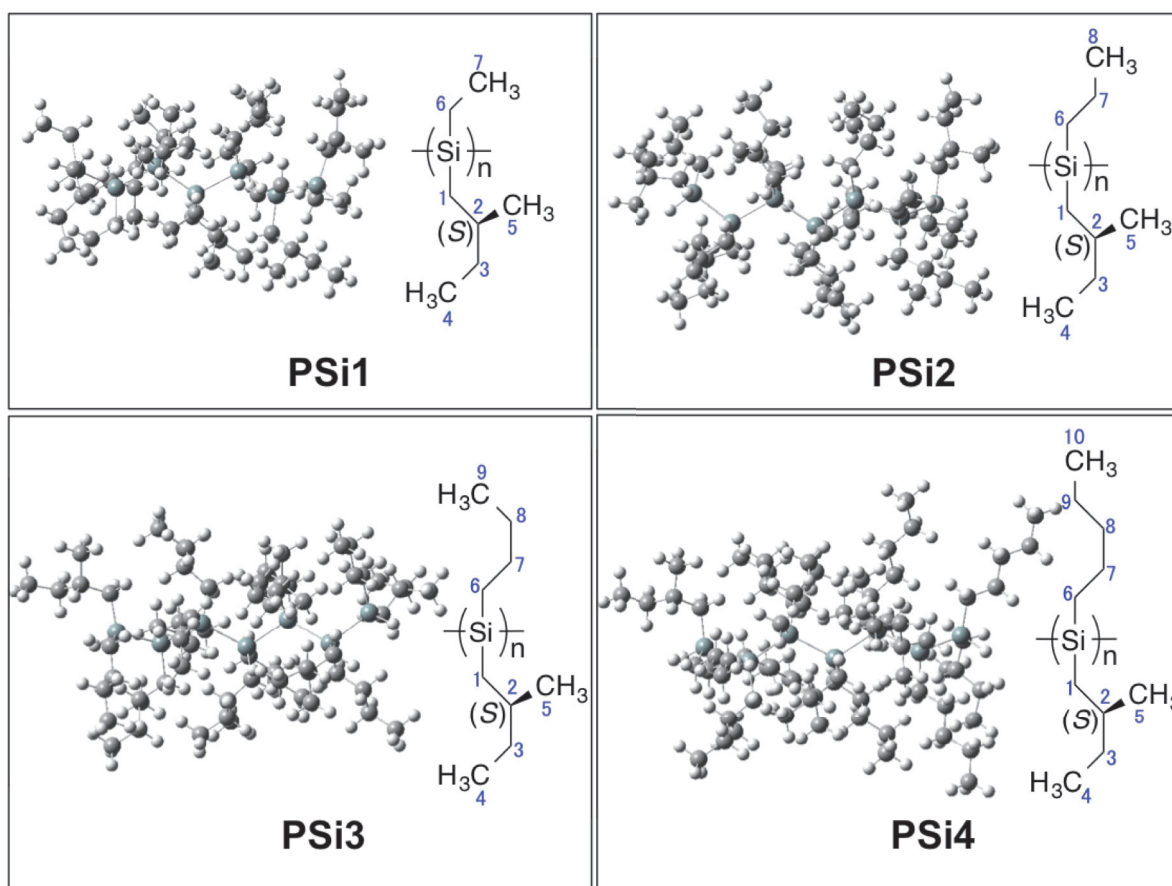


Table 5.16. Conformation of the main chain and side chains of **PSi1–PSi4**.

PSi1							
Main chain		Chiral side chain			Achiral side chain		
Si-Si-Si-Si(H)		C6-Si-C1-C2	Si-C1-C2-C3	C1-C2-C3-C4	C1-Si-C6-C7		
H-Si1-Si2-Si3	-176.5	1	-173.9	-75.3	171.5	1	-57.7
Si1-Si2-Si3-Si4	149.2	2	-73.6	-147.6	173.6	2	-51.3
Si2-Si3-Si4-Si5	155.5	3	-72.5	-146.5	172.7	3	-51.3
Si3-Si4-Si5-Si6	156.1	4	-66.0	-148.5	172.8	4	-56.3
Si4-Si5-Si6-Si7	148.6	5	-56.9	-161.2	70.2	5	-58.7
Si5-Si6-Si7-H	-179.6	6	-46.8	-105.4	172.0	6	-56.8
		7	-167.4	-162.3	173.5	7	66.3

PSi2								
Main chain		Chiral side chain			Achiral side chain			
Si-Si-Si-Si(H)		C6-Si-C1-C2	Si-C1-C2-C3	C1-C2-C3-C4	C1-Si-C6-C7	Si-C6-C7-C8		
H-Si1-Si2-Si3	159.0	1	90.4	-154.0	-60.5	1	-60.0	-176.3
Si1-Si2-Si3-Si4	-174.4	2	87.5	-142.5	175.6	2	-60.3	-173.1
Si2-Si3-Si4-Si5	156.0	3	44.6	-93.0	168.2	3	-170.5	-178.4
Si3-Si4-Si5-Si6	163.0	4	-72.0	-151.2	171.9	4	-51.0	174.1
Si4-Si5-Si6-Si7	150.5	5	-49.5	-147.8	-59.2	5	-167.2	-178.4
Si5-Si6-Si7-H	177.6	6	-47.2	-98.5	172.2	6	-49.8	179.5
		7	-167.8	-162.7	174.5	7	71.3	179.2

PSi3									
Main chain		Chiral side chain			Achiral side chain				
Si-Si-Si-Si(H)		C6-Si-C1-C2	Si-C1-C2-C3	C1-C2-C3-C4	C1-Si-C6-C7	Si-C6-C7-C8	C6-C7-C8-C9		
H-Si1-Si2-Si3	162.2	1	35.2	-168.1	66.7	1	-174.7	179.1	-179.7
Si1-Si2-Si3-Si4	160.2	2	-75.9	-154.3	170.0	2	-46.6	-177.0	-180.0
Si2-Si3-Si4-Si5	154.0	3	-65.2	-146.0	173.1	3	-166.4	-175.1	-176.3
Si3-Si4-Si5-Si6	163.2	4	-69.1	-153.2	168.5	4	-51.3	178.4	178.8
Si4-Si5-Si6-Si7	154.1	5	-57.0	-146.4	173.7	5	-168.4	-175.8	-176.7
Si5-Si6-Si7-H	177.6	6	-65.5	-150.1	172.2	6	-56.7	178.1	180.0
		7	-58.2	-76.5	174.5	7	175.8	-173.5	-178.6

PSi4										
Main chain		Chiral side chain			Achiral side chain					
Si-Si-Si-Si(H)		C6-Si-C1-C2	Si-C1-C2-C3	C1-C2-C3-C4	C1-Si-C6-C7	Si-C6-C7-C8	C6-C7-C8-C9	C7-C8-C9-C10		
H-Si1-Si2-Si3	-177.8	1	-175.2	-77.1	172.3	1	-58.7	-177.6	-179.7	180.0
Si1-Si2-Si3-Si4	149.4	2	-70.4	-146.2	175.8	2	-54.4	177.1	177.4	-179.8
Si2-Si3-Si4-Si5	157.4	3	-71.9	-147.8	177.0	3	-51.2	178.7	178.8	-179.8
Si3-Si4-Si5-Si6	155.9	4	-62.2	-150.5	175.1	4	-59.3	178.3	177.7	-179.7
Si4-Si5-Si6-Si7	153.9	5	-65.5	-148.3	173.0	5	-54.4	175.1	-176.7	-177.0
Si5-Si6-Si7-H	156.4	6	-58.0	-146.3	173.2	6	-62.1	173.4	-175.6	-177.1
		7	-42.8	-71.8	175.3	7	-64.5	178.5	-178.3	-177.6

5.5.2. Optimization of Two Body Structures

To answer (3), the two 7-mer dialkyloligosilanes (**PSi1–PSi4**) were set with various orientations (Figure 5.17). For each dialkyloligosilanes, the most stable conformation that was obtained in the previous section was used. For γ , ϕ_1 , and ϕ_2 , 12 data points were taken, so 1728 initial structures were generated to cover the aggregation possibilities. For γ , only the oligomer 2 was rotated along the axis. For the inter-helix distance (l), 15, 15, 16, and 17 Å were used for **PSi1**, **PSi2**, **PSi3**, and **PSi4** so that those two polymers do not to overlap each other at the initial structure. For each possible orientation, geometry optimization was carried out. Each polymer was optimized sequentially for 1 time (freezing one polymer when optimizing the other).

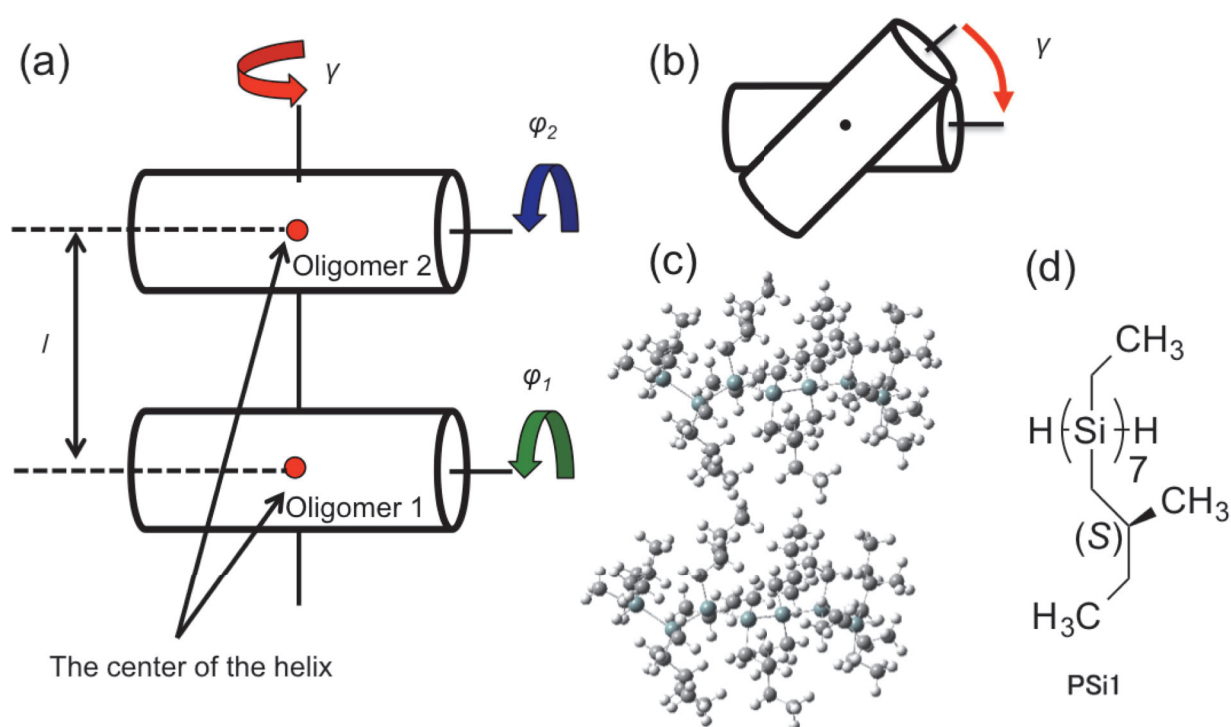


Figure 5.13. The defined orientation of the two dialkyloligosilanes taking **PSi1** as example. (a) Side view of the defined orientation of two oligomers. (b) Top view of the model in (a). (c) Actual molecular alignment of two **PSi2**. (d) Structure of the 7-mer **PSi2**.

The resulting potential is shown in Figure 5.14. The blue dots represent initial structure and red dots are the optimized structure. The potential energy did not give plausible explanation for the inversion of chiroptical activity because most stable structure always located in the right handed ($0^\circ < \gamma < 90^\circ$) higher order structure region. The energy differences were 1.56, 0.08, 1.88, and 0.52 kcal/mol for **PSi1**, **PSi2**, **PSi3**, and **PSi4**, respectively and the energy difference was extremely small for **PSi2**.

The discrepancy between the result and experimental fact could be arisen by (i) a relaxation of side chain conformation after their approach and (ii) tacticity of the dialkylpolysilane. Therefore consideration of relaxation by MD could be necessary for the each two body structures as well as consideration of syndiotactic structure in addition to isotactic structure.

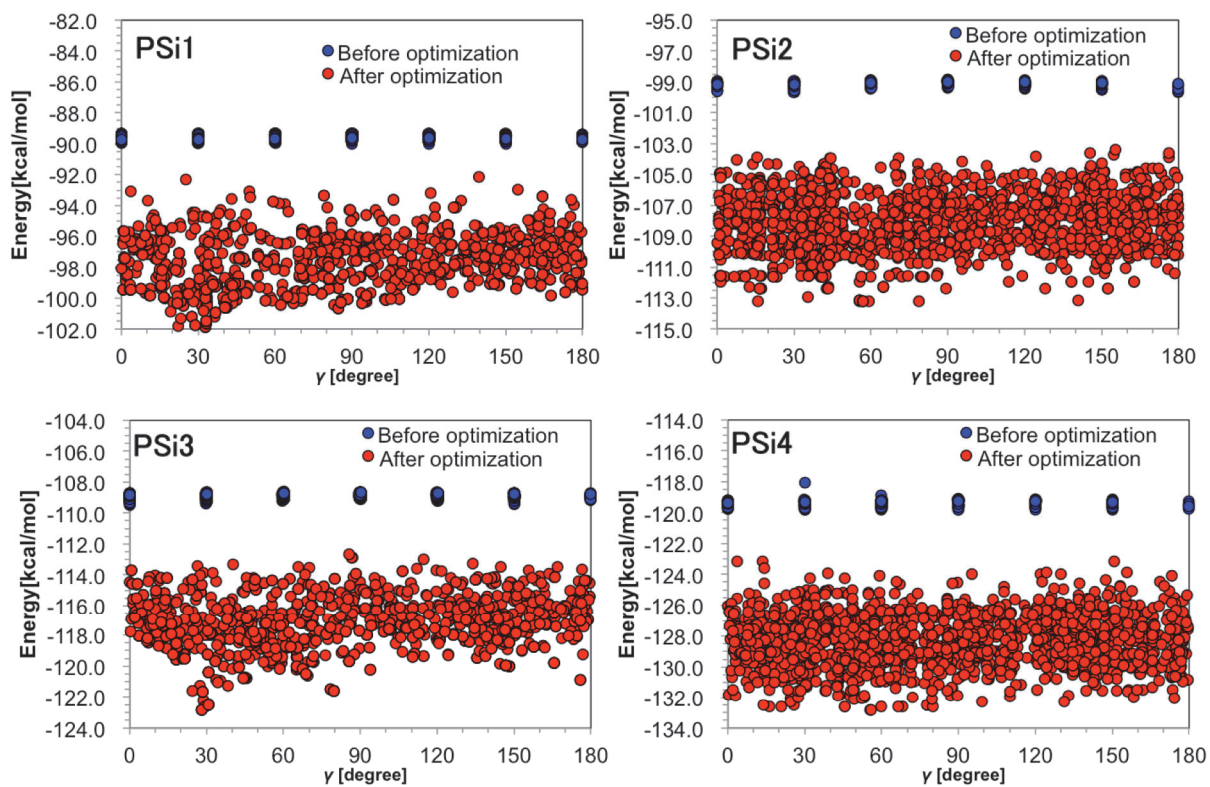


Figure 5.14. The energy of the two interacting oligomers depending on the angle γ .

5.6. References

- (1) Halgren, T. A. *J. Am. Chem. Soc.* **1992**, *114*, 7827.
- (2) Halgren, T. A. *J. Comput. Chem.* **1996**, *17*, 490.
- (3) Halgren, T. A. *J. Comput. Chem.* **1996**, *17*, 520.
- (4) Halgren, T. A. *J. Comput. Chem.* **1996**, *17*, 553.
- (5) Halgren, T. A. *J. Comput. Chem.* **1996**, *17*, 616.
- (6) Halgren, T. A.; Nachbar, R. B. *J. Comput. Chem.* **1996**, *17*, 587.
- (7) Halgren, T. A. *J. Comput. Chem.* **1999**, *20*, 720.
- (8) Halgren, T. A. *J. Comput. Chem.* **1999**, *20*, 730.
- (9) Sun, H. *Macromolecules* **1995**, *28*, 701.
- (10) Durig, J. R.; Church, J. S. *J. Chem. Phys.* **1980**, *73*, 4784.
- (11) Puzzarini, C. *Phys. Chem. Chem. Phys.* **2003**, *5*, 26.
- (12) Duncan, J. L.; Harvie, J. L.; McKean, D. C.; Cradock, S. *J. Mol. Struct.* **1986**, *145*, 225.
- (13) Gutowsky, H. S.; Stejskal, E. O. *J. Chem. Phys.* **1954**, *22*, 939.
- (14) Belyakov, A. V.; Haaland, A.; Shorokhov, D. J.; West, R. *J. Organomet. Chem.* **2000**, *597*, 87.
- (15) Piqueras, M. C.; Crespo, R.; Michl, J. *J. Phys. Chem. A* **2003**, *107*, 4661.
- (16) Sigfridsson, E.; Ryde, U. *J. Comput. Chem.* **1998**, *19*, 377.
- (17) García, G.; Atilhan, M.; Aparicio, S. *J. Mol. Liq.* **2015**, *211*, 506.
- (18) Bordner, A. J.; Cavasotto, C. N.; Abagyan, R. A. *J. Phys. Chem. B* **2003**, *107*, 9601.
- (19) Mahlanen, R.; Pakkanen, T. A. *Chem. Phys.* **2011**, *382*, 121.
- (20) Scott, A. P.; Radom, L. *J. Phys. Chem.* **1996**, *100*, 16502.
- (21) Chen, K. S.; Allinger, N. L. *J. Phys. Org. Chem.* **1997**, *10*, 697.

Chapter 6. Concluding remarks

In this thesis, bistability of chiral polysilane aggregate was investigated experimentally and theoretically. Moreover, several computational tools suited to the simulation of such system were developed and verified.

In Chapter 1, the concept of chiroptical switching capability in molecule and higher order structure (supramolecular structure) was described in detail. The viewpoints of the structure and property were clearly distinguished and some kinds of the stimuli to introduce the switching have been overviewed. The emphasis was made on the importance of observing switching behavior in solid state for the application. Cholesteric hard-core model was introduced as a concept to control the switching behavior of helical polymers in the solid state. An interesting statement of this model was that right handed state and left handed state in higher order structure do not depend only on the handedness of each helical polymer but also on its helical pitch (p) and diameter (D). This lead to an idea that side chain length switchable or main chain switchable helical polymer (i.e. cis-trans isomerism) could be attractive candidate as switching substance in solid state because those moieties in helical polymer could alter p and D . The author focused on the chiral system that exhibit optical activity switching in aggregate states in this work.

In Chapter 2, dialkylpolysilane system was prepared based on the idea of cholesteric hard-core model by varying the side chain length of the polymer. The chiral polymers used for the experiment has tetravalent silicon atoms in the backbone, two out of the four bonds were connected to the other silicon atoms to form Si-Si backbone and another connected to chiral alkyl side chain and the other to achiral alkane. The chiral side chain was (*S*)-2-methylbutyl group and achiral alkanes were ethyl, *n*-propyl, *n*-butyl, *n*-pentyl and *n*-hexyl group. A side chain dependent chiroptical inversion and a solvent induced chiroptical switching were reported for this system. The former was a configurational change in the chemical structure and it was not suitable for application

to information storage but such phenomenon supported the idea of cholesteric hard-core model. For polysilanes with relatively shorter side chain showed positive bisigned Cotton effect and longer side chain showed negative bisigned Cotton effect in aggregate state. The polysilane with proper side chain length that is not too long or too short showed the bistability and the chiroptical property was switched depending on the toluene/methanol solvent ratio. At relatively high toluene ratio, the negative bisigned CD was observed, but at relatively high methanol ratio, the aggregates showed positive bisigned CD.

In Chapter 3, the geometrical feature of the helical polymer and its structural bistability at aggregated form was described theoretically. The concept of cholesteric hard-core model was introduced which define the structure of helical compound by p and D . Qualitative and quantitative descriptions of the model were presented. The cholesteric hard-core model described the structural aspect but the optical property could depend on the molecules, therefore, exciton chirality method was combined with the model. Assuming that left handed helical conjugated polymer which electric transition dipole moment is directed along the longitudinal axis, it was concluded that the helical polymer with larger p/D value results in a positive bisigned Cotton effect while polymer with the smaller p/D value results in a negative bisigned Cotton effect. This tendency was consistent with the experimental results described in Chapter 2. The model predicts that the critical point of the p/D value should be around π . Three approaches were made to evaluate p and D , (i) an optimized structure by PM3 assuming side chain conformation is all-*trans* and main chain has P -7₃-helix structure, (ii) an optimized structure by MMFF94S force field (described in Chapter 4 and 5) with a most stable conformation found by CONFLEX method, and (iii) indirect estimation by wide angle X-ray diffraction (WAXD) of poly[*n*-alkyl-(*S*)-2-methylbutylsilane]s (number of carbon atoms in *n*-alkyl side chain = 10, 11, 12, 13, 14, and 15). Estimation of critical value of p/D by PM3 resulted in 2.0 smaller value compared to π . On the other hand, conformation search based on MMFF94S

and WAXD result estimated this value as 3.1 and 3.2, which were close to π . The discrepancy between PM3 and MMFF94S could come from conformational difference between the two especially for the side chain. The limitation of the theory could be raised when consider solvent effect and number of the constituents in the aggregates but those could be covered by taking into account of the solvent effect by contact surface area between polymer and solvents, and observation of relatively small aggregates in experimental system, respectively.

In Chapter 4, the parameter optimization program was developed to optimize the MMFF94S force field parameters for the polydialkylsilane system. The specific interest of developing the force field was to carry out conformation search based on an accurate force field. The program was coupled with CONFLEX 7B and designed to fit the MM parameters to the quantum mechanics calculation calculated by Gaussian 09. The performance of the program was tested using relatively small molecules (methylsilane for internal coordinates and vibrations and propylsilane for conformational energy). The RMSD from the quantum mechanics data for bond length, angle, vibrational frequency and conformational energies at ground state and transition states were 0.002 Å, 0.003°, 41 cm⁻¹, and ~ 0.001 kcal/mol, respectively, which are accurate enough to optimize the parameters.

In Chapter 5, the force field parameters for silicon, carbon, and hydrogen system were optimized utilizing the program described in Chapter 4. Approximately 40 kinds of silicon compounds were prepared as model structures. Parameters involved in bond charge increments, van der Waals parameter, bond stretching, angle bending, stretch-bend interaction, and torsion interaction were optimized using the program described in Chapter 4. MP4(sdq)/cc-pVTZ//MP2/6-311G(d,p) level of the structures and energies were chosen as reference except for optimization of the van der Waals interaction where aug-cc-pVTZ was used as the basis set. The RMSD from the quantum mechanics data for bond length [Å], angle, vibrational frequency

and conformational energies at ground state and transition states were 0.013 \AA , 0.6° , 41 cm^{-1} , and $\sim 0.001 \text{ kcal/mol}$, respectively. Further verification could be necessary by applying this force field to actual experimental systems such as dialkylpolysilane in solution state. However at least for the model compounds, those values reproduced the quantum mechanics data well.

The applicability of the cholesteric hard-core theory has been tested based on dialkylpolysilanes and alkylphenylsilanes. The model explains the chiroptical inversion phenomena well and it paves the way for designing compound that undergo chiroptical inversion by side chain length switching or main chain switching of helical polymers. Mixing two helical polymers A and B with different p/D could also be interesting if one could control the stability among the combination AA, AB, and BB. This is because such system could also control the chiroptical inversion.

Since the tested dialkylpolysilane are rigid rod-like molecule and cholesteric hard-core model assumes rod-like structure, the model could not be applied to an assembly of globular polymers though the geometry of the contacting surface of the two polymers should be important for the globular polymer as well.

Appendix

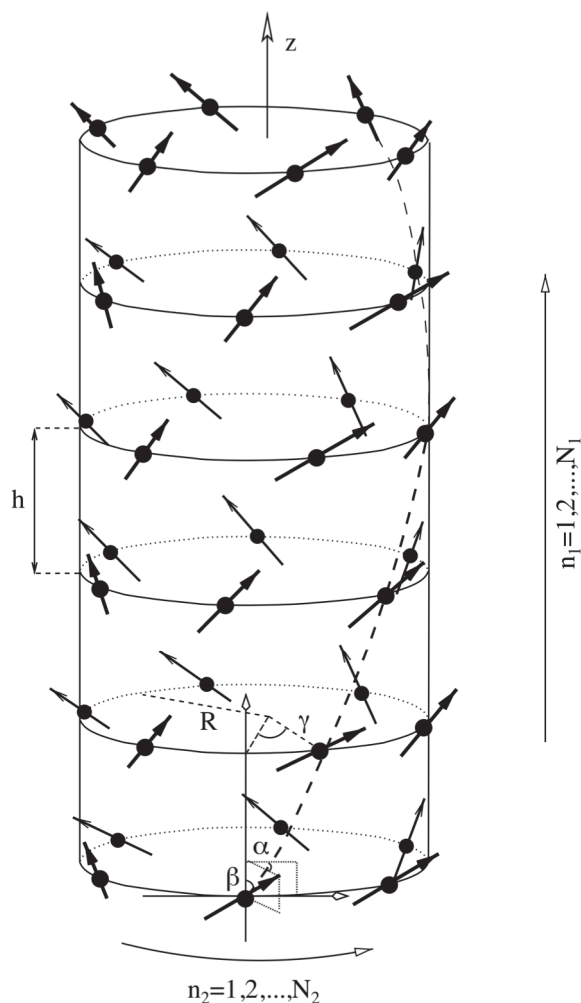


Figure A.2.1. The cylindrical aggregate consisting of a stack of N_1 rings that each contains N_2 molecules.¹ The arrows indicate the transition dipoles, which are equal in magnitude (μ) and make an angle β with the cylinder axis. The projection of each dipole on the plane of the rings makes an angle α with the local tangent to the ring. Each ring is rotated with respect to the previous one over an angle γ so that we may view the aggregate as a collection of N_2 parallel helices (dashed) on the cylinder's surface. Reprinted from Journal of Luminescence, Vol. 102–103, C. Didraga, and J. Knoester "Absorption and dichroism spectra of cylindrical J aggregates and chlorosomes of green bacteria", pp. 60–66, Copyright (2003), with permission from Elsevier.

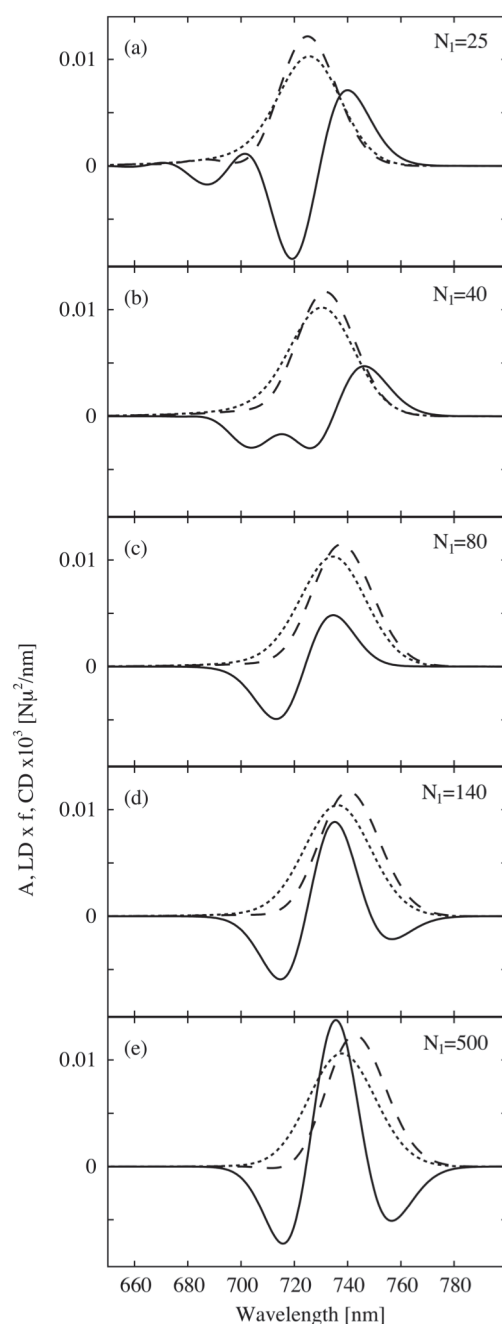


Figure A.2.2. Linear absorption (dotted), LD (dashed), and CD (solid) spectra calculated for cylindrical aggregates with geometry applicable to the rod elements in the chlorosomes of *Chlorofexus aurantiacus*.¹ The panels (a)–(e) give the spectra for five different cylinder lengths N_l . The factor f multiplying the LD is defined by $f=2/(3[\cos^2\beta-1])$ and was introduced to give the absorption and the LD spectrum the same area ($N\mu^2/3$). Reprinted from *Journal of Luminescence*, Vol. 102–103, C. Didraga, and J. Knoester "Absorption and dichroism spectra of cylindrical J aggregates and chlorosomes of green bacteria", pp. 60–66, Copyright (2003), with permission from Elsevier.

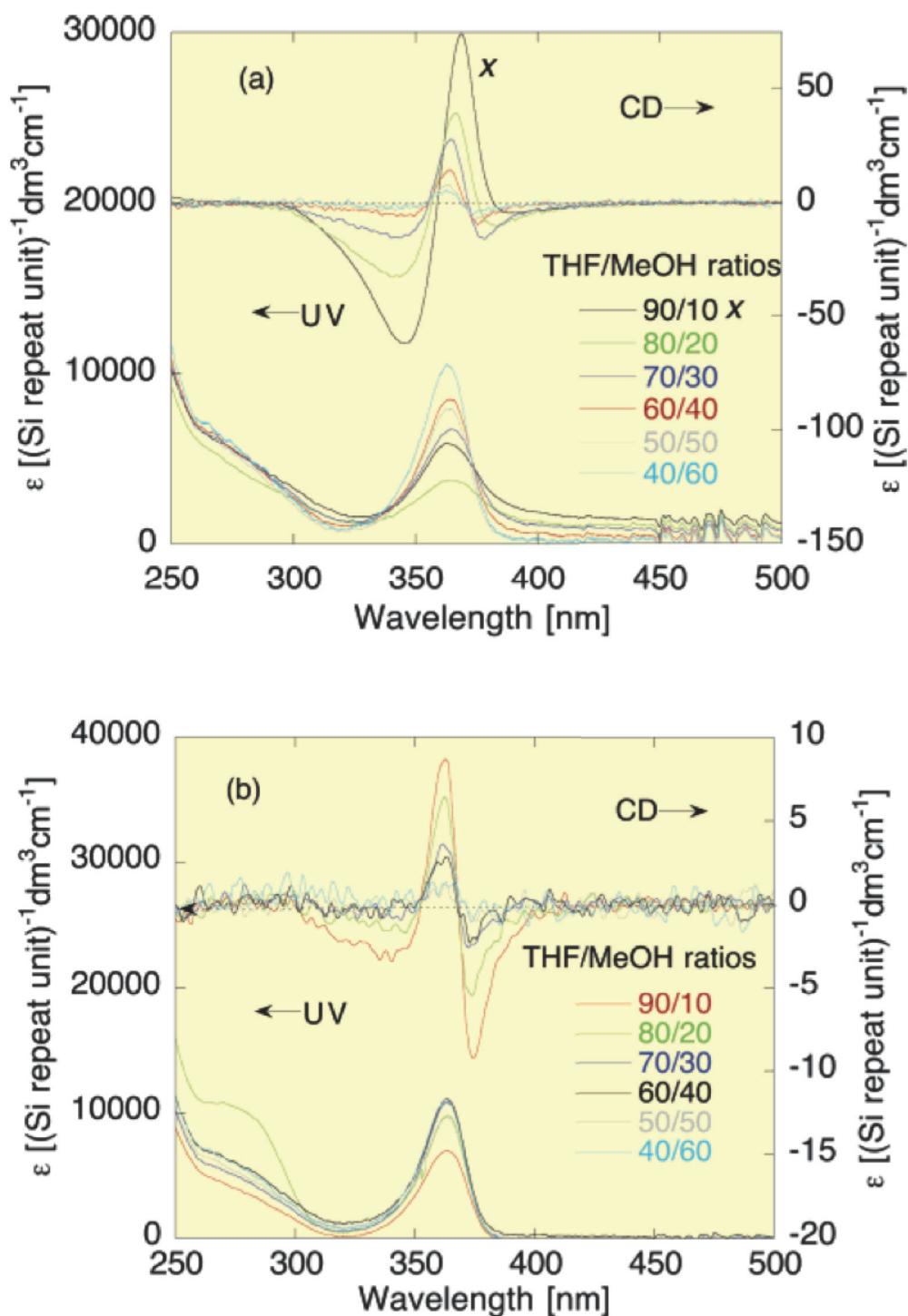


Figure A.2.3. CD spectra of **Poly-B3** and **Poly-B4** polymer aggregates. (a) **Poly-B4** and (b) **Poly-B3**, prepared at various THF/MeOH ratios (20 °C). Reprinted with permission from Peng, W.; Motonaga, M.; Koe, J. R. *J. Am. Chem. Soc.* **2004**, *126*, 13822. Copyright 2004 American Chemical Society.

A.4.1. Root Mean Square Deviation

For the parameter fitting, the author employed the method to develop consistent force field by Rasmussen^{2,3} and steepest decent method (see Section A.4.2) was implemented. The purpose of the program is to minimize the root mean square deviation (RMSD) from the reference value. Before going over the optimization step, it is beneficial to describe the function of RMSD $f(\mathbf{x})$ in detail for clarity. The variable \mathbf{x} denotes a set of parameters.

$$\mathbf{x} = (x_1, x_2, \dots, x_n, \dots, x_N)^T \quad (\text{Eq. A.4.1})$$

When parameter vector \mathbf{x} is given, function of $f(\mathbf{x})$ can be expressed as follows.

$$f(\mathbf{x}) = \sqrt{f_R(\mathbf{x}) + f_\theta(\mathbf{x}) + f_N(\mathbf{x}) + f_E(\mathbf{x})} \quad (\text{Eq. A.4.2})$$

Where $f_R(\mathbf{x}), f_\theta(\mathbf{x}), f_N(\mathbf{x}), f_E(\mathbf{x})$ denotes averaged value of squared difference between MM and QM of bond length, angle, vibration, and energy scaled by certain value. For example, the equation for bond length is described as follows.

$$f_R(\mathbf{x}) = \frac{F_R}{\sum_{i=1}^I J_i} \sum_{i=1}^I \sum_{j=1}^{J_i} \frac{\sum_{k=1}^{K_{ij}} (R_{ijk}(\mathbf{x}) - R'_{ijk})^2}{K_{ij}} \quad (\text{Eq. A.4.3})$$

Where $R_{ijk}(\mathbf{x})$ and R'_{ijk} denotes bond length from MM and from QM, respectively. F_R is a scaling factor for bond length, and the K_{ij} denotes number of bonds belong to j th bond type in i th molecule.

The error of the each bond is averaged within each bond type and this is to treat each bond type as equal and not to put higher weight on abundant bond type in molecule. For example, Si-H is abundant compared to Si-Si in disilane. Each bond that belongs to bond type j in i th molecule is described by k . To obtain the $f_N(\mathbf{x})$, vibration modes were assigned based on eigenvector of each vibration mode.⁴ For the excited state structure, vibration frequency was omitted. To decide the scaling factors including F_R , 1.0 divided by squared value of typical RMSD values of MMFF94S

with respect to experimental data were used (bond length error= 0.014 angstrom, angle error = 1.2°, and torsion angle error = 1.2°, vibration frequency error = 61.0 cm⁻¹, steric energy error = 0.38 kcal/mol).⁵

A.4.2. Steepest Descent Method

Steepest descent method is a popular method to solve optimization problem and documented in textbooks.⁶ The method is often used for geometry optimization in the field of molecular mechanics as the first scheme. In this thesis, the author briefly describes the method not in general form as many of the books do but describe the specific case for optimization of the parameters.

Assume that there are two parameters $\mathbf{x}(x_1, x_2)$ and one wishes to optimize the vector so that the RMSD value become minimum (Fig. A.4.1). The start and goal are represented in red point in the Fig. A.4.1 and the goal is the bottom of the valley. At each point \mathbf{x} , the gradient unit vector ($\Delta\mathbf{x}$) is calculated towards the lower $f(\mathbf{x})$ (white arrow in Fig. A.4.2) as follows.

$$\Delta\mathbf{x} = \frac{-\nabla f(\mathbf{x})}{|\nabla f(\mathbf{x})|} \quad (\text{Eq. A.4.4})$$

The coordinates of the \mathbf{x} are moved along the gradient unit vector for given step size ($t_i > 0$) (the points that the blue arrows are pointing). At the coordinates after the movement, $f(\mathbf{x})$ is calculated and the program determines whether it is preferable change or not. If $f(\mathbf{x})$ *decreases* after the coordinates change, if the change preferable, so keep the changed coordinate and repeats the process from getting the gradient unit vector. If $f(\mathbf{x})$ *increases*, it means that the RMSD become worse after the alternation, so it is necessary to decrease the step size (divided by 2 in Fig. A.4.2) and change the coordinate (pointed by purple arrow in Fig. A.4.2) and the $f(\mathbf{x})$ is calculated and reevaluated. Until the $f(\mathbf{x})$ becomes better than previous step, this process is repeated. The process to reach to the minimum from the start is described in Figure A.4.2. Actual implementation of the steepest descent method in the parameter optimization is described in Section 4.2.

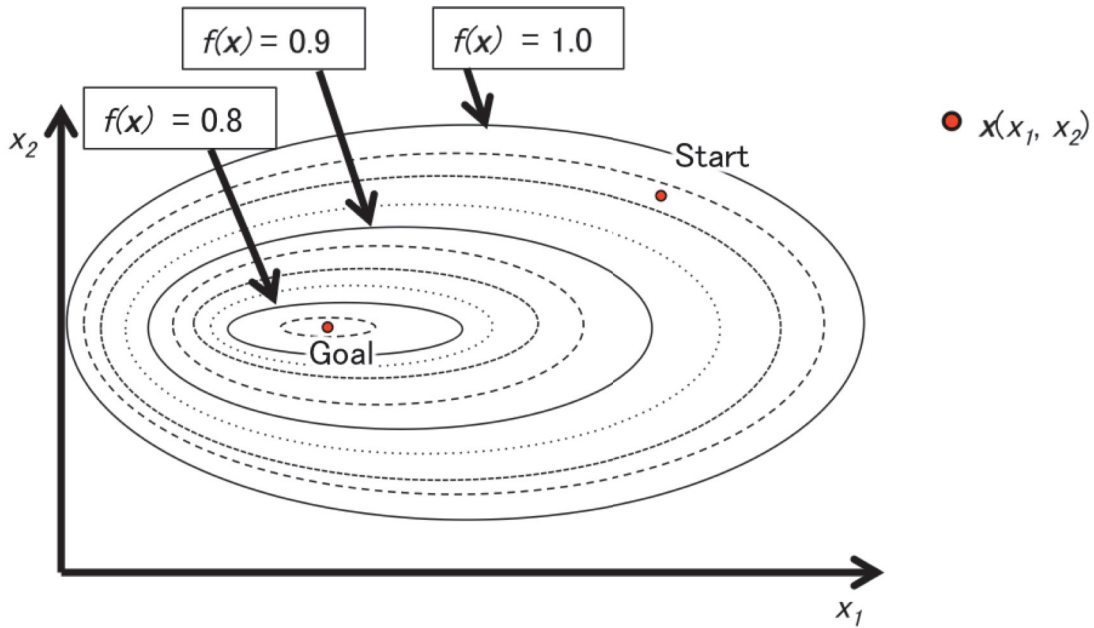


Figure A.4.1. A typical example of RMSD optimization problem. RMSD is represented by $f(x)$ and the purpose is to reduce the value as much as possible by optimizing two parameters x_1 and x_2 which is represented by vector \mathbf{x} .

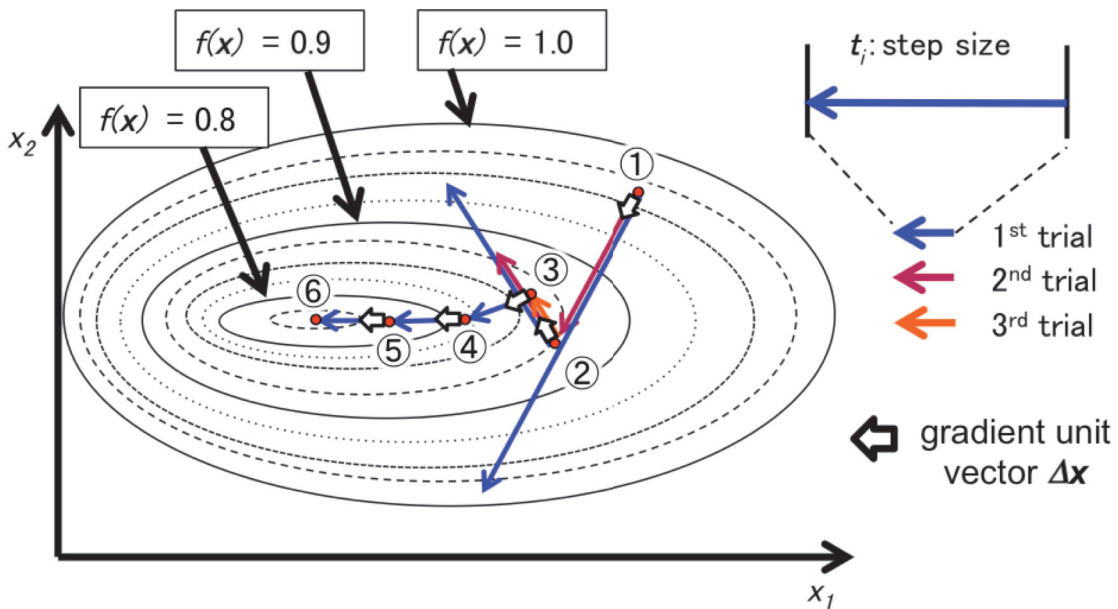



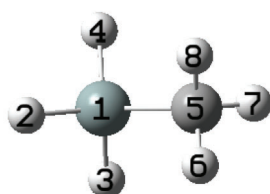
Figure A.4.2. Schematic drawing of the steepest descent method to solve the RMSD minimization problem.

Partial charges of silicon compounds containing one silicon atom and four silicon atoms are shown in Figure A.5.1–A.5.11. Charges were calculated using CHELPG method at MP4(sdq)/cc-pVTZ//MP2/6-31G(d,p) level. Charges calculated based on optimized BCI are also shown. For compounds with four silicon atoms, the charges are average over each conformation. Charges of 1-19 and 5-19 are set to 0.1996 and 0.1452.



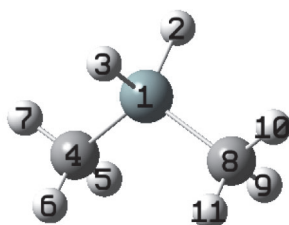
		Original ChelpG charge	BCI
1	Si	0.70	0.58
2	H	-0.18	-0.15
3	H	-0.18	-0.15
4	H	-0.18	-0.15
5	H	-0.18	-0.15

Figure A.5.1. Partial charges of silane. Charges using CHELPG method at MP4(sdq)/cc-pVTZ//MP2/6-31G(d,p) level and charges calculated based on optimized BCI are shown.



		Original ChelpG charge	H charge added to C	BCI
1	Si	0.74	0.74	0.64
2	H	-0.20	-0.20	-0.15
3	H	-0.20	-0.20	-0.15
4	H	-0.20	-0.20	-0.15
5	C	-0.35	-0.14	-0.20
6	H	0.07	0.00	0.00
7	H	0.07	0.00	0.00
8	H	0.07	0.00	0.00

Figure A.5.2. Partial charges of methylsilane. Charges using CHELPG method at MP4(sdq)/cc-pVTZ//MP2/6-31G(d,p) level and charges calculated based on optimized BCI are shown.



		Original ChelpG charge	H charge added to C	BCI
1	Si	0.83	0.83	0.69
2	H	-0.23	-0.23	-0.15
3	H	-0.23	-0.23	-0.15
4	C	-0.44	-0.18	-0.20
5	H	0.09	0.00	0.00
6	H	0.09	0.00	0.00
7	H	0.08	0.00	0.00
8	C	-0.44	-0.18	-0.20
9	H	0.09	0.00	0.00
10	H	0.08	0.00	0.00
11	H	0.09	0.00	0.00

Figure A.5.3. Partial charges of dimethylsilane. Charges using CHELPG method at MP4(sdq)/cc-pVTZ//MP2/6-31G(d,p) level and charges calculated based on optimized BCI are shown.



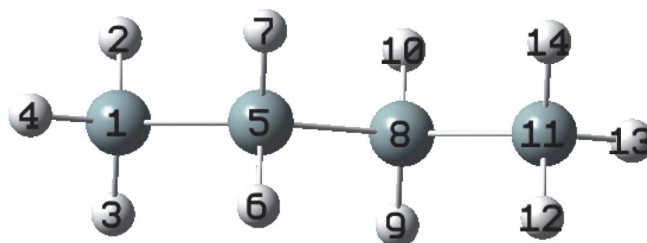
		Original ChelpG charge	H charge added to C	BCI
1	Si	0.90	0.90	0.74
2	H	-0.26	-0.26	-0.15
3	C	-0.47	-0.21	-0.20
4	H	0.09	0.00	0.00
5	H	0.09	0.00	0.00
6	H	0.09	0.00	0.00
7	C	-0.47	-0.21	-0.20
8	H	0.09	0.00	0.00
9	H	0.09	0.00	0.00
10	H	0.09	0.00	0.00
11	C	-0.47	-0.21	-0.20
12	H	0.09	0.00	0.00
13	H	0.09	0.00	0.00
14	H	0.09	0.00	0.00

Figure A.5.4. Partial charges of trimethylsilane. Charges using CHELPG method at MP4(sdq)/cc-pVTZ//MP2/6-31G(d,p) level and charges calculated based on optimized BCI are shown.



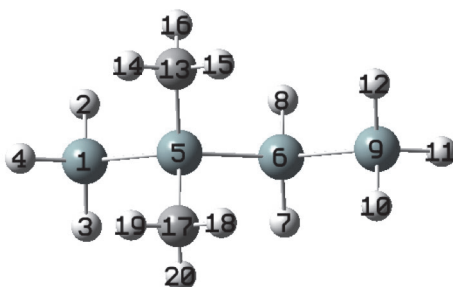
	Original	ChelpG	H charge	BCI	RMS
	charge	charge	added to C		
1	Si	0.98	0.98	0.80	0.03
2	C	-0.51	-0.24	-0.20	0.00
3	H	0.09	0.00	0.00	0.00
4	H	0.09	0.00	0.00	0.00
5	H	0.09	0.00	0.00	0.00
6	C	-0.51	-0.24	-0.20	0.00
7	H	0.09	0.00	0.00	0.00
8	H	0.09	0.00	0.00	0.00
9	H	0.09	0.00	0.00	0.00
10	C	-0.50	-0.24	-0.20	0.00
11	H	0.09	0.00	0.00	0.00
12	H	0.09	0.00	0.00	0.00
13	H	0.09	0.00	0.00	0.00
14	C	-0.51	-0.24	-0.20	0.00
15	H	0.09	0.00	0.00	0.00
16	H	0.09	0.00	0.00	0.00
17	H	0.09	0.00	0.00	0.00

Figure A.5.5. Partial charges of tetramethylsilane. Charges using CHELPG method at MP4(sdq)/cc-pVTZ//MP2/6-31G(d,p) level and charges calculated based on optimized BCI are shown.



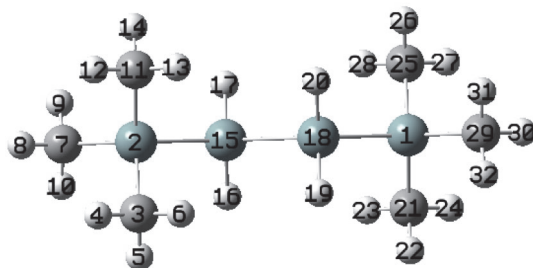
		Original ChelpG charge			
		G ($\omega=61.9$)	A ($\omega=180.0$)	Averaged	BCI
1	Si	0.43	0.51	0.47	0.44
2	H	-0.14	-0.16	-0.15	-0.15
3	H	-0.14	-0.16	-0.15	-0.15
4	H	-0.13	-0.16	-0.14	-0.15
5	Si	0.23	0.22	0.22	0.29
6	H	-0.11	-0.13	-0.12	-0.15
7	H	-0.13	-0.13	-0.13	-0.15
8	Si	0.23	0.22	0.22	0.29
9	H	-0.11	-0.13	-0.12	-0.15
10	H	-0.13	-0.13	-0.13	-0.15
11	Si	0.43	0.51	0.47	0.44
12	H	-0.14	-0.16	-0.15	-0.15
13	H	-0.13	-0.16	-0.14	-0.15
14	H	-0.14	-0.16	-0.15	-0.15

Figure A.5.6. Partial charges of tetrasilane. Charges using CHELPG method at MP4(sdq)/cc-pVTZ//MP2/6-31G(d,p) level and charges calculated based on optimized BCI are shown.



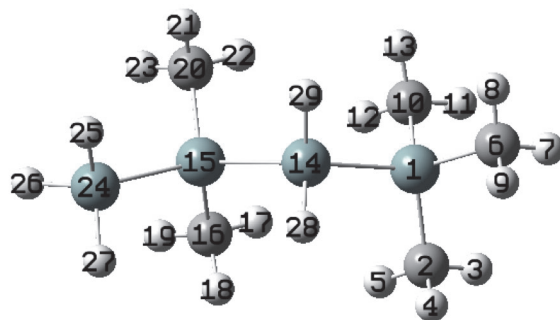
		Original ChelpG charge		H charge added to C		Averaged	BCI
		G ($\omega=61.2$)	A ($\omega=180.0$)	G ($\omega=61.2$)	A ($\omega=180.0$)		
1	Si	0.37	0.45	0.37	0.45	0.41	0.44
2	H	-0.14	-0.16	-0.14	-0.16	-0.15	-0.15
3	H	-0.14	-0.16	-0.14	-0.16	-0.15	-0.15
4	H	-0.13	-0.15	-0.13	-0.15	-0.14	-0.15
5	Si	0.29	0.30	0.29	0.30	0.30	0.40
6	Si	0.17	0.18	0.17	0.18	0.17	0.29
7	H	-0.11	-0.13	-0.11	-0.13	-0.12	-0.15
8	H	-0.12	-0.13	-0.12	-0.13	-0.13	-0.15
9	Si	0.43	0.50	0.43	0.50	0.46	0.44
10	H	-0.14	-0.16	-0.14	-0.16	-0.15	-0.15
11	H	-0.14	-0.16	-0.14	-0.16	-0.15	-0.15
12	H	-0.15	-0.16	-0.15	-0.16	-0.15	-0.15
13	C	-0.23	-0.26	-0.11	-0.12	-0.12	-0.20
14	H	0.05	0.05	0.00	0.00	0.00	0.00
15	H	0.04	0.05	0.00	0.00	0.00	0.00
16	H	0.02	0.03	0.00	0.00	0.00	0.00
17	C	-0.13	-0.26	-0.08	-0.12	-0.10	-0.20
18	H	0.03	0.05	0.00	0.00	0.00	0.00
19	H	0.01	0.05	0.00	0.00	0.00	0.00
20	H	0.00	0.03	0.00	0.00	0.00	0.00

Figure A.5.7. Partial charges of 2,2-dimethyltetrasilane. Charges using CHELPG method at MP4(sdq)/cc-pVTZ//MP2/6-31G(d,p) level and charges calculated based on optimized BCI are shown.



		Original ChelpG charge		H charge added to C		Averaged	BCI
		G ($\omega=59.0$)	A ($\omega=180.0$)	G ($\omega=59.0$)	A ($\omega=180.0$)		
1	Si	0.57	0.70	0.57	0.70	0.63	0.599
2	Si	0.57	0.70	0.57	0.70	0.63	0.599
3	C	-0.37	-0.41	-0.16	-0.12	-0.14	-0.20
4	H	0.06	0.08	0.00	0.00	0.00	0.00
5	H	0.08	0.06	0.00	0.00	0.00	0.00
6	H	0.07	0.07	0.00	0.00	0.00	0.00
7	C	-0.30	-0.40	-0.16	-0.12	-0.14	-0.20
8	H	0.06	0.08	0.00	0.00	0.00	0.00
9	H	0.04	0.06	0.00	0.00	0.00	0.00
10	H	0.05	0.06	0.00	0.00	0.00	0.00
11	C	-0.32	-0.41	-0.17	-0.12	-0.14	-0.20
12	H	0.07	0.08	0.00	0.00	0.00	0.00
13	H	0.03	0.07	0.00	0.00	0.00	0.00
14	H	0.05	0.06	0.00	0.00	0.00	0.00
15	Si	0.17	0.13	0.17	0.13	0.15	0.290
16	H	-0.13	-0.13	-0.13	-0.13	-0.13	-0.15
17	H	-0.12	-0.13	-0.12	-0.13	-0.12	-0.15
18	Si	0.17	0.13	0.17	0.13	0.15	0.290
19	H	-0.13	-0.13	-0.13	-0.13	-0.13	-0.15
20	H	-0.12	-0.13	-0.12	-0.13	-0.12	-0.15
21	C	-0.37	-0.41	-0.16	-0.12	-0.14	-0.20
22	H	0.07	0.06	0.00	0.00	0.00	0.000
23	H	0.06	0.07	0.00	0.00	0.00	0.000
24	H	0.08	0.08	0.00	0.00	0.00	0.000
25	C	-0.32	-0.41	-0.17	-0.12	-0.14	-0.20
26	H	0.05	0.06	0.00	0.00	0.00	0.000
27	H	0.07	0.08	0.00	0.00	0.00	0.000
28	H	0.03	0.07	0.00	0.00	0.00	0.000
29	C	-0.30	-0.40	-0.16	-0.12	-0.14	-0.20
30	H	0.06	0.08	0.00	0.00	0.00	0.000
31	H	0.04	0.06	0.00	0.00	0.00	0.000
32	H	0.05	0.06	0.00	0.00	0.00	0.000

Figure A.5.9. Partial charges of 1,1,1,4,4,4-hexamethyltetrasilane. Charges using CHELPG method at MP4(sdq)/cc-pVTZ//MP2/6-31G(d,p) level and charges calculated based on optimized BCI are shown.



		Original ChelpG charge		H charge added to C		Averaged	BCI
		G ($\omega=49.6$)	T ($\omega=165.2$)	G ($\omega=49.6$)	T ($\omega=165.2$)		
1	Si	0.63	0.70	0.63	0.70	0.66	0.60
2	C	-0.42	-0.40	-0.19	-0.20	-0.19	-0.20
3	H	0.09	0.08	0.00	0.00	0.00	0.00
4	H	0.07	0.06	0.00	0.00	0.00	0.00
5	H	0.06	0.06	0.00	0.00	0.00	0.00
6	C	-0.28	-0.37	-0.16	-0.18	-0.17	-0.20
7	H	0.05	0.07	0.00	0.00	0.00	0.00
8	H	0.03	0.06	0.00	0.00	0.00	0.00
9	H	0.05	0.06	0.00	0.00	0.00	0.00
10	C	-0.39	-0.43	-0.18	-0.19	-0.19	-0.20
11	H	0.08	0.08	0.00	0.00	0.00	0.00
12	H	0.06	0.08	0.00	0.00	0.00	0.00
13	H	0.07	0.07	0.00	0.00	0.00	0.00
14	Si	0.05	0.07	0.05	0.07	0.06	0.29
15	Si	0.33	0.31	0.33	0.31	0.32	0.40
16	C	-0.26	-0.28	-0.13	-0.12	-0.13	-0.20
17	H	0.05	0.06	0.00	0.00	0.00	0.00
18	H	0.03	0.04	0.00	0.00	0.00	0.00
19	H	0.05	0.05	0.00	0.00	0.00	0.00
20	C	-0.13	-0.22	-0.09	-0.12	-0.10	-0.20
21	H	0.00	0.02	0.00	0.00	0.00	0.00
22	H	0.03	0.04	0.00	0.00	0.00	0.00
23	H	0.01	0.04	0.00	0.00	0.00	0.00
24	Si	0.34	0.45	0.34	0.45	0.40	0.44
25	H	-0.14	-0.16	-0.14	-0.16	-0.15	-0.15
26	H	-0.13	-0.16	-0.13	-0.16	-0.14	-0.15
27	H	-0.12	-0.16	-0.12	-0.16	-0.14	-0.15
28	H	-0.12	-0.12	-0.12	-0.12	-0.12	-0.15
29	H	-0.10	-0.12	-0.10	-0.12	-0.11	-0.15

Figure A.5.10. Partial charges of 1,1,1,3,3-pentamethyltetrasilane. Charges using CHELPG method at MP4(sdq)/cc-pVTZ//MP2/6-31G(d,p) level and charges calculated based on optimized BCI are shown.



		Original ChelpG charge			H charge added to C				
		G	O	T	G	O	T		
		($\omega=53.8$)	($\omega=89.9$)	($\omega=162.8$)	($\omega=53.8$)	($\omega=89.9$)	($\omega=162.8$)	Averaged	BCI
1	Si	0.58	0.67	0.70	0.58	0.67	0.70	0.65	0.60
2	C	-0.43	-0.37	-0.52	-0.19	-0.20	-0.22	-0.20	-0.20
3	H	0.09	0.07	0.10	0.00	0.00	0.00	0.00	0.00
4	H	0.08	0.05	0.10	0.00	0.00	0.00	0.00	0.00
5	H	0.07	0.05	0.10	0.00	0.00	0.00	0.00	0.00
6	C	-0.25	-0.30	-0.39	-0.15	-0.18	-0.20	-0.18	-0.20
7	H	0.03	0.04	0.07	0.00	0.00	0.00	0.00	0.00
8	H	0.04	0.04	0.06	0.00	0.00	0.00	0.00	0.00
9	H	0.03	0.04	0.06	0.00	0.00	0.00	0.00	0.00
10	C	-0.40	-0.55	-0.37	-0.19	-0.23	-0.21	-0.21	-0.20
11	H	0.09	0.12	0.07	0.00	0.00	0.00	0.00	0.00
12	H	0.06	0.11	0.05	0.00	0.00	0.00	0.00	0.00
13	H	0.07	0.10	0.05	0.00	0.00	0.00	0.00	0.00
14	Si	0.15	0.18	0.20	0.15	0.18	0.20	0.18	0.40
15	Si	0.15	0.18	0.20	0.15	0.18	0.20	0.18	0.40
16	C	-0.09	-0.11	-0.23	-0.08	-0.09	-0.12	-0.10	-0.20
17	H	0.02	0.02	0.04	0.00	0.00	0.00	0.00	0.00
18	H	0.00	0.01	0.03	0.00	0.00	0.00	0.00	0.00
19	H	0.00	0.00	0.04	0.00	0.00	0.00	0.00	0.00
20	C	-0.25	-0.41	-0.37	-0.12	-0.15	-0.15	-0.14	-0.20
21	H	0.02	0.06	0.07	0.00	0.00	0.00	0.00	0.00
22	H	0.05	0.11	0.08	0.00	0.00	0.00	0.00	0.00
23	H	0.05	0.09	0.08	0.00	0.00	0.00	0.00	0.00
24	Si	0.58	0.67	0.70	0.58	0.67	0.70	0.65	0.60
25	C	-0.43	-0.37	-0.52	-0.19	-0.20	-0.22	-0.20	-0.20
26	H	0.07	0.05	0.10	0.00	0.00	0.00	0.00	0.00
27	H	0.09	0.07	0.10	0.00	0.00	0.00	0.00	0.00
28	H	0.08	0.05	0.10	0.00	0.00	0.00	0.00	0.00
29	C	-0.40	-0.55	-0.37	-0.19	-0.23	-0.21	-0.21	-0.20
30	H	0.07	0.10	0.05	0.00	0.00	0.00	0.00	0.00
31	H	0.09	0.12	0.07	0.00	0.00	0.00	0.00	0.00
32	H	0.06	0.11	0.05	0.00	0.00	0.00	0.00	0.00
33	C	-0.25	-0.30	-0.39	-0.15	-0.18	-0.20	-0.18	-0.20
34	H	0.03	0.04	0.07	0.00	0.00	0.00	0.00	0.00
35	H	0.04	0.04	0.06	0.00	0.00	0.00	0.00	0.00
36	H	0.03	0.04	0.06	0.00	0.00	0.00	0.00	0.00
37	C	-0.09	-0.11	-0.23	-0.08	-0.09	-0.12	-0.10	-0.20
38	H	0.00	0.00	0.04	0.00	0.00	0.00	0.00	0.00
39	H	0.02	0.02	0.04	0.00	0.00	0.00	0.00	0.00
40	H	0.00	0.01	0.03	0.00	0.00	0.00	0.00	0.00
41	C	-0.25	-0.41	-0.37	-0.12	-0.15	-0.15	-0.14	-0.20
42	H	0.05	0.11	0.08	0.00	0.00	0.00	0.00	0.00
43	H	0.05	0.09	0.08	0.00	0.00	0.00	0.00	0.00
44	H	0.02	0.06	0.07	0.00	0.00	0.00	0.00	0.00

Figure A.5.11. Partial charges of permethyltetrasilane. Charges using CHELPG method at MP4(sdq)/cc-pVTZ//MP2/6-31G(d,p) level and charges calculated based on optimized BCI are shown.

Bond length and angle of experiment, quantum mechanics (QM) at MP2/6-311G(d,p), optimized MMFF94S(MMFF), MM3 are shown in Table A.5.1–A.5.7. The experimental microwave spectroscopy data (MW) and MM3 data are reprinted from reference ⁷. Vibrational frequencies are listed in Table 5.8–5.12.

Table A.5.1. Internal coordinates of silane.

Silane								
	Exp. (IR+MW)	QM	MMFF	MM3	Δ_{QM}	Δ_{MMFF}	$\Delta_{MM3-exp}$	$\Delta_{MMFF-QM}$
Si–H [Å]	1.481185(3)	1.475	1.486	1.483	-0.006	0.005	0.002	0.011
\angle HSiH [deg]	---	109.5	109.5	109.5	---	---	---	0.000

Table A.5.2. Internal coordinates of methylsilane.

Methylsilane								
	Exp. (IR+MW)	QM	MMFF	MM3	Δ_{QM}	Δ_{MMFF}	$\Delta_{MM3-exp}$	$\Delta_{MMFF-QM}$
Si–C [Å]	1.8686(2)	1.876	1.877	1.876	0.007	0.009	0.007	0.001
Si–H	1.4832(4)	1.478	1.488	1.483	-0.005	0.004	0.000	0.010
C–H	1.0957(5)	1.093	1.093	1.112	-0.003	-0.003	0.016	0.000
\angle HSiH [deg]	---	108.5	108.9	108.3	---	---	---	0.375
\angle HCH	---	107.9	107.7	108.7	---	---	---	-0.221
\angle CSiH	110.50(3)	110.4	110.1	110.6	-0.1	-0.4	0.1	-0.339
\angle SiCH	110.88(3)	111.0	111.2	110.2	0.1	0.3	-0.7	0.209

Table A.5.3. Internal coordinates of dimethylsilane.

Dimethylsilane								
	Exp. (MW)	QM	MMFF	MM3	Δ_{QM}	Δ_{MMFF}	$\Delta_{MM3-exp}$	$\Delta_{MMFF-QM}$
Si–C [Å]	1.867(3)	1.878	1.878	1.873	0.011	0.011	0.006	0.000
Si–H	1.483(5)	1.481	1.491	1.482	-0.002	0.008	-0.001	0.010
C–H	1.095(5)	1.094	1.093	1.112	-0.001	-0.002	0.017	-0.001
\angle HSiH [deg]	107.8(5)	107.8	108.3	107.5	0.0	0.5	-0.3	0.449
\angle CSiC	111.0(2)	111.0	111.1	111.3	0.0	0.1	0.3	0.160
\angle CSiH	---	109.5	109.4	109.5	---	---	---	-0.150
\angle SiCH	---	111.0	111.2	110.2	---	---	---	0.173

Table A.5.4. Internal coordinates of trimethylsilane.

Trimethylsilane								
	Expt. (MW)	QM	MMFF94S	MM3	Δ_{QM}	Δ_{MMFF}	$\Delta_{MM3-exp}$	$\Delta_{MMFF-QM}$
Si-C [Å]	1.868(3)	1.879	1.879	1.876	0.011	0.011	0.008	0.000
Si-H	1.489(3)	1.485	1.497	1.484	-0.004	0.008	-0.005	0.012
C-H	1.095(3)	1.094	1.093	1.112	-0.001	-0.002	0.017	-0.002
\angle CSiC [deg]	110.2(2)	110.2	110.3	110.1	0.0	0.1	-0.1	0.137
\angle HCH	107.9(3)	107.8	107.7	108.7	-0.1	-0.2	0.8	-0.104
\angle CSiH		108.8	108.6	108.8	---	---	---	-0.142
\angle SiCH		111.1	111.2	110.2	---	---	---	0.105

Table A.5.5. Internal coordinates of tetramethylsilane.

Tetramethylsilane								
	Expt. (MW)	QM	MMFF	MM3	Δ_{QM}	Δ_{MMFF}	$\Delta_{MM3-exp}$	$\Delta_{MMFF-QM}$
Si-C [Å]	1.877(2)	1.881	1.882	1.876	0.004	0.005	-0.001	0.001
C-H	1.117(7)	1.095	1.093	1.112	-0.022	-0.024	-0.005	-0.002
\angle CSiC [deg]		---	109.5	109.5	---	---	---	0.000
\angle HCH	109.8(8)	107.7	107.7	108.7	-2.1	-2.1	-1.1	-0.047
\angle SiCH	109.2(8)	111.2	111.2	110.2	2.0	2.0	1.0	0.044

Table A.5.6. Internal coordinates of ethylsilane.

Ethylsilane								
	Expt.(MW)	QM	MMFF	MM3	Δ_{QM}	Δ_{MMFF}	$\Delta_{MM3-exp}$	$\Delta_{MMFF-QM}$
Si-C [Å]	1.866(3)	1.883	1.891	1.882	0.017	0.025	0.016	0.008
Si-H _s	1.483(5)	1.479	1.488	1.483	-0.004	0.005	0.000	0.009
Si-H _a	1.480(5)	1.479	1.488	1.483	-0.001	0.008	0.003	0.008
C-C	1.540(3)	1.537	1.519	1.542	-0.003	-0.021	0.002	-0.018
C ₁ -H	1.093(3)	1.096	1.093	1.114	0.003	0.000	0.021	-0.003
C ₂ -H	1.097(3)	1.094	1.094	1.113	-0.003	-0.003	0.016	0.000
\angle SiCC [deg]	113.2(2)	113.2	113.0	113.3	0.0	-0.2	0.1	-0.247
\angle SiCH		---	108.7	109.3	---	---	---	0.643
\angle CSiH		---	110.3	110.1	---	---	---	-0.112
\angle H _a SiH _a	108.3(5)	108.4	109.0	108.3	0.1	0.7	0.0	0.567
\angle H _a SiH _s	108.2(5)	108.8	108.7	108.3	0.6	0.5	0.1	-0.106
\angle H _a C ₁ H _a	107.0(5)	107.6	108.3	106.8	0.5	1.3	-0.2	0.730
\angle H _a C ₁ H _s	107.3(5)	107.7	108.3	107.3	0.4	1.0	0.0	0.624
\angle C ₂ C ₁ H	110.5(5)	111.3	110.6	109.3	0.8	0.1	-1.2	-0.625
\angle C ₁ C ₂ H	112.0(5)	109.9	109.1	111.6	-2.1	-2.9	-0.4	-0.829

Table A.5.7. Internal coordinates of ethylmethylsilane.

Ethylmethylsilane								
	Expt.(MW)	QM	MMFF	MM3	Δ_{QM}	Δ_{MMFF}	$\Delta_{MM3-exp}$	$\Delta_{MMFF-QM}$
Si-C(Me) [Å]	1.873	1.879	1.877	1.873	0.006	0.004	0.000	-0.001
Si-C(Et)	1.879	1.884	1.890	1.879	0.005	0.011	0.000	0.007
Si-H	1.483	1.483	1.491	1.482	0.000	0.008	-0.001	0.008
C-C	1.540	1.537	1.519	1.542	-0.003	-0.021	0.002	-0.018
\angle SiCC [deg]	114.2(20)	113.5	112.8	113.4	-0.7	-1.4	-0.8	-0.766
\angle CSiC	111(assumed)	111.6	110.9	111.2	0.6	-0.1	0.2	-0.739
\angle SiC2H	109.2(30)	108.6	109.4	109	-0.6	0.2	-0.2	0.842
\angle CCH	109.2(20)	109.8	108.9	110.6	0.6	-0.3	1.4	-0.947
\angle HC2H	105.8(assumed)	106.1	107.2	106.7	0.3	1.4	0.9	1.099

Table A.5.8. Rotational and vibrational frequencies of silane.

Silane					
Exp.	QM		MMFF		MM3
	original	scaled	Original	Optimized	
2189	2331.48	2214.91	2038.85	2224.32	2162
2185	2326.91	2210.56	1909.39	2172.99	2111
972	1017.12	966.26	758.37	993.83	1028
913	974.02	925.32	447.08	849.01	877

Table A.5.9. Vibrational frequencies of methylsilane.

Methylsilane					
Exp.	QM		MMFF		MM3
	original	scaled	Original	Optimized	
2982	3178.50	3020.21	2905.77	2991.98	2984
2929	3083.67	2929.49	3049.78	2874.22	2881
2166	2310.20	2194.69	2075.21	2214.16	2158
2169	2311.57	2195.99	2004.45	2191.49	2126
1403	1479.80	1405.81	1425.57	1421.77	1417
1264	1321.16	1255.1	1240.85	1243.66	1271
946	1006.27	955.96	732.72	954.77	983
871	908.76	863.32	792.32	753.92	892
946	989.58	940.1	795.82	916.65	841
701	718.53	682.6	591.43	643.08	702
545	524.71	498.47	418.55	595.23	590
183	197.81	187.92	216.12	200.79	208

Table A.5.10. Rotational and vibrational frequencies of dimethylsilane.

Dimethylsilane						
Exp.	QM		MMFF		MM3	
	original	scaled	Original	Optimized		
2970	3174.04	3015.97	3015.97	2992.3	2984	
2970	3174.21	3016.13	3016.13	2990.71	2984	
-	3170.61	3012.71	3012.71	2992.13	2984	
2970	3171.53	3013.59	3013.59	2991.29	2984	
2920	3077.76	2924.49	2924.49	2874.01	2881	
2920	3077.20	2923.96	2923.96	2873.88	2881	
2142	2285.75	2171.92	2171.92	2182.95	2171	
2145	2289.27	2175.26	2175.26	2176.02	2153	
1430	1484.92	1410.97	1410.97	1424.49	1417	
1410	1480.80	1407.06	1407.06	1418.98	1417	
1410	1473.94	1400.54	1400.54	1418.72	1417	
-	1472.82	1399.47	1399.47	1424.28	1417	
1260	1312.76	1247.38	1247.38	1245.66	1274	
1260	1320.35	1254.6	1254.6	1244.64	1272	
963	1008.35	958.13	958.13	947.73	904	
919	955.69	908.1	908.1	902.02	899	
867	904.40	859.36	859.36	763.26	897	
838	874.83	831.26	831.26	750.84	890	
-	910.60	865.25	865.25	802.44	883	
728	744.65	707.57	707.57	728.72	783	
-	587.69	558.42	558.42	725.52	713	
643	649.20	616.87	616.87	728.72	698	
659	672.73	639.23	639.23	618.78	671	
467	467.55	444.27	444.27	492.77	465	
223	207.84	197.49	197.49	203.39	224	
-	171.25	162.72	162.72	168.68	180	
-	152.53	144.93	144.93	161.17	170	

Table A.5.11. Rotational and vibrational frequencies of trimethylsilane.

Trimethylsilane						
Exp.	QM		MMFF		MM3	
	original	scaled	Original	Optimized		
-	3168.73	3010.93	3047.93	2990.86	2985	
2969	3164.92	3007.31	3047.99	2991.88	2984	
-	3163.47	3005.93	3046.12	2991.88	2984	
-	3168.11	3010.34	3046.07	2990.12	2984	
2912	3071.50	2918.54	2903.44	2873.75	2882	
-	3071.40	2918.44	2903.28	2873.57	2881	
2125	2262.97	2150.27	2211.14	2129.79	2139	
-	1489.25	1415.09	1425.17	1424.68	1419	
1446	1480.21	1406.5	1424.61	1418.79	1418	
-	1309.83	1244.6	1248.39	1246.88	1417	
-	1467.08	1394.02	1423.54	1418.17	1416	
1257	1472.47	1399.14	1424.79	1424.18	1272	
1263	1321.26	1255.46	1245.68	1245.27	1270	
907	941.12	894.25	878.03	871.05	915	
835(s)	891.91	847.49	809.2	769.5	909	
849	866.13	823	791.91	752.79	884	
-	691.75	657.3	784.42	735.95	878	
616(1)	624.08	593	763.42	733.34	779	
714	728.86	692.56	657.95	663.1	721	
625	635.70	604.04	592.01	583.46	624	
216(1)	241.07	229.06	233.56	229.75	250	
252(1)	201.96	191.9	257.41	194.61	229	
-	167.03	158.71	163.05	161.42	177	
-	145.10	137.87	159.72	158.14	171	

Table A.5.12. Rotational and vibrational frequencies of disilane.

Disilane						
Exp.		QM		MMFF		MM3
IR(gas)	Ra(liquid)	original	scaled	Original	Optimized	
2178	-	2316.86	2201.02	2055.11	2211.16	2163
-	2155	2308.82	2201.02	2052.14	2209.31	2162
2154	-	2316.86	2193.38	2035.43	2178.15	2129
-	2152	2299.84	2184.85	2032.21	2175.69	2128
940	-	981.93	932.83	788.04	948.41	968
-	929	997.65	947.77	774.68	948.41	962
-	909	896.88	852.04	757.35	852.7	771
844	-	976.92	928.07	788.28	894.37	765
-	625	665.27	632.01	541.86	546.35	555
379	-	395.78	375.99	531.6	505.51	509
-	434	446.20	423.89	449.62	441.96	428
-	-	148.59	141.16	136.11	135.58	147

Table A.5.13. Conformational energy of various monosilane derivatives.

Compound		Exp.	QM	MMFF	MM3
Methylsilane	Methyl barrier	1.67	1.56	1.56	1.65
Dimethylsilane	Methyl barrier	1.65	1.53	1.52	1.74
Trimethylsilane	Methyl barrier	1.83	1.50	1.49	1.81
Tetramethylsilane	Methyl barrier	2.00	1.47	1.47	1.90
Ethylsilane	Methyl barrier	2.62	2.63	2.63	2.64
	SiH ₃ barrier	1.98	1.79	1.78	2.01
Propylsilane	ΔE	0.60 – 0.65	0.68	0.68	0.60
Ethylmethylsilane	Methyl barrier	1.54(3)	1.52	1.52	1.74
	Ethyl barrier				2.14

References

- (1) Didraga, C.; Knoester, J. J. *Lumin.* **2003**, *102-103*, 60.
- (2) Niketic, S. R.; Rasmussen, K. *The Consistent Force Field: A Documentation*; Springer-Verlag Berlin • Heidelberg: Berlin; Heidelberg; New York, 1977; pp. 169–179.
- (3) Engelsen, S. B.; Fabricius, J.; Rasmussen, K. *Comput. Chem.* **1994**, *18*, 397.
- (4) Vaiana, A. C.; Cournia, Z.; Costescu, I. B.; Smith, J. C. *Comput. Phys. Commun.* **2005**, *167*, 34.
- (5) Halgren, T. A. *J. Comput. Chem.* **1996**, *17*, 490.
- (6) Leach, A. R. *Molecular modelling : principles and applications*; 2nd ed.; Pearson Education: Harlow ; Tokyo, 2001; pp. 262–267.
- (7) Chen, K. S.; Allinger, N. L. *J. Phys. Org. Chem.* **1997**, *10*, 697.

List of Publications

Academic Journals

- (1) Suzuki, N.; Fujiki, M.; Kimpinde-Kalunga, R.; Koe, J. R. *J. Am. Chem. Soc.* **2013**, *135*, 13073.
- (2) Suzuki, N.; Wang, Y.; Elvati, P.; Kim, K.; Qu, Z.-B.; Jiang, S.; Baumeister, E.; Lee, J.; Yeom, B.; Bahng, J. H.; Lee, J.; Violi, A.; Kotov, N. A. *ACS Nano*, DOI : 10.1021/acsnano.5b06369.
- (3) Taguchi, M.; Suzuki, N.; Fujiki, M. *Polym. J.* **2013**, *45*, 1047.
- (4) Wang, L.; Suzuki, N.; Liu, J.; Matsuda, T.; Rahim, N. A. A.; Zhang, W.; Fujiki, M.; Zhang, Z.; Zhou, N.; Zhu, X. *Polym. Chem.* **2014**, *5*, 5920.
- (5) Amako, T.; Harada, T.; Suzuki, N.; Mishima, K.; Fujiki, M.; Imai, Y. *RSC Adv.* **2013**, *3*, 23508.
- (6) Amako, T.; Nakabayashi, K.; Suzuki, N.; Guo, S.; Rahim, N. A. A.; Harada, T.; Fujiki, M.; Imai, Y. *Chem. Commun.* **2015**, *51*, 8237.
- (7) Fujiki, M.; Jalilah, A. J.; Suzuki, N.; Taguchi, M.; Zhang, W.; Abdellatif, M. M.; Nomura, K. *RSC Adv.* **2012**, *2*, 6663.
- (8) Fujiki, M.; Yoshida, K.; Suzuki, N.; Zhang, J.; Zhang, W.; Zhu, X. *RSC Adv.* **2013**, *3*, 5213.
- (9) Kitayama, Y.; Amako, T.; Suzuki, N.; Fujiki, M.; Imai, Y. *Org. Biomol. Chem.* **2014**, *12*, 4342.
- (10) Lee, D.; Kim, H.; Suzuki, N.; Fujiki, M.; Lee, C.-L.; Lee, W.-E.; Kwak, G. *Chem. Commun.* **2012**, *48*, 9275.
- (11) Watanabe, K.; Koyama, Y.; Suzuki, N.; Fujiki, M.; Nakano, T. *Polym. Chem.* **2014**, *5*, 712.
- (12) Kim, H.; Lee, D.; Lee, S.; Suzuki, N.; Fujiki, M.; Lee, C.-L.; Kwak, G. *Macromol. Rapid Commun.* **2013**, *34*, 1471.

- (13) Lee, D.; Jin, Y.-J.; Kim, H.; Suzuki, N.; Fujiki, M.; Sakaguchi, T.; Kim, S. K.; Lee, W.-E.; Kwak, G. *Macromolecules* **2012**, *45*, 5379.
- (14) Liu, J.; Zhang, J.; Zhang, S.; Suzuki, N.; Fujiki, M.; Wang, L.; Li, L.; Zhang, W.; Zhou, N.; Zhu, X. *Polym. Chem.* **2014**, *5*, 784.
- (15) Fujiki, M.; Donguri, Y.; Zhao, Y.; Nakao, A.; Suzuki, N.; Yoshida, K.; Zhang, W. *Polym. Chem.* **2015**, *6*, 1627.
- (16) Shiraki, T.; Tsuchiya, Y.; Noguchi, T.; Tamaru, S.-i.; Suzuki, N.; Taguchi, M.; Fujiki, M.; Shinkai, S. *Chem. Asian J.* **2014**, *9*, 218.

Presented Works

A. Presentations at International Conference

- (1) ○Suzuki, N.; Goto, H.; Fujiki, M.
Side Chain Length Dependent Chiroptical inversion of Helical Polysilane Aggregates
15th International Conference on Chiroptical Spectroscopy (CD2015), P01, poster, August 30–September 3, 2015, (Sapporo, Hokkaido, Japan)
- (2) Suzuki, N.; Fujiki, M.; ○Koe, J. R.
Systematical Conformation Search of Helical Dialkyloligosilane
The 10th SPSJ International Polymer Conference (IPC2014), 4P-G2-076b, poster, December 2–5, 2014, (Tsukuba, Ibaraki, Japan)
- (3) ○Suzuki, N.
Chiroptical Inversion in Polymer Aggregates Induced by Geometrical Effect of Helical Structure
GIST-NCTU-NAIST International Joint Symposium 2013 (GNN Joint Symposium 2013), oral, November 21–22, 2013, (Ikoma, Nara, Japan)
- (4) ○Suzuki, N.; Fujiki, M.; Koe, J. R.
Helical Polysilane Aggregates: Novel Side-Chain Length and Solvent Dependent (Chir)optical Properties
International Association of Colloid and Interface Scientists (IACIS2012), S1P15-06, poster, May 13–18, 2012, (Sendai, Miyagi, Japan)
- (5) ○Suzuki, N.; Fujiki, M.; Koe, J.
Understanding Chiroptical Switching of Helical Polymer Supramolecules Based on a Mathematical Model
The 9th International Polymer Conference (IPC2012), 13E01, oral, December 11–14, 2012,

(Kobe, Hyogo, Japan)

- (6) ○Suzuki, N.; Fujiki, M.; Kimpinde-Kalunga, R.; Koe, J.

Chirality in Polysilane Aggregates

4th Asian Silicon Symposium (ASiS-4), PO-047, poster, October 21–24, 2012, (Tsukuba, Ibaraki, Japan)

B. Presentations at Domestic Conference

- (1) ○鈴木 望; 藤木 道也; コウ ジュリアン

らせん構造の幾何的性質による高分子高次構造体の光学活性反転機構

第 62 回高分子討論会, 口頭, 2013/9/11–13, (金沢)

- (2) ○渡辺 顕士; 小山 靖人; 中野 環; 鈴木 望; 藤木 道也

ハイパーブランチ型主鎖構造を有する光学活性ポリフルオレン誘導体の合成と物性

第 62 回高分子討論会, 口頭, 2013/9/11–13, (金沢)

- (3) コウ ジュリアン; ○鈴木望; 藤木道也

貧溶媒・良溶媒系における光学活性ジアルキルポリシランのキロプティカルクロミズム

第 57 回高分子研究発表会, ポスター, 2011/7/15, (神戸)

- (4) ○鈴木 望; コウ ジュリアン; 藤木道也

光学活性反転を示すケイ素高分子の構造: 貧溶媒/良溶媒とアルキル鎖長依存性

第 20 回ポリマー材料フォーラム, ポスター, 2011/11/24–25, (東京)

Acknowledgements

The works in this thesis could not be achieved alone. I am thankful to my supervisor Prof. Michiya Fujiki for his suggestions, encouragement, and patience. His deep knowledge in the field of polysilane and spectroscopy broadened my view in science. He also gave me opportunities to visit University of Michigan (UM) where I worked with Prof. Nicholas Kotov for a half a year in 2014 and visiting Toyohashi University of Technology (TUT) in 2015 where I have developed the program in Chapter 4 and 5 with Prof. Hitoshi Goto. Those were not possible without his generous attitude.

I also appreciate other faculty members in Nara Institute of Science and Technology (NAIST). My gratitude to Prof. Hiroshi Daimon who had keen eyes for direction of the research. His questions were sometimes hard to answer but struggling on getting the answers for his questions sometimes led me to new ideas to explain the experimental results. I am also thankful to Prof. Hironari Kamikubo for his kind advise and suggestion that was not limited to the obstacle that I was confronting but he also pointed out the potential future problem that will be encountered after solving the confronting problem. His encouragement to develop silicon force field motivated me very much when I felt the work tedious. My gratitude also goes to Prof. Takeshi Inagaki who kindly responded me when I had difficulty in understanding the functions that describe exciton chirality method. He did not hesitate to spend his own time to the student in different laboratory. I am thankful to Prof. Shinji Koh who was in NAIST but moved to Aoyama Gakuin University (Tokyo) in 2013. He was a good educator and he suggested not only about the research theme I had but also how to develop the carrier as a researcher.

I am also thankful to highly talented technical staffs in NAIST. I am thankful to Fumio Asanoma who helped me with the measurement using ^{29}Si -NMR, and 2D NMR such as COSY, HMQC, and HMBC. Not only the measurement but also the discussion about my research was

beneficial to verify assumptions. I appreciate the help by Shunsuke Kawabata who was responsible for Material Simulation Analysis System in NAIST. He properly provided the computational environment for the calculation and kindly helped me when I met hardware memory issue and several difficulties in starting up the Materials Studio.

This work includes experimental, theoretical, and computational methods, and such various approaches could not have been taken without helps of researchers in the other universities. I would like to express my great gratitude to Prof. Hitoshi Goto at TUT who developed molecular mechanics software package CONFLEX 7B. The author requested him to supervising me during the development of the parameterization program in 2015 and also the force field for silicon system and he did not let me down. He had deep insight in the field and told me the importance of “observation” not only for the experiment but also for the results obtained from computational method. His advice was always accurate and clear. I am indebted to Assistant Prof. Shigeaki Obata in TUT who had helped me starting up the heavy quantum mechanics calculation using the facilities in TUT. I am also thankful to Dr. Naofumi Nakayama in CONFLEX Corporation who supported me evaluating the method for the quantum mechanics.

I am thankful to Prof. Julian Koe at International Christian University who was my former supervisor during the senior thesis writing while I was an undergraduate student. This project was started in his laboratory and the project was taken over by Prof. Fujiki with their agreement in 2011. I could not complete writing the paper *J. Am. Chem. Soc.* **2013**, *135*, 13073–13079 without his advice on how to build-up the logic to persuade the readers.

I am also thankful to Prof. Nicholas Kotov and Prof. Sharon Glotzer at UM. The work is not written in this thesis but Nick gave me the opportunity to work on the chiral graphene project in 2014 and the work was accepted by ACS Nano in Dec. 31, 2015. During the laboratory stay, I was in Sharon Glotzer’s laboratory since the computational facilities are much better in her lab. During

the stay I have learned the python programming language and how to work on supercomputers from her post doctoral researcher and students including, Ryan Marson, Andrew Karas, and Pablo F. Damasceno. Without this valuable experience I could not achieve the work described in Chapters 4 and 5.

I am also thankful for laboratory members in Advanced Polymer Science Laboratory including students who were already graduated from NAIST. Not only the discussion in laboratory but also spending time out side the school with them was enjoyable.

Finally but not the least, I appreciate the support from my parents, two elder brothers and two younger sisters. Especially my father Hiroshi Suzuki who is a mathematician encouraged me to work hard, advised me how to design the carrier as a researcher, and told me some mathematics related to chemistry during the Ph.D. course.

February 2016

Nozomu SUZUKI